SYNCHROPHASORS: MULTILEVEL ASSESSMENT AND DATA QUALITY IMPROVEMENT FOR ENHANCED SYSTEM RELIABILITY

A Dissertation

by

TAMARA BECEJAC

Submitted to the Office of Graduate and Professional Studies of
Texas A&M University
in partial fulfillment of the requirements for the degree of

DOCTOR OF PHILOSOPHY

Chair of Committee,	Thomas Overbye
Committee Members,	Katherine Davis
	Alexander Sprintson
	Erick Moreno-Centeno
Head of Department,	Miroslav Begovic

May 2019

Major Subject: Electrical Engineering

ABSTRACT

This study presents a comprehensive framework for testing and evaluation of Phasor Measurement Units (PMUs) and synchrophasor systems under normal power system operating conditions, as well as during disturbances such as faults and transients. The proposed framework suggests a performance assessment to be conducted in three steps: (a) *type testing*: conducted in the synchrophasor calibration laboratory according to accepted industrial standards; (b) *application testing*: conducted to evaluate the performance of the PMUs under faults, transients, and other disturbances in power systems; (c) *end-to-end system testing*: conducted to assess the risk and quantify the impact of measurement errors on the applications of interest.

The suggested calibration toolset (*type testing*) enables performance characterization of different design alternatives in a standalone PMU (e.g., length of phasor estimation windows, filtering windows, reporting rates, etc.). In conjunction with the standard performance requirements, this work defines new metrics for PMU performance evaluations under any static and dynamic conditions that may unfold in the grid. The new metrics offer a more realistic understanding of the overall PMU performance and help users choose the appropriate device/settings for the target applications. Furthermore, the proposed probabilistic techniques quantify the PMU accuracy to various test performance thresholds specified by corresponding IEEE standards, rather than having only the pass/fail test outcome, as well as the probability of

specific failures to meet the standard requirements defined in terms of the phasor, frequency, and rate of change of frequency accuracy.

Application testing analysis encompasses PMU performance evaluation under faults and other prevailing conditions, and offers a realistic assessment of the PMU measurement errors in real-world field scenarios and reveals additional performance characteristics that are crucial for the overall application evaluation.

End-to-end system tests quantify the impact of synchrophasor estimation errors and their propagation from the PMU towards the end-use applications and evaluate the associated risk.

In this work, extensive experimental results demonstrate the advantages of the proposed framework and its applicability is verified through two synchrophasor applications, namely: Fault Location and Modal Analysis. Finally, a data-driven technique (Principal Component Pursuit) is proposed for the correction and completion of the synchrophasor data blocks, and its application and effectiveness is validated in modal analyzes.

DEDICATION

To my sister

ACKNOWLEDGEMENTS

First, I would like to express my sincere gratitude and deepest respect to my advisor, Dr. Thomas Overbye, for his endless encouragement, guidance, and support throughout the course of this research. His knowledge and patience are invaluable to the completion of this work. Working with Dr. Overbye during the last year is my greatest honor.

I also wish to thank my committee members, Dr. Katherine Davis, Dr. Erick Moreno-Centeno, Dr. Alexander Sprintson, and Prof. Sunil Khatri, for their suggestions, time, and support. Special thanks to Dr. Harold Kirkham from Pacific Northwest National Laboratory (PNNL) for all the informative discussions and his helpful advices regarding my research.

Thanks also go to my friends and colleagues, Ms. Ana Maria Ospina Sierra, and other group members for their help and support throughout my graduate study.

I am also grateful to the department faculty and staff for making my time at Texas A&M University a great experience, particularly Melissa Sheldon, Andrea Kishne, Katie Bryan, Jeanne Prestwood, Wayne Matous, Rebecca Rice, Holley Toschlog, Anni Brunker, and Alexandra Bello.

Finally, I wish to thank my sister, and my grandmother for their unconditional love, patience, and encouragement.

CONTRIBUTORS AND FUNDING SOURCES

This work was supervised by a dissertation committee consisting of Professors Thomas Overbye, Katherine Davis, and Alexander Sprintson of the Department of Electrical and Computer Engineering, and Professor Erick Moreno-Centeno of the Department of Industrial and Systems Engineering. Part of the work was supervised by Professor Mladen Kezunovic of the Department of Electrical and Computer Engineering.

All work conducted for the dissertation was completed by the student independently.

My research was mainly funded by financial resources from two projects. One is funded by Texas A&M – CAPES: “Development of Advanced Open-Source PMU/PDC Lab and Applications with Synchronized Data Obtained from Simulation and Actual Power Network”. The other is funded by Power System Engineering Research Center (PSERC): “High Impact Project Title: Life-cycle Management of Mission-Critical Systems through Certification, Commissioning, In-Service Maintenance, Remote Testing, and Risk Assessment.”

This work was made possible in part by a Thomas Powell’62 fellowship from Texas A&M University and a dissertation research fellowship from DEED (Demonstration of Energy & Efficiency Developments) and the American Public Power Association.

I would like to acknowledge the financial support from all the sponsors.

TABLE OF CONTENTS

Page

LIST OF FIGURES

Page

LIST OF TABLES

Page

1. INTRODUCTION

1.1 Motivation and Overview

The electricity grid is a critical infrastructure of the modern society, yet vulnerable to numerous sources of uncertainties and disturbances, due to its noticeable growth of both electricity demand and penetration of non-conventional generators. Unfortunately, the number of failures in the grid is also increasing as a result of the grid's aging infrastructure, and more severe weather conditions [1]. Hence, advanced monitoring and control strategies need to be properly planned and deployed to mitigate and minimize the impact of such risks on the grid performance.

Following the catastrophic Northeastern US blackout in 2003, the American Recovery and Reinvestment Act (Recovery Act) of 2009 supported the DOE with $4.5 billion for the modernization of the power grid, which offered a new impetus for the development of synchrophasor technology [2]. With up to 120 measurements per second, synchrophasor technology is deemed a solution for more advanced and high-resolution monitoring, protection, and control of the grid. PMU measurements help capture and track real-time system dynamics and allow development of new, groundbreaking applications that can improve situational awareness of the grid states [3]-[8]. Deployment of PMUs and PMU-capable IEDs over the last 30 years has facilitated a better understanding of modern power systems. PMUs now serve as the backbone for many system-wide mission-critical applications in the electric industry, such as state estimation, fault detection,

remedial actions, oscillation detection, and wide area monitoring. Nevertheless, those applications require synchrophasor data to be reliable, accurate, and delivered "on-time."

The synchrophasor infrastructure is a mission-critical system and, it is expected to operate reliably each time it is called upon. To ensure the reliability and security of the infrastructure for synchrophasor-based applications, good synchronization (accuracy of the timing reference is higher than 1 us), a fast and reliable communication network, and accurate phase angle and magnitude measurements are needed [9]. On the other hand, PMU data is often delivered with various data quality issues, hindering PMUs to be fully incorporated and deployed in control and operation practices [40]. Several IEEE standards and guides provide requirements for installation, performance and testing procedures for synchrophasor devices (i.e., PMU, PDC), but considering the lack of enforcement, data quality is still not sufficient for many downstream applications. California ISO reported that the typical bad data ratio of synchrophasor measurements in the US ranges from 10% to 17%, where 80% of the problems are the invalid data problem (incorrect magnitude, phase and/or frequency measurement) while 10% are the unsynchronized data problems [39].

Regardless of the application, certain testing and performance validation of PMUs and the end-to-end synchrophasor system are essential to confirm measurement accuracy and continuously ensure high reliability and trustworthiness. Over the past decades, many synchrophasor applications have been developed, although the performance under various PMU errors has not been explored and is unknown for most applications. This research strives to examine a number of procedures and testing tool implementation techniques to

reach a better understanding of the PMU measurement limitations imposed on the applications, and improve quality of synchrophasor data by looking in the following problems:

1) Performance of the single PMU device under standard-defined test and beyond

While compatibility of commercial PMUs with the industrial standards (e.g., IEEE standard C37.118.1a-2014) is expected, calibration laboratory tests reveal noticeable inconsistencies among the measurements obtained by PMUs from various manufacturers due to different phasor estimation techniques and hardware solutions [32]. Furthermore, hardware in the loop testing reveals evident discrepancies among the phasor estimates under the conditions not specified in the standards (e.g., transients, faults) [31]-[34], [41]. Such observations suggest that there is no guarantee that different end-use applications would perform satisfactorily even if the PMUs have passed all the standard *type test* requirements. Thus, development of advanced testing facilities and procedures that will help to understand the behavior of different implementations is crucial.

2) Synchrophasor end-to-end system evaluation

Even though all components (e.g., PMUs, PDC, and communication gear) may pass the laboratory tests, there is no guarantee that everything will work properly together after installation and deployment in the field. To preserve a satisfactory level of service quality, system components need to be tested keeping in mind different stages of the deployment. Therefore, developing the testing environment for not only PMUs but also an assessment of the complete system solution is critical. Moreover, the risk of failure of the end-use applications caused by inaccuracy and abnormality of PMU measurements,

especially in the face of different system operating conditions such as faults and transients should be researched.

3) Synchrophasor data quality improvement

Data issues in the synchrophasor system can arise because of topology errors, meter failures, improper configurations. Additionally, communication infrastructure brings vulnerabilities to the power system allowing intruders to launch various types of cyber-attacks and jeopardize the reliability of the electric grid. Hence, it is crucial to have a proper mechanism for the detection and mitigation of the corrupted PMU data. In spite of its importance, limited effort has been made to characterize and understand the source nature, detect and finally, if possible correct PMU data [40].

Having a rigorous procedure and adequate tools to test different aspects of the hardware and software design, from the component to the overall system level, and over different time spans is the only way to assure a robust and reliable operation of the mission-critical systems.

1.2 State of the art

1.2.1 Associated Standards and Guides

Multiple efforts have resulted in standards and guides for PMU testing and calibration. IEEE Standards Association and North American Synchro Phasor Initiative (NASPI) have issued several standards and guidelines providing information on how to test and safeguard mission-critical infrastructure such as PMUs and Phasor Data Concentrators (PDCs) [10]-[17]. Since 2005, standards for the static and dynamic performance of the PMUs, as well as communication requirements for the synchrophasor

data transfer have been developed and eventually adopted. The IEEE C37.118.1-2011 standard defines acceptable performance requirements for synchrophasor measurement [10]. In 2014, this standard was revised, where some tests were removed, and some of the requirements were relaxed because none of the PMUs and IEDs with PMU capabilities available at that time in the market could comply with the standard [12]. Testing procedures and requirements for the test equipment, such as timing reference, signal source, calibration device, and environmental conditions, are given in IEEE Synchrophasor Measurement Test Suite Specification (TSS) document published by IEEE Conformity Assessment Program (ICAP) [13]. TSS provides a suite of unambiguous test procedures by following the Smart Grid Interoperability Panel (SGIP) Recommendations contained in the Interoperability Process Reference Manual [14]. IEEE C37.118.2-2011 standard covers the requirements for the PMU data transfer in power systems [11]. IEEE C37.242 document provides guidance for synchronization, calibration, testing, and installation of PMUs applied in power system protection and control [16]. Testing procedures for the Phasor Data Concentrators (PDCs) are given in the IEEE C37.244 Guide for Phasor Data Concentrators Requirements for Power System Protection, Control, and Monitoring [17].

According to the above standards, two performance classes of PMUs, namely P and M, are defined where the P-class is intended for protection applications demanding fast measurement response time, while the M performance class is utilized in applications that require high measurement accuracy [10]. A standard-compliant PMU should meet all

the requirements, at least for one class, for the *type test* steady-state and dynamic performance.

1.2.2 Synchrophasor System Assessment Methodologies

Type tests are conducted in a controlled environment where the PMUs are exposed to known input waveforms defined in the IEEE standards. Many organizations, government agencies, and researchers have developed calibration and testing facilities for performance evaluation of PMUs and PMU-embedded devices (e.g., relays and recorders) according to standard requirements [18]-[29] and field-testing procedures [30]-[34]. For instance, the National Institute of Standard and Technology (NIST) lead the way in this area, and Synchro-Metrology lab was built in 2006 [18], and has advanced to reference calibration system for all other testing facilities [19]. Since the National Metrology Institute (NMI) did not provide support for the calibration of these devices, and due to the lack of the reference calibration system, NIST took the lead to develop such facility. This calibration system is capable of testing PMUs only under the signal conditions given in the standard and it is not fully automated. Additionally, PMU testing laboratories have been developed and used to evaluate PMUs in Brazil [20], China [21], Europe [22], [23], Canada [27], and in the USA [28]. However, the traceability of those testing systems to the NIST system was not demonstrated, hence the trustworthiness of the acquired testing results is uncertain. Recently, Fluke Company has promoted a commercial PMU calibration system, which complies with IEEE C37.118.1-2011a-2014 [29].

Furthermore, a team at the Bonneville Power Administration (BPA) in collaboration with the Pacific Northwest National Laboratory (PNNL) was involved in

testing the PMUs in laboratory and field environments under both static and dynamic conditions [30]. However, details about the calibration system and its accuracy are not provided. In [31], several issues related to PMU measurements under transient conditions were discussed and procedures for PMU testing under such scenarios were proposed. Authors in [33] analyzed the impact of PMU frequency and phase angle errors on a number of synchrophasor applications among which are: islanding detection, event location detection, dynamic line rating, and oscillation detection. The main issue with the proposed approach is the assumption that the maximum frequency error present in the PMU measurement is equal to 0.005 Hz, which is many cases, is not correct. We showed that in the certain test cases, frequency error exceeds the assumed value; hence, the results from [33] are underestimating the impact of the flawed PMU data.

Besides, all these facilities are focused only on the particular test set, while this dissertation proposes the comprehensive framework that includes multiple stages of testing, ranging from evaluation of the PMUs according to standard requirements and beyond, as well as the assessment of entire synchrophasor system under normal power conditions and during system disturbances. Also, the traceability of the developed PMU calibration system has been demonstrated to a NIST system.

The concept of end-to-end testing has been established in the literature [35]-[38]. An example of such end-to-end testing of protection system and fault clearing system is discussed in [36], [37] where the overall engineering process of system study, protection concept, design, purchase, build, and installation is described. However, this concept is not yet being applied the synchrophasor systems [110].

1.2.3 Bad Data Detection and Management

Presence of bad data in power system application is not a novel issue. Conventional measurements collected from the meters contain the errors due to the imperfections in the current/voltage transformers, rounding in the calculation, communication gear, etc. Within energy management system, state estimation (SE) is widely used as a tool for data "pre-screening" having a capability of the measurement correctness and timeliness. With the introduction of the modern devices such as PMUs and advancement in the network infrastructure, power system has become more vulnerable, imposing a need for the better solutions in regards to data protection and bad data detection [115]. In general, bad data detection (BDD) techniques can be divided into five categories: 1) traditional approach based on the SE [42]-[45]; 2) methods that utilize Kalman filter [46]-[50]; 3) data-driven analyses [51]-[65]; 4) machine learning algorithms [66] and 5) logic-based techniques [67]-[69].

Many of the bad data detection methods are still based on SE, though it has been shown that when smart cyber-attack is launched, traditional SE methods will fail (bypass) to detect it, putting the system in danger. To deploy the SE-based BDD technique, previous knowledge on the system model is necessary, which in turn may result in non-reliable bad data detection when system topology is inaccurate. Therefore, the detection accuracy of the SE-based approaches may be affected when gross errors are presented in system topology or parameters. Furthermore, these methods cannot operate successfully when state estimation diverges because of gross measurement errors, system physical disturbances, or stressful operating conditions. The techniques based on the Kalman filter

are model-free since the estimate of the state is based on the previously predicted values of the same state, however, usually those are computationally expensive.

Techniques that require prior knowledge of the network parameters and/or system topology might be affected by the errors in the topology/parameters, giving the significant advantage to the purely data-driven methods, among which are: Principal Component Analyses (PCA), low-rank matrix approach, density based Local Outlier Factor detection techniques (LOF), clustering. However, some data-driven approaches [53], [54] are defined as nonlinear optimizations problem. The problem with nonlinear functions is that it can make the minimization problem to be non-convex, making it computationally expensive. References [53], [55] pioneered purely data-driven approach to improve the PMU measurements quality.

To be applied onto PMU measurement blocks, PCA based data detection requires a prior estimation of error-free measurement matrix as well as a certain training period. Low-rank matrix techniques are block-based processing methods, and potential applications include the recovery of missing PMU data, detection of the outliers, cyber-attacks. One interesting approach for the recovery of a low-rank matrix is the Principal Component Pursuit (PCP), which is based on a convex problem that can be solved by applying an augmented Lagrangian multiplier (ALM)-based algorithm [64]. In contrast to PCA, PCP guaranties recovery of the low-rank matrix despite the gross sparse errors. Algorithms such as Singular Value Thresholding (SVT) and the Information Cascading Matrix Completion (ICMC) are just some of the examples applied in the synchrophasor domain [58], [59]. In addition, a few more algorithms were proposed to solve the matrix

completion problem in other research areas such as ADMiRa, and Singular Value Projection (SVP).

Although the proposed recovery techniques are capable of filling the missing points, and bad data detection due to high computational complexity those are not suitable for on-line applications. In [59], an online algorithm for PMU data processing (OLAP) has been proposed and is built upon the recent art in subspace tracking, continuously updating the dominant singular values and singular vectors, and the missing data is recovered by filling the empty point space based on the singular vectors.

Authors in [61], [62] applied density based LOF analyses to identify the low-quality synchrophasor measurement leveraging the spatial-temporal correlation between the measurements. LOF method is threshold-based, and it is system dependent, which imposes the need for the algorithm to pass the off-line training using the historical system data. A drawback of the methods that use outliers for the BD detection is that it can mislead the detection methods when disturbances occur in the system or produce false alarms because of insufficient PMU redundancy.

Sometimes, simple plausibility checks combined with the engineering judgment can greatly help in mitigating some basic, still common issues that arise in the PMU data sets. It has been shown that this type of basic checks are very efficient, nevertheless, in some cases, the “logical rules” do not catch bad measurements (especially when a cyber-attack is executed), or incorrectly reject valid data points which can result in increased loss of data. In [68] authors proved that the largest residual location does not mean that it is the location of the bad data occurrence, which results in removing the good data. The

computational burden is very low, allowing this method to be used online for the detection and correction purpose.

In this work, the Principal Component Pursuit technique that has been widely used in the image processing is applied for the correction of PMU data, and its effectiveness is demonstrated on the synthetic PMU frequency measurements.

1.3 Research Approach and Main Contributions

This dissertation proposes the synchrophasor measurement evaluation to be accomplished in three layers: *type testing*, *application testing*, and *system end-to-end testing*. Figure 1 depicts the proposed synchrophasor testing framework.

- *Type tests* are conducted in a calibration laboratory environment where PMUs are exposed to known signal patterns defined in the IEEE standard 37.118.1a and the PMU response to such static and dynamic patterns are assessed. Proposed comprehensive evaluation of PMUs assesses the performance of different design alternatives such as length of the phasor estimation windows, type of the filtering windows (i.e., Raised Cosine, Hamming, Flat-Top, Blackman, etc.), reporting rates, by subjecting PMUs to known waveforms.
- *Application tests* are conducted to evaluate the PMU performance under faults and other disturbances in power systems. At this stage of testing, the performance of the stand-alone PMU device is evaluated when PMU is exposed to a set of input waveforms from the field. Phasor estimates and frequency measurements of the Device Under Test (DUT) are compared with those estimated from the reference PMU (with the very accurate algorithm). The accuracy of the reference algorithm

is confirmed in the calibration laboratory to ensure applicability of the developed algorithm to serve as a valid reference even under the unknown inputs.

- *System end-to-end tests* are conducted by feeding the end-use synchrophasor applications with the measurements from real PMUs and quantify the impact of measurement errors on the application of interest.
- Finally, purely data-driven technique, namely Principal Component Pursuit is used for the correction and completion of the synchrophasor data blocks, and its application in the modal analyzes is verified.

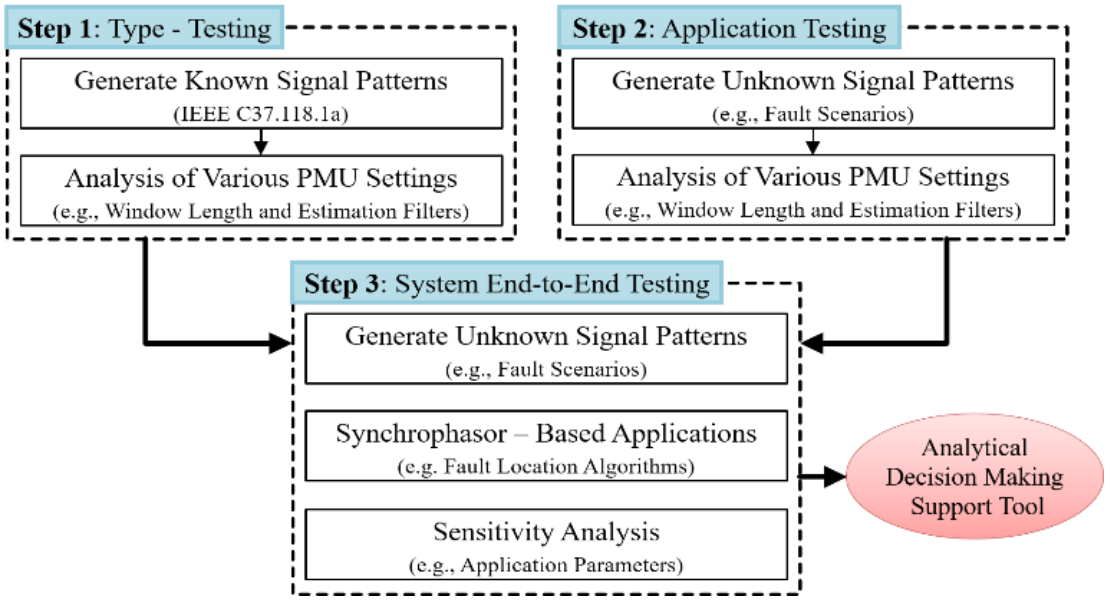

Figure 1. Proposed architecture for multilevel testing of synchrophasor systems.

1.4 Dissertation Organization

This dissertation is organized as follows. In Section 2, a background of the synchrophasor technology is introduced, including the basic synchrophasor concepts and the phasor estimation challenges. Furthermore, brief overview of the typical synchrophasor system infrastructure and its devices is reviewed.

Section 3 focuses on the performance evaluation of the standalone PMUs according to the IEEE standard requirements. Detailed hardware and software solution for the calibration test set is provided. Issues with the standard requirements are recognized and the novel metrics for the performance evaluation are introduced.

In Section 4, the concepts of the *application* and *system end-to-end testing* in the hardware environment are elaborated. We explored the performance of different PMUs when exposed to the waveforms generated from the system under disturbance, specifically faults in the transmission network. Risk assessment of the purely synchrophasor fault – location algorithm is studied and quantified.

Next, Section 5 studies are focused on the risk assessment of the PMU data in the modal analyses in the simulation environment. The Matrix Pencil Method for the modal extraction was presented and we quantified the impact of the various PMU data issues on the application outcome. Different quality data issues are applied to the input data (i.e. PMU frequency measurements), among which are noise, un-updated data and outliers. In this section, we also introduced the Principal Component Pursuit technique for the data correction and applied it as a pre-screening tool for the modal extraction.

The conclusions of the dissertation and the main contributions are given in Section 6.

2. BACKGROUND

2.1. Introduction

The concept of phasor representation of alternate current and voltage signals was introduced in early 1893. by Charles Proteus Steinmetz [70]. Almost a century later, in 1992 at Virginia Tech, the idea of the complex representation of the electrical waves evolved and the first Phasor Measurement Unit (PMU) prototype was developed. The PMU is capable of calculating the voltage/current waveform phasors that are synchronized to the absolute time reference provided by the Global Positioning System (GPS). Since synchrophasor technology was introduced, developed, and partly integrated into the electric power systems, it has shown great advantages in control and monitoring of the grid, detection of network problems in early stages, maximization of power system security, and reliability. Extensive research efforts on the use of PMUs in power systems have been reported in the literature, particularly on Wide Area Measurement Systems (WAMS) for monitoring, control, and protection applications. PMUs now serve as the backbone of various critical applications in the electric industry, such as state estimation, fault detection, remedial actions, and wide area monitoring [3]-[8].

Issues such as inconsistent accuracy due to the use of different synchrophasor estimation methods in various PMU products, and difficulties in the integration of proprietary software and hardware features of different products from different vendors, hindered the wide implementation of synchrophasor technology [9]. Such a wide range of phasor estimation techniques and resulting performance differences necessitate quality assessment, compliance analysis, calibration, and field-testing.

2.2. Phasors and Phasor Estimation Challenges

In an ideal scenario when power system is in normal operation mode, voltage/current waveforms appear as a pure sinusoidal wave with a frequency of 60 Hz (or 50 Hz). A normal operation implies all electricity demand being supplied with stable frequency, and transmission line flows are within the desirable margins. Using the phasor representation concept, a pure sinusoidal time dependent signal in (2.1) can be represented with the unique constant number, called phasor, as in (2.2).

$$a(t) = A_m \cos(\omega t + \theta) = A_m \cos(2\pi f_0 t + \theta) \tag{2.1}$$

$$\bar{A} = \frac{A_m}{\sqrt{2}}(\cos\theta + j\sin\theta) = Ae^{i\theta} \tag{2.2}$$

where, θ is the phase angle of the sine waveform defined relative to a time reference signified by $t=0$, and magnitude A is the root mean square (rms) value of the signal in (2.1) with the amplitude A_m. Sinusoidal signal with phase angle θ and its phasor representation are depicted in Fig. 2. Note that the nominal signal frequency (f_0) is not part of the phasor representation.

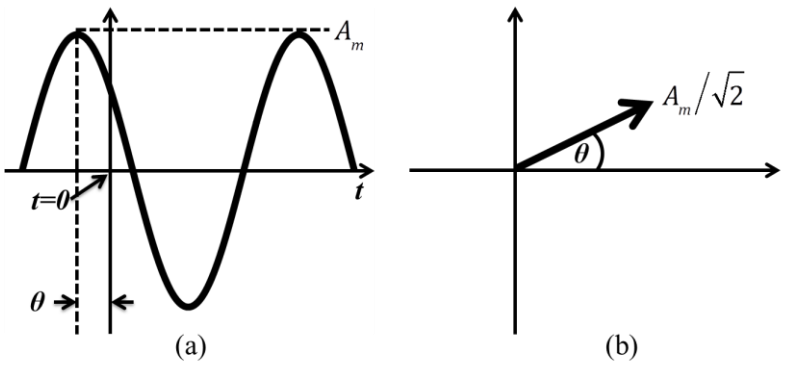

Figure 2. Sinusoidal waveform (a) and its phasor representation (b).

Phasor representation indicates that signal continuously residues stationary and that its complaint has constant value. However, power system frequency may vary from its nominal value during disturbances, faults, and transients, while voltage and current waveforms can suffer from different types of distortions, e.g., harmonics, amplitude and phase distortions, modulations [41]. In such circumstances, assumption made regarding the pure stationary sinusoidal signals is not valid any longer and the concept of phasor representation needs to be modified.

In general case when the amplitude and the signal frequency are the functions of time, we can define the function $g = f - f_0$ where f_0 is the nominal signal frequency (50 or 60 Hz) and g is the difference between actual and nominal frequency. In this case, the equation (2.1) can be rewritten as follows:

$$a(t) = A_m(t)\cos\left(2\pi\int f dt + \theta\right) = A_m(t)\cos\left(2\pi f_0 t + \left(2\pi\int g dt + \theta\right)\right) \tag{2.3}$$

Phasor representation of this waveform is then given in (2.4).

$$\bar{A} = \frac{A_m(t)}{\sqrt{2}} e^{j2\pi\int g dt + \theta} \tag{2.4}$$

The most common practice for phasor estimation in commercial PMUs is to apply the Discrete Fourier Transform (DFT) technique. The DFT deconstructs a finite number of time domain waveform samples into the frequency domain representation that comprises of voltage/current spikes at varying frequencies.

$$A_{(k)} = \frac{\sqrt{2}}{N}\sum_{n=0}^{N-1} a_{(k+n)} e^{-j\frac{2\pi n}{N}} \tag{2.5}$$

where *N* represents the number of samples in data window and *k* denotes the first sample of the data set. The transformation in the frequency domain may be done using an optimized version of the DFT, the Fast Fourier Transformation (FFT), after which the pure sinusoidal signal has only one spike at the nominal frequency when sampling frequency is an integer multiplication of the 60 Hz. FFT assumes that the endpoints of the waveform are interpreted as they are connected together (circular topologies) and that the acquisition interval is equal to an integer number of signal periods.

When the frequency differs from the nominal value, the sampling frequency is no longer the integer multiplication of the nominal frequency; hence, artificial discontinuities or sharp changes will be observed in the measured signals, the consequence of which is a phenomenon called *specter leakages*. It appears as the energy is "*leaking*" from one frequency into another and FFT is not capable to accurately estimate the parameters of the signal in frequency domain. In the meantime, there exist many techniques in digital signal processing domain to deal with this phenomenon, example of which are various windowing techniques used to minimize the effect of errors introduced by the frequency deviations [71]. However, there is no perfect filter that can make estimation of all parameters (i.e. frequency, magnitude, and phase) equally accurate, and using the proposed testing framework impact of various filter parameters on the estimation accuracy is studied in this dissertation.

2.3. Synchrophasor System

A typical synchrophasor system consists of several layers as depicted in Fig. 3:

- *Substation layer*, including timing references created using GPS/GNSS receivers, PMUs and a PDC (in the case there are multiple PMUs) that will merge the measurement streams sent from the substation.
- *Communication layer*, connecting the equipment in substations, as well as between substations and control center allowing the measurement streams from substations to be sent to PDCs located at the Control Center.
- *Control Center layer*, receiving the streams from substations and merging them through a PDC that makes them available to the decision making environment where the application software, data management and visualization tools are located, and forwards them to the next layer.
- *Regional System Operator* or an *Independent System Operator layer*, receiving the synchrophasor measurement streams from the Control Centers PDCs, and aligning them based on the reported time tags and combining them in a unique stream of measurements that represent the wide area system dynamics, which is further processed and used in various wide-area grid applications.

The described synchrophasor system is quite complex with multiple components that can influence the performance and accuracy of the applications and it signifies a need for multilevel testing and evaluation of the measurements.

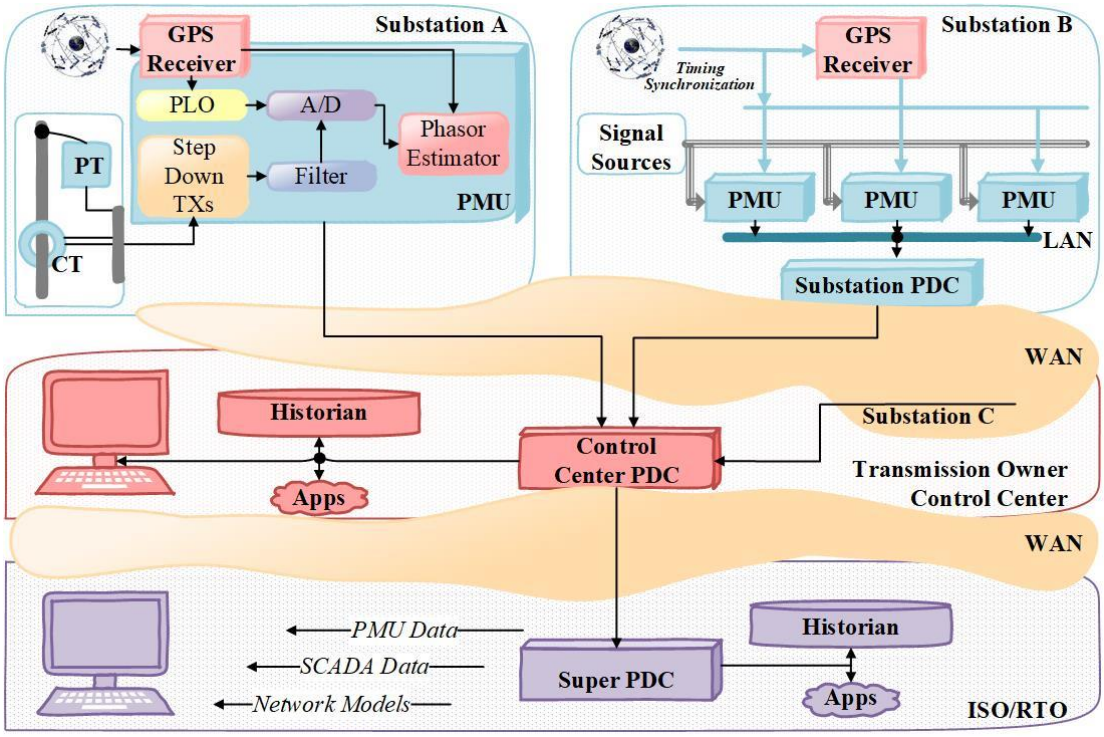

Figure 3. Typical configuration of the synchrophasor systems.

2.4. Phasor Measurement Unit (PMU)

Housing the estimation algorithms, PMUs are devices capable of providing the synchrophasors of the voltage and/or current electrical signals, as well as frequency and the rate of change of frequency of the system. Synchrophasor is a term that designates time-imprinted phasor with associated time tag synchronized to Universal Coordinate Time (UTC) at the nominal system frequency. All measurements that belong to the exact same point of time can be time-aligned and provide a big picture of the entire system or interconnected region. Depending on the hardware and technology, precise and accurate timing reference is provided to PMUs directly using the Global Positioning System (GPS)

signal or using the IRIG-B signal generated by separate GPS receivers. Typical configuration of the PMU is depicted in Fig. 4.

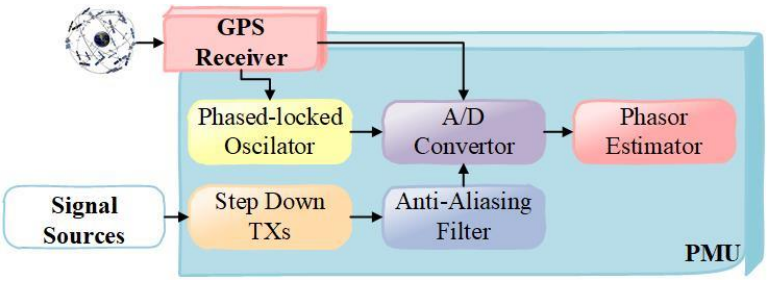

Figure 4. Typical PMU configuration.

Nominal voltage/current signals (signal sources) provided to PMU device are not specified in any standard, though typical value for the voltage is 70 V_{rms} while for current signal is 2 or 5 A_{rms}. However, these values are still too high to be directly digitally sample with an analog-to-digital converter (ADC); thus, each PMU device has smaller step-down transformers. Before signal are converted to the digital values, stepped-down inputs pass the anti-aliasing filters that aid in the selection of the fundamental frequency component that is desired for measurement. Next, ADC digitally sampling point-on-wave values, that are used by the signal processor (phasor estimator) for estimating the phasor values of the input signals.

3. CONFORMANCE OF THE SINGLE PHASOR MEASUREMENT UNIT TO THE IEEE STANDARD SPECIFICATION*

3.1. IEEE Standard Requirements

According to the IEEE standard C37 118.1, each device that is capable of providing GPS synchronized measurements has to undergo various test scenarios while being calibrated. The tests can be generally categorized into steady state or dynamic tests as specified in the IEEE C37.118.1, and as shown in Table 1. Further, two performance classes of PMUs, namely P and M, are defined where the P-class is intended for protection applications demanding fast measurement response time, while the M performance class is utilized in applications that require high measurement accuracy.

During the steady state tests, PMUs are exposed to various *type test* scenarios where all variables are kept unchanged during each test and the measurements are captured according to the standard procedure [13]. Such static *type tests* include performance evaluation of PMUs over a range of frequency values, voltage/current amplitudes as well as influence of harmonic and inter-harmonic interferences. Dynamic *type tests* involve testing PMUs with the modulated signals, checking their performance during the step occurrence in amplitude and angle, as well as testing the PMU response to the frequency ramp events. Dynamic tests are devised to account for the dynamic signal changes that a PMU would face when applied in a real-world power grid. As a part of the standard requirements, latency of a PMU device has to be measured as well.

* Part of this section is reprinted with permission from "Probabilistic Assessment of PMU Integrity for Planning of Periodic Maintenance and Testing" by T. Becejac, P. Dehghanian, and M. Kezunovic, Oct. 2016 IEEE Conference on Probabilistic Methods Applied to Power Systems, ©2016 IEEE, with permission from IEEE.

Table 1. PMU steady state and dynamic standard *type tests.*

Test Category	Test Name	Input Range	
		P Class	M Class
Steady Tests	Magnitude Sweeping	0.8-2 pu	0.1-2 pu
	Frequency Sweeping	±2Hz	±2Hz, or ±5Hz
	Harmonic Distortion	1% each harmonic up to 50th	10% each harmonic up to 50th
	Latency	1000 consecutive messages	1000 consecutive messages
	Out-of-Band Interference	N/A	Depending on reporting frequency, harmonic infiltration from 10Hz to twice nominal frequency; interfering signal 10% of signal magnitude
Dynamic Tests	Amplitude Modulation	Modulation frequency from 0.1Hz to 2Hz Modulation level 0.1	Modulation frequency from 0.1Hz to 5Hz Modulation level 0.1
	Angle Modulation		
	Frequency Ramp	±1Hz/s, frequency range within ±2Hz	±1Hz/s, frequency range within ±5Hz
	Magnitude Step Change	±10% Step	
	Angle Step Change	±pi/18 radians	

Mathematical representation of the input signals during the dynamic tests, namely modulation, ramping and step changes, as well as the frequency, frequency deviation and the rate of change of frequency (ROCOF) during those tests, are given respectively by, Equation (3.1), Equation (3.2), and Equation (3.3):

$$
\begin{aligned}
A_a &= A_m\left[1+k_x\cos\left(\omega t\right)\right]\times\cos\left[\omega_0 t+k_a\cos\left(\omega t-\pi\right)\right]\\
A_b &= A_m\left[1+k_x\cos\left(\omega t\right)\right]\times\cos\left[\omega_0 t-2\pi/3+k_a\cos\left(\omega t-\pi\right)\right]\\
A_c &= A_m\left[1+k_x\cos\left(\omega t\right)\right]\times\cos\left[\omega_0 t+2\pi/3+k_a\cos\left(\omega t-\pi\right)\right]\\
f\left(nT\right) &= \frac{\omega_0}{2\pi}-k_a\left(\frac{\omega}{2\pi}\right)\sin\left(\omega nT-\pi\right)\\
\Delta f\left(nT\right) &= -k_a\left(\frac{\omega}{2\pi}\right)\sin\left(\omega nT-\pi\right)\\
ROCOF\left(nT\right) &= -k_a\left(\frac{\omega^2}{2\pi}\right)\cos\left(\omega nT-\pi\right)
\end{aligned}
\tag{3.1}
$$

where A_m is the amplitude of the input signal, ω_0 is the nominal power system frequency, ω is the modulation frequency in radians/s, k_x is the amplitude modulation factor, and k_a is the phase angle modulation factor. $t = nT$ represents the reporting time tags, where T is equal to the phasor reporting interval.

$$
\begin{aligned}
A_a &= A_m\cos\left[\omega_0 t+\pi R_f t^2\right]\\
A_b &= A_m\cos\left[\omega_0 t-2\pi/3+\pi R_f t^2\right]\\
A_c &= A_m\cos\left[\omega_0 t+2\pi/3+\pi R_f t^2\right]\\
f\left(nT\right) &= \frac{\omega_0}{2\pi}+\left(R_f\right)\left(nT\right)\\
\Delta f\left(nT\right) &= \left(R_f\right)\left(nT\right)\\
ROCOF(nT) &= R_f
\end{aligned}
\tag{3.2}
$$

A_m is the amplitude of the input signal, ω_0 is the nominal power system frequency and R_f is the frequency ramp rate given is Hz/s. $t = nT$ represents the reporting time tags, where T is equal to the phasor reporting interval.

$$
\begin{aligned}
A_a &= A_m\left[1+k_x f_1(t)\right]\times\cos\left[\omega_0 t + k_a f_1(t)\right] \\
A_b &= A_m\left[1+k_x f_1(t)\right]\times\cos\left[\omega_0 t - 2\pi/3 + k_a f_1(t)\right] \\
A_c &= A_m\left[1+k_x f_1(t)\right]\times\cos\left[\omega_0 t + 2\pi/3 + k_a f_1(t)\right]
\end{aligned} \tag{3.3}
$$

where A_m is the amplitude of the input signal, ω_0 is the nominal power system frequency, $f_1(t)$ is a unit step function, k_x is the magnitude step size and k_a phase step size.

Metrics for PMU performance evaluation according to the IEEE standard are: Total Vector Error (TVE), Frequency Error (FE), and Rate of Change of Frequency Error (RFE). TVE is defined as the deviation of the estimated phasor from the reference true value, and is calculated as follows:

$$
TVE = \sqrt{\frac{\left(A_r - A_r^t\right)^2 + \left(A_i - A_i^t\right)^2}{\left(A_r^t\right)^2 + \left(A_i^t\right)^2}} \times 100\% \tag{3.4}
$$

where subscript *r* stands for real, and *i* for imaginary parts of the phasor, and superscript *t* designates the true value of the input signal for each reported measurement; A_r and A_i are, respectively, the real and imaginary parts of PMU estimated phasor. TVE contains errors in both magnitude and phase angles. The FE and RFE are defined as absolute values of the estimated frequency (Hz) and ROCOF (Hz/s) deviation from the true values at the same time instant, given in (3.5) and (3.6):

$$
FE = \left| f^t - f \right| \tag{3.5}
$$

$$
RFE = \left| \left(df/dt\right)^t - \left(df/dt\right) \right| \tag{3.6}
$$

The PMU performance conformity under the aforementioned static and dynamic conditions needs to be ensured during the life-cycle of the PMUs and, hence, periodic

maintenance and testing of the PMUs can help checking the desired functionality over time. A standard-compliant PMU should meet all the requirements, at least for one class, for the *type test* steady state and dynamic performance.

3.2. Development of the Facility for the Synchrophasor Unit Assessment

3.2.1. Hardware Architecture of the Testing Facility

In this effort, a unique PMU calibration lab is constructed to execute standardized PMU acceptance tests according to IEEE and IEC standards, such as the IEEE C37.118.1a among others. PMU test platform is developed to verify the performance of PMU device exposed to *type tests*. In particular, the *type test* implementation is done based on mathematical signal models defined in the standard using very accurate signal generators to replay the generated waveforms into the device under test. The measurements acquired from the device under test are compared against the true phasor values derived from the signal model. In order to implement the PMU *type tests*, a synchrophasor testing and calibration set-up is developed using the National Instrument (NI) PXIe-1062Q Chassis equipped with the following PXI boards: (a) PXIe-8105n 2.0 GHz Dual Core controller; (b) PXI-6683H Synchronization module, and (c) PXI-7854R FPGA-based IO module; all controlled in graphical system design software platform, LabVIEW. Full testing of PMUs on 50/60Hz for each reporting rate defined in the IEEE standard and considering various PMU communication protocols is automated. Functional architecture of the implemented test set-up is depicted in Fig. 5 and the actual implementation of such testing environment is illustrated in Fig. 6.

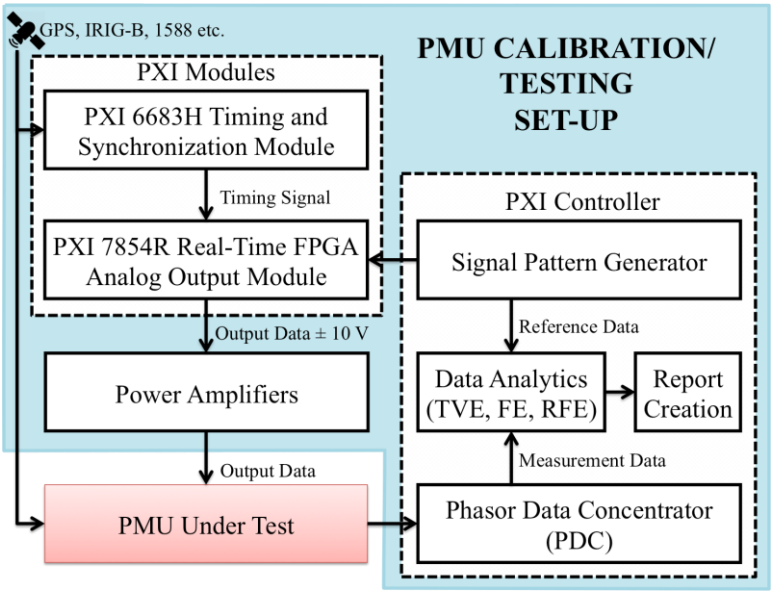

Figure 5. Functional diagram of the PMU calibration/testing set up.

Using the PXI controller, signal pattern generator calculates the waveform parameters according to the IEEE C37.118.1 std. definitions [10]. Parameters are then transferred to the Virthex-5 LX110 FPGA board and six voltage and current waveforms are generated using the PXI-7854R analog I/O module equipped with eight 16-bit digital-to-analog converters (DACs). Generated waveforms are low-level signals (±10V) with a sampling rate controlled with 40MHz clock that are amplified to a given nominal value ($70V_{rms}$ for three phase voltage and $5A_{rms}$ for the current signals).

Synchronization and time alignment with respect to the Coordinate Universal Time (UTC) of all modules are ensured in the calibration system through the PXI 6683H module with the accuracy of higher than 100 ns. PMU measurements are then directed over Ethernet or Serial communication ports back to the PXI system, where they are parsed in a local PDC developed on the PXI controller. Received measurements are compared

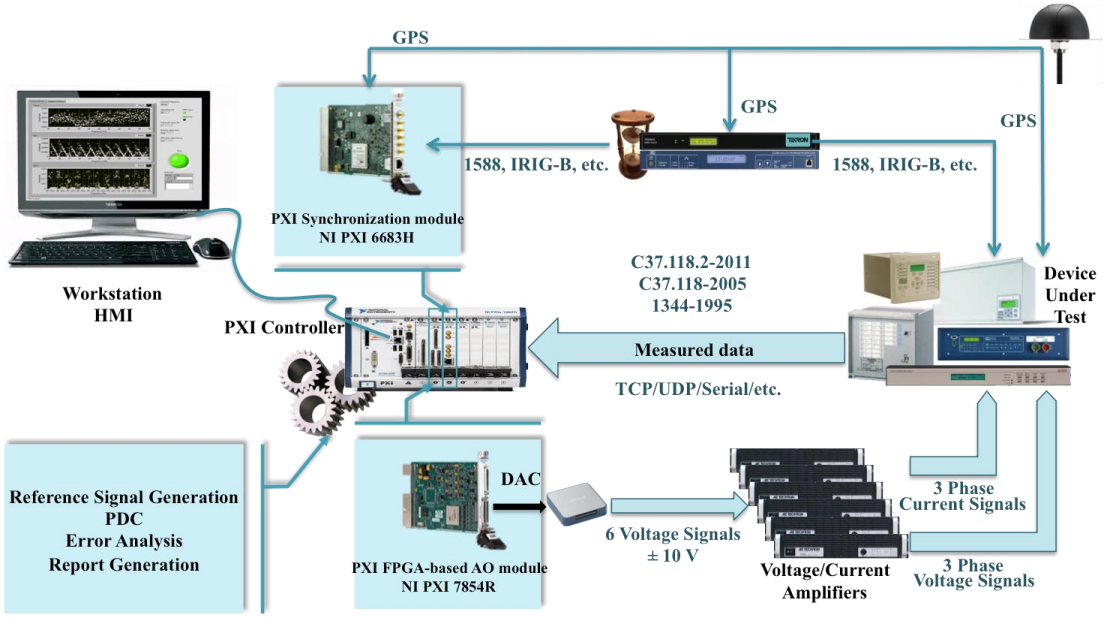

Figure 6. The developed PMU calibration and automated testing set up. Adapted with permission from[111]

against the reference values and the TVE, FE and RFE performance metrics are calculated. Values of the reference phasors are compensated, through compensation factors, to take into account the influence of the hardware response (signal generator and power amplifiers) and correspondingly the induced errors.

3.2.2. Quality Assessment of the Calibration Testing Facility

To ensure the validity of the testing and calibration procedure, systematic characterization of the testing hardware and software modules is carried out in all stages of testing. Overall accuracy of the calibration system depends on (a) the accuracy and stability of the timing reference, and (b) the ability to curtail the angle and magnitude uncertainties in the generated waveforms. Impact of uncertainties in the developed signal

generation and synchronization modules is carefully studied and the results are presented as follows:

Timing Reference: with the onboard temperature-compensated crystal oscillator (TCXO) that can be disciplined with the GPS source, 6683H module allows the long-term stability of the real time calibration system. Quality of the timing reference is evaluated by measuring the maximum synchronization error with respect to the UTC reference over a 24-hour period. Fig. 7 reflects the maximum uncertainty and the corresponding mean and standard deviation. It can be seen that the maximum uncertainty over the entire range of measurements is limited to 60 ns, which in turn, causes a maximum phase angle error of less than 1.3 mdeg. for the reference system.

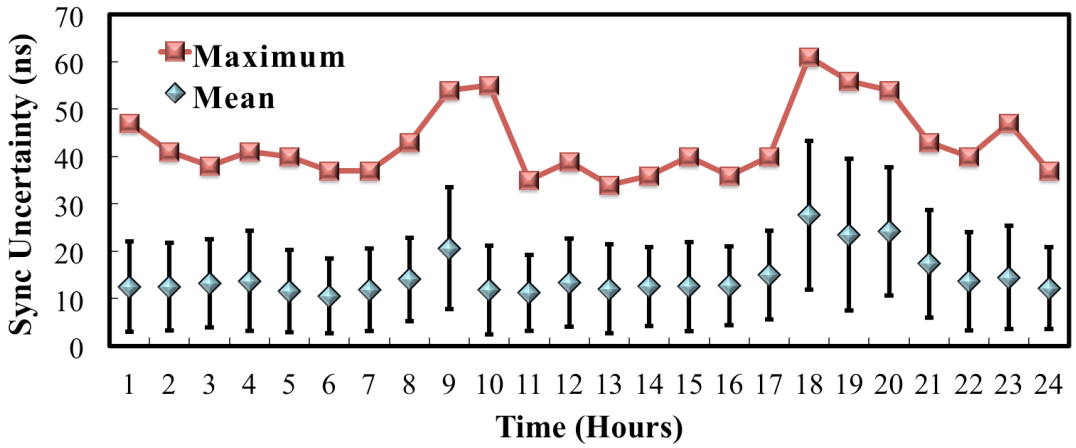

Figure 7. Synchronization error of the calibration system over a 24-hour period.

Signal Generation: two metrics are used to assess the power quality of the generated waveforms: (a) total harmonic distortion (THD) over the first 50 harmonics, and

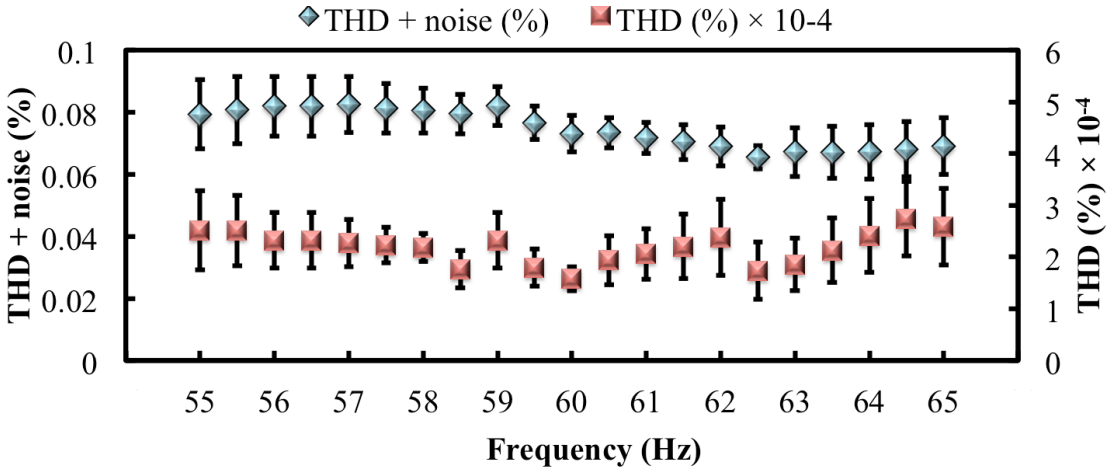

Figure 8. Total Harmonic Distortion (THD) over a frequency range of 55-65 Hz.

(b) signal to noise and distortion ratio (SINAD). Measurements are taken using the very accurate oscilloscope [72] equipped with a software for power quality assessments and interfaced with the testing software module where the metrics are assessed. For THD evaluation, the nominal frequency is swept in the range from 55 to 65 Hz (for nominal system frequency of 60Hz), while keeping the voltage/current values at nominal ($70V_{rms}/5A_{rms}$, respectively). According to Fig. 8, observations revealed that the THD is independent of the nominal frequency and is limited to 4e-4%, which is two orders of magnitude better than specified in the standard. Furthermore, the quality of the generated signals is evaluated by measuring the THD with noise. Similarly, the results confirmed the accuracy of the designed calibration set-up for PMU testing, and that the impact of the THD is negligible.

Next, the SINAD metric is calculated as presented in Fig. 9. One can see in Fig. 9 that the SINAD keeps around 70 dB for all tests performed, but the harmonic distortion

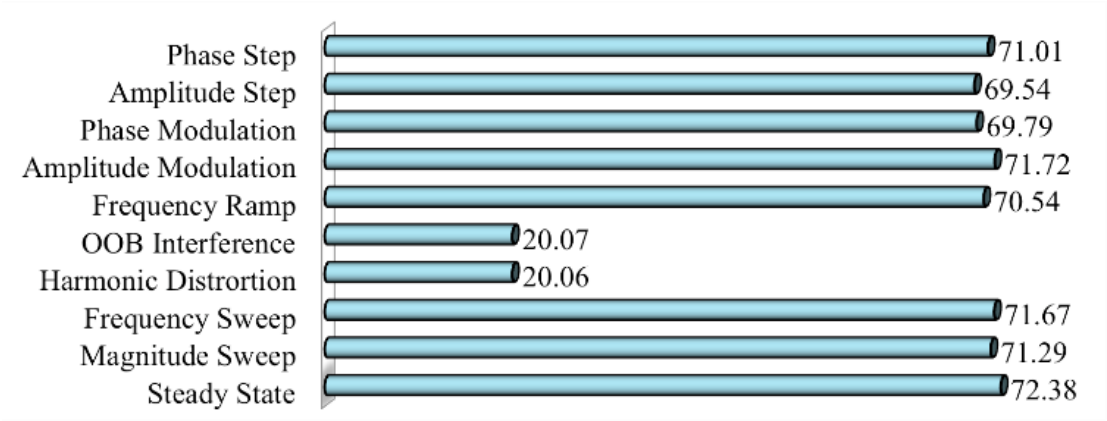

Figure 9. Signal to noise distortion ratio (SINAD) (dB) over the set of *type tests* defined in the IEEE standard for M-class PMUs.

and out of band (OOB) interference tests where the interfering components with magnitude equal to 10% of the fundamental are added to the fundamental component.

Magnitude and Phase Angle Error: As mentioned before, the reference synchrophasors are derived from the mathematical models defined in the IEEE C37.118.1 std. [10]. The "true" values are compared against the oscilloscope measurements and the offsets, resulting from the DAC and power amplifier responses to generated signals, are compensated in the calibration system software module.

3.3. Testing Procedure Implementation and Numerical Results

3.3.1. PMU Under Test: Settings and Phasor Estimation Functions

Some of the PMU devices are equipped with various options for the estimation algorithms (in both P and M performance classes). The options include different windowing functions and filters, adaptive tuning capability of the estimation algorithm, number of cycles used for calculation of the phasors (WL), reporting rate, and are provided

to user as the optional parameters to be defined and used within a given PMU device. Window function is a mathematical function used to minimize the effect of the specter leakage and improve the signal quality before applying the DFT by removing the corrupting influence of noise, harmonics, modulation, etc.

The filters used in the PMUs may seriously affect the accuracy of the output estimate by introducing magnitude attenuation and phase offset [71]. In this study, the PMU under test has a built-in setting allowing the user to select between four windowing functions, namely the Raised-Cosine, Flat-Top, Hamming, and Blackman. The frequency-domain magnitude characteristics (dB) of four window functions are demonstrated in Fig. 10. The window length (WL) is set to 6 cycles of the nominal frequency (100ms). Each window function consists of the main-lobe and several side-lobes, characteristics (width

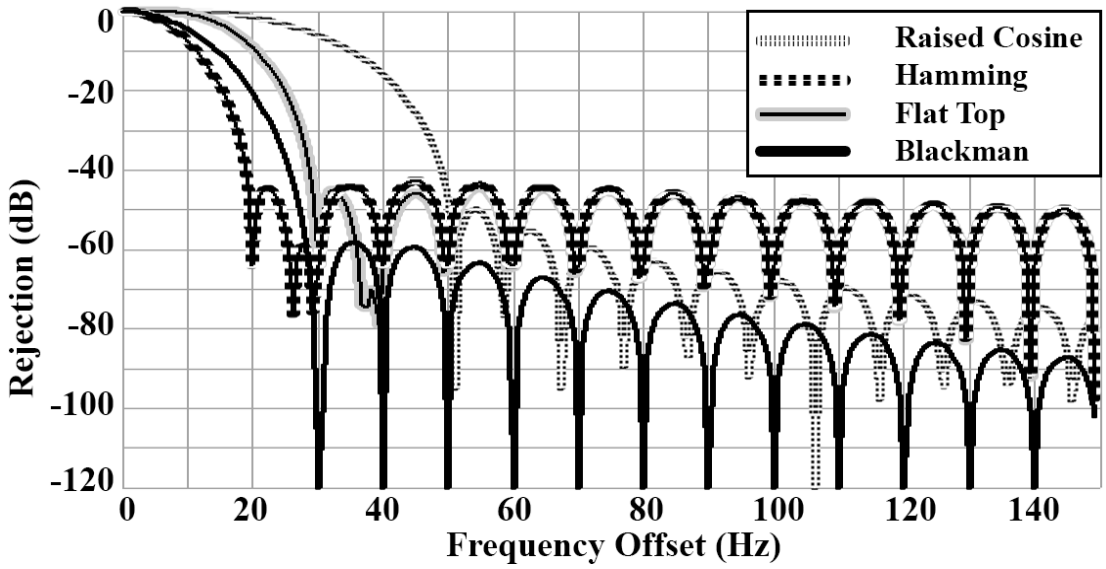

Figure 10. Magnitude response (dB) of different window functions in the tested PMU.

of the main-lobe, roll-off of the side-lobes, attenuation factor, etc.), which determine the filter performance. Selecting the most appropriate settings for synchrophasor measurement depends on the target end-use application, which involves a compromise on the filter characteristic (e.g. bandwidth, the amplitude accuracy, and the decrease rate of the spectral leakage into other frequencies).

The Raised-Cosine and Hamming window functions, both of the Hamming family of functions, are constructed by multiplying a rectangular window by one period of a cosine signal, offering it two degrees of freedom. General definition of the Hamming family of functions is given in (3.7).

$$w(n) = \alpha + 2\beta \cos\left(\frac{2\pi n}{N}\right), n = -\frac{N-1}{2}, ..., -1, 0, 1, ..., \frac{N-1}{2} \tag{3.7}$$

where, N is the length of the window function in samples. Raised-Cosine function is characterized by the parameters $\alpha = 0.5$ and $\beta = 0.25$, while they are $\alpha = 25/46 \approx 0.54$ and $\beta = (1- \alpha)/2 \approx 0.23$ for the Hamming functions.

Adding one more degree of freedom compared to the Hamming family results in the family of Blackman windows.

$$w(n) = \alpha_0 + \alpha_1 \cos\left(\frac{2\pi n}{N}\right) + \alpha_2 \cos\left(2\frac{2\pi n}{N}\right) \tag{3.8}$$

Classic Blackman window is defined with $\alpha_0 = 0.42$, $\alpha_1 = 0.50$, and $\alpha_2 = 0.08$.

The Flat-Top window functions are basically the sum of few cosine terms designed to have smooth and flat filtering characteristics in frequency domain, especially to determine the amplitude of the signal with excellent precision. However, they typically lack a reasonably good frequency resolution.

Additionally, WL also plays an important role on the frequency response of the functions. The PMU device under test has an option to choose WL from set of {1,2,3,4,5,6} cycles of fundamental frequency. Fig. 11 depicts the influence of the WL on the frequency response of the Blackman window function taking values in the set {1, 2, 4, 6}. As *N* increases, the main-lobe narrows, providing a better frequency resolution with no impact on the side-lobes but at the same time introduces the additional delay in estimate. One can also see that decreasing the WL degrades the estimation accuracy while the phasor estimates are available faster in time.

Furthermore, the reporting rate of the synchrophasor estimates is selected by taking values from a set of {10,12,15,20,30,60} frames per second (fps) as required by the IEEE standard when considering a nominal frequency of 60 Hz. Depending on the selected

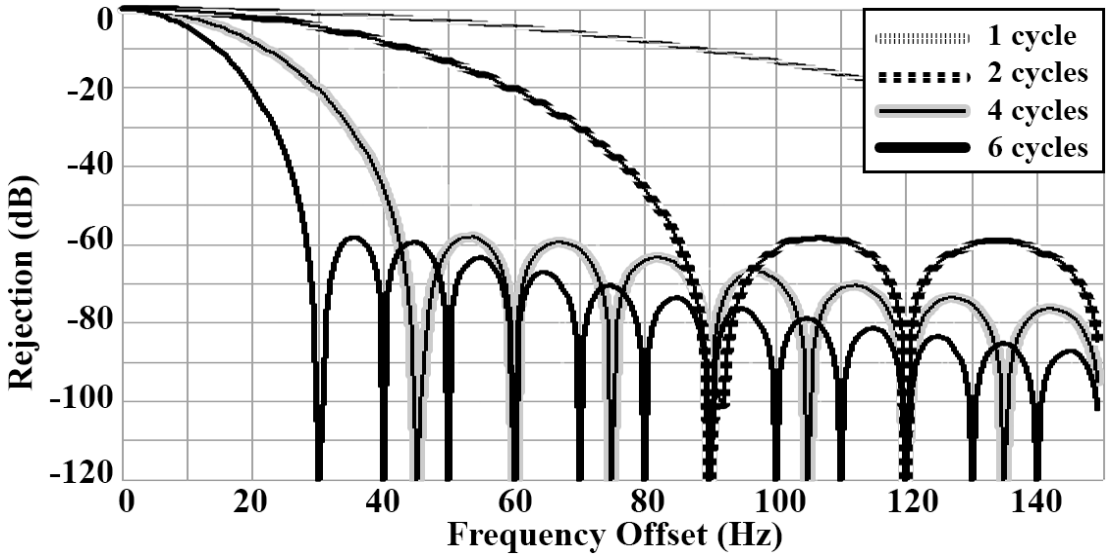

Figure 11. Magnitude response (dB) of the Blackman window function, when WL changes values from 1-6 cycles.

value, coefficients of the filter functions vary which in return influence the overall performance of the PMU. Correct choice of such parameters is crucial for an accurate synchrophasor measurement. Once again, trade-offs between the required accuracy and the estimation speed should be made depending on the target application of interest.

3.3.2. Testing Results

Full set of static and dynamic *type tests* according to the IEEE C37.118.1 Std. [12] and following the test procedures defined in the IEEE Test Suit Specification [13] is carried out considering various settings for the PMU under test. In order to assess the impact of different settings, only one parameter was changed at a time while the rest remained unchanged. Fig. 12 illustrates the sample results of one static (i.e., out-of-band test) and Fig. 13 depicts the sample results of one dynamic *type test* (i.e., frequency ramping test). The selected settings of the PMU under test for the presented results in Fig. 12 and Fig. 13 are given in Table 2. PMU is evaluated applying the requirements for the M performance class. For the Out of Band (OOB) compliance test, frequency of the fundamental power signal is set equal to the system nominal frequency; and measurements are not evaluated in the "excluded frequency range", defined as the nominal frequency half of the reporting rate (i.e., 30-90 Hz). Frequency ramping compliance for the M-class

Table 2. Selected settings of the PMU under test.

Nominal Frequency (*Hz*)	60	**Window Length (*cycles of nominal frequency*)**	6
Reporting Rate (*frames per second*)	60	**Window Function**	Variable

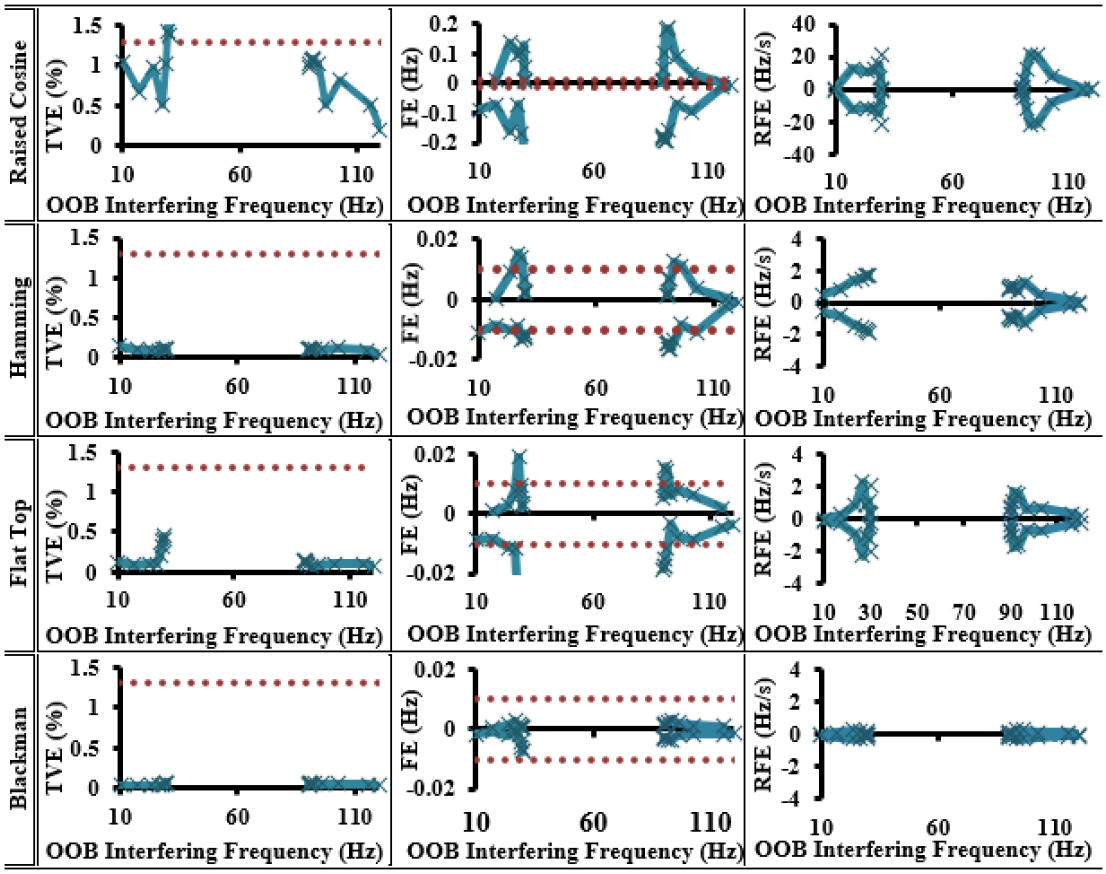

Figure 12. TVE, FE and RFE metrics for PMU performance assessment during the standard static *type test* (i.e., out-of-band test).

PMU is executed with the ramp of frequency applied to three phase balanced input signals in the range of ±5 Hz, with the rate of 1 Hz/s.

The TVE, FE and RFE metrics evaluated for four different window functions reveal a significant difference in their performance while exposed to test signals. The Raised-Cosine is attributed the worst performance in all the fulfilled tests, mainly due to its low frequency resolution and the lowest side-lobe attenuation. The Hamming window function revealed a better performance, but was still prone to off-nominal frequencies

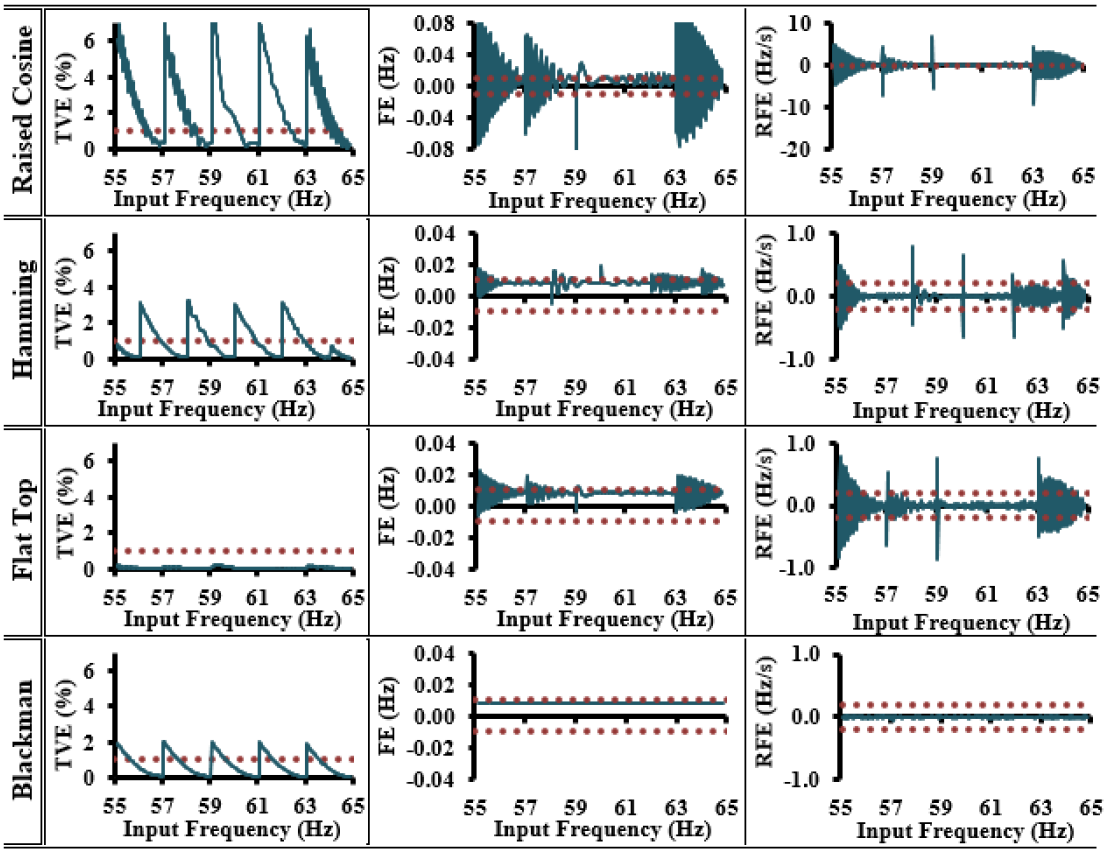

Figure 13. TVE, FE and RFE metrics for PMU performance assessment during the dynamic *type tests* (i.e., ramping frequency test).

during dynamic tests where it violated the desired estimation error. Flat Top windowing approach has the best comparative performance regarding the voltage magnitude and angle measurements during the static test. While measuring voltage vectors precisely, it can be seen that the error in measuring the frequency is higher using the Flat Top algorithm compared to the Blackman windowing function (Fig. 13). The reason for this observation is activation of the adaptive frequency tracking option for better estimation performance during the off-nominal frequency measurements. Consequently, the time offset is present

and the measurement of the frequency is not deemed accurate. On the other hand, the Blackman filtering approach has the best performance regarding the accurate measurements of the frequency, while the TVE is insignificantly above the allowed limits. In addition, even though the limits for the existing errors in the measurements of the ROCOF are not specified in the IEEE standard for all tests, it is worth to mention that among the different algorithms studied, the deviation is noticeable (Fig. 12 and Fig 13), and if this measurement is going to be used as the application input parameter, one should be careful in choosing an appropriate filter function.

From the results obtained in this testing stage, one can foresee that a synchrophasor-based fault location algorithm based on only voltage/current estimates will have the best performance and accuracy if the Flat-Top window function is implemented in the corresponding PMU. This hypothesis is verified in the next stages of the proposed testing framework.

3.4. Proposed Novel Assessment Metrics Beyond the Scope of the Standards*

3.4.1. Introduction - Why do we need them?

Some conditions that PMU under test is seeing during the evaluation according to the IEEE std., take into account wide range of signals (i.e. frequency range from 45 to 65 Hz, or voltage magnitude equal to 10% of nominal value). These conditions are not very likely to happen in real-world, nevertheless, are important to certify a PMU calibration procedure. Consequently, even if the PMU under test fails in one of such test conditions, that does not imply that the tested device is 100% unreliable while exposed to extreme signal conditions. Moreover, the outcome from the testing results can be even incorrect,

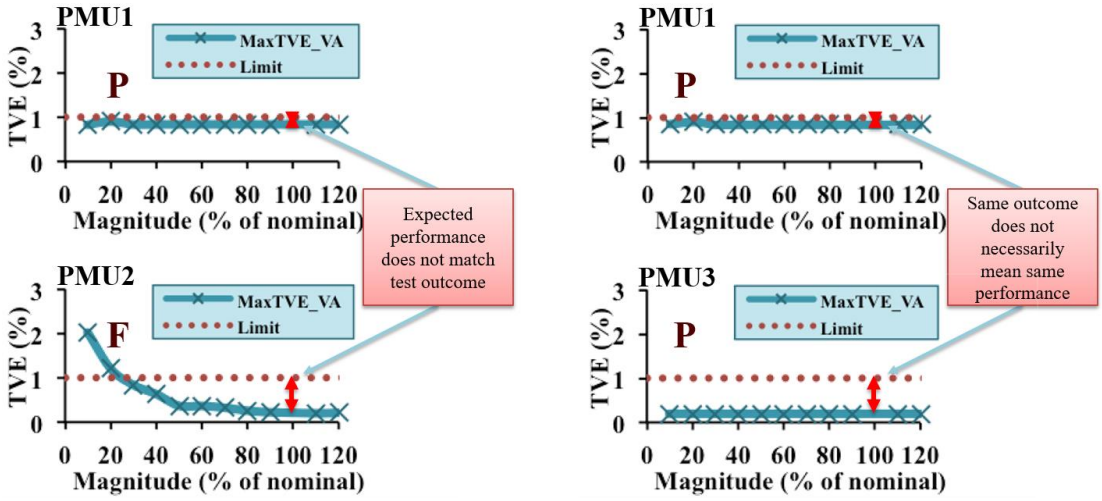

(a) (b)

Figure 14. Sample test results from three different PMUs showing the TVE trend during the magnitude sweep test.

and the PMU that does not comply with the standard could perform better in the filed environment, than the PMU that passed the test, as it can be seen from the sample results acquired during the calibration process of the commercial PMUs, Fig. 14a. Therefore, rather than solely a pass/failed status, we proposed new metric that highlights the success rate of all the test scenarios within a given *type test* and, as a result, it is a reliable measure to recognize sustainable problems in a PMU device and differentiate them from ephemeral conditions that might have led to a test failure.

Furthermore, the PMUs may pass all the static and dynamic tests, but the test results do not reflect the uncertainty level of the test acceptance. In other words, the original test results do not reveal how close the errors are to the standard thresholds, Fig.

14b, giving the incorrect imprint of the performance quality of different PMUs that are in compliance with the relevant standard.

In addition to standard *type test* practices that need to be performed during acceptance tests in the calibration lab environment and during the early commissioning stages of PMU deployment, testing is also desirable after the PMU has been in-service for a longer time to ensure that the PMU functionality over time still complies with the standard requirements.

By utilizing the standard *type test* results under both dynamic and static test conditions, and with the proposed new metrics, this dissertation offers a methodology to probabilistically evaluate the deterioration of PMU performance over time with regards to the standard requirements. The proposed probabilistic technique can quantitatively reveal the PMU response to various test performance thresholds specified by corresponding IEEE standards and the probability of specific failures to meet the standard requirements. The trends revealed by such probabilistic metrics could help in better planning the maintenance periods and future in-filed testing procedures.

Focusing on the applications, periodic testing of the PMUs under static and dynamic test conditions provides a database containing valuable information to the users on how the PMU measurements are affected over time in face of device wear and tear mechanism and environmental/operational conditions in real-world. Such information further can help in detecting possible origins of the measurement abnormalities and can be used to develop risk mitigation plans to constantly ensure the synchrophasor application trustworthiness.

3.4.2. PMU Vulnerability and Integrity Metrics: Definitions

Reports acquired during the *type tests* consist of all data resulting from PMU tests which allows extensive post-analysis of the collected results. A practical approach to evaluate the performance degradation of PMUs considering various steady state and dynamic test signals is devised. Conducting the standard tests on the PMUs, altogether PMU responses corresponding to each *type test* and sets of data in terms of error indicators are captured and recorded. The calculated error indicators are: Total Vector Error (TVE), Frequency Error (FE), and error in estimation of Rate of Change of Frequency (RFE). A normal probability distribution is then assigned to each test measurement error data as demonstrated in Fig. 15. The proposed approach is, however, generic enough to be

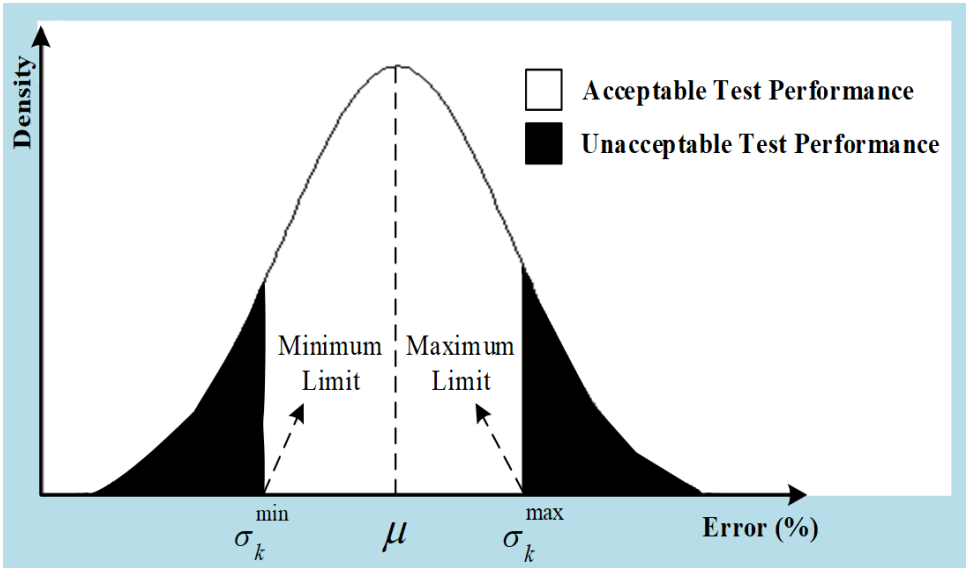

Figure 15. Probability distribution and the bands assigned to the error indicators for each PMU *type test* k. Adapted with permission form [111]

adopted with different types of probability distributions as data may dictate in various applications [111].

To proceed with the methodology, the minimum and maximum bands are adopted from the IEEE standard for each test signal. If one value x_i falls in the desirable margin, then it indicates a proper functionality of the PMU reflected by that specific test. Similarly, one new value of x_i may fall out of the desirable band leading to the test failure. In general, and according to the probability distribution assigned, the probability of a given test success can be calculated in (3.9)-(3.10), respectively for the steady state and dynamic conditions

$$P_{e_k,i}^{ST_k} = \int_{k=\sigma_{e_k}^{\min}}^{k=\sigma_{e_k}^{\max}} f_{e_k,i}^{ST_k}(k)dk \tag{3.9}$$

$$P_{e_k,i}^{DT_k} = \int_{k=\sigma_{e_k}^{\min}}^{k=\sigma_{e_k}^{\max}} f_{e_k,i}^{DT_k}(k)dk \tag{3.10}$$

Where the following nomenclature applies:

$P_{e_k,i}^{[.]_k}$ = Success probability of a *type test k* regarding the error indicator e_k for PMU *i* in the system.

e_k = Error indicator for test type *k* (i.e., TVE, FE, RFE).

ST_k = Steady-state *type test k.*

DT_k = Dynamic *type test k.*

$\sigma_{e_k}^{\min}$ = Minimum threshold for error indicator for test *k.*

$\sigma_{e_k}^{\max}$ = Maximum threshold for error indicator for test *k.*

$f_{e_k,i}^{[.]_k}(k)$ = Probability density function of an error indicator for *type test k* of PMU *i* in the system.

There are several error indicators for some PMU tests that all need to be in compliance with standard requirements. In order to be able to conclude a probabilistic measure for the success/failure of a given test on a PMU, equations (3.11)-(3.12) are proposed to integrate such indicators, where applicable, into one metric:

$$P_i^{ST_k} = \prod_{k=1}^{3} P_{e_k,i}^{ST_k} \quad e_k = \text{TVE, FE, RFE} \tag{3.11}$$

$$P_i^{DT_k} = \prod_{k=1}^{3} P_{e_k,i}^{DT_k} \; e_k = \text{TVE, FE, RFE} \tag{3.12}$$

Where, $P_i^{ST_k}$ and $P_i^{DT_k}$ are the success probability of the static and dynamic tests, respectively, considering all the required error indicators within the desirable thresholds.

In order to have an overall evaluation of the PMU performance robustness considering all the requisite static and dynamic tests, a probabilistic measure representing the integrity of the PMU *i* in terms of testing results in face of all the static and dynamic test conditions is suggested in (3.13).

$$P_i^{Integrity} = \left(\prod_{k=1}^{K} P_i^{ST_k} \right) \times \left(\prod_{k'=1}^{K'} P_i^{DT_{k'}} \right) \tag{3.13}$$

In which *K* and *K'* represent the sets of static and dynamic tests, respectively. Observations on the $P_i^{Integrity}$ using the proposed in-field tests over time show how the PMU *type test* errors are moving with respect to the desirable thresholds representing the

degradation of the PMU measurements as the time goes on. The trend on such observations could also help better plan for periodic maintenance over the PMU life-cycle as needed.

Even though PMUs may pass the standard tests, it may be desirable for the user to know how far the measurement errors corresponding to various tests are from the desirable standard thresholds. The equation (3.14) indicates a probabilistic metric for the distance of the reported error mean values from the desirable standard thresholds.

$$\eta_{e_k,i}^{[.]_k} = \frac{1}{n}\sum_{n=1}^{N}\left(\sigma_{e_k}^{\max} - \left|e_{k,n}\right|\right) \tag{3.14}$$

where, $\eta_{e_k,i}^{[.]_k}$ is the probabilistic metric representing the distance between the mean error value and the maximum standard threshold; *N* is the total number of error observations for a given *type test k*.

This metric is useful in trying to understand how reliable a given PMU is with regards to a given test and what adjustments need to be made and how fast. That is, it can differentiate various PMUs that need periodic maintenance and troubleshooting by knowing which test requirements are more likely to cross the standard requirements over time.

3.4.3. Testing Results

The proposed technique for PMU in-field testing is applied to several PMUs from various manufacturers with different operational characteristics and settings. Sample test results on a given PMU are presented in Fig. 16 using the aforementioned calibration test set. Various PMUs were exposed to different test signals and the performance of each

product was thoroughly analyzed. As can be seen in Fig. 16, one of the PMU under test has failed most of the tests (e.g., voltage magnitude sweep, frequency sweep, out-of-band interfering frequency) while it has passed only one (i.e., harmonic distortion).

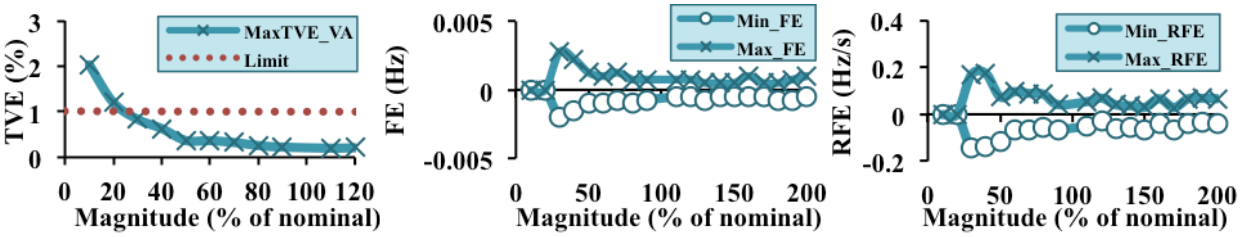

(a) voltage magnitude sweeping test

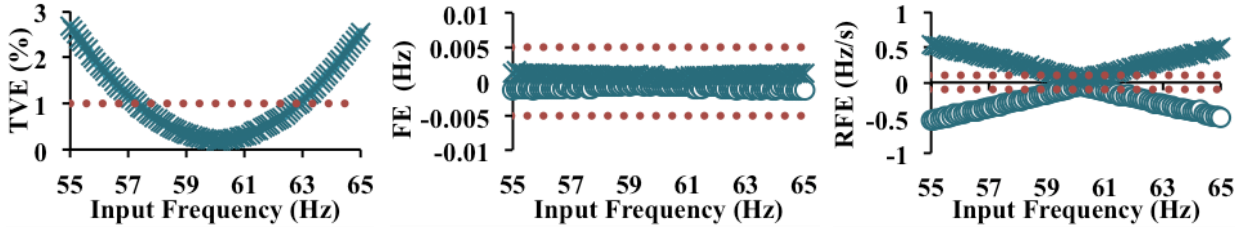

(b) frequency sweeping test

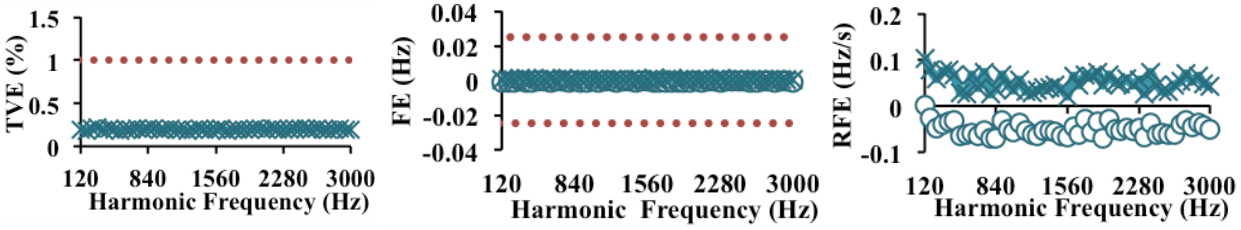

(c) harmonic distortion test

Figure 16. Test results of a given PMU under various static and dynamic test conditions. Adapted with permission from [111]

Figure 16. Continued.

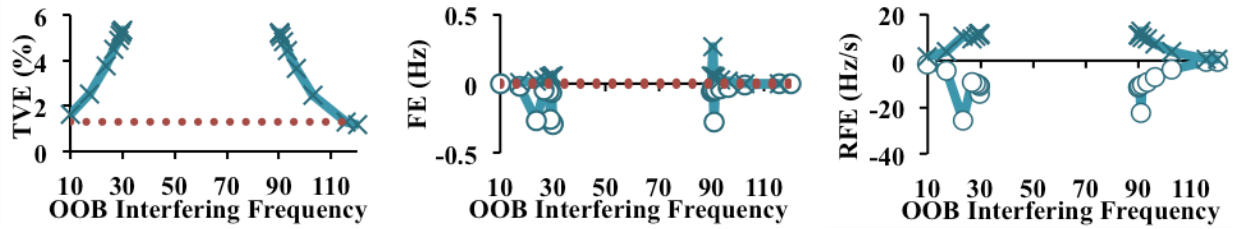

(d) out-of-band distortion test

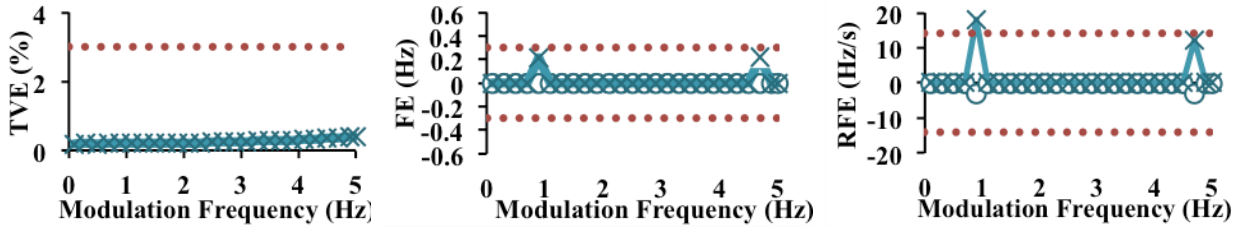

(e) amplitude modulation test

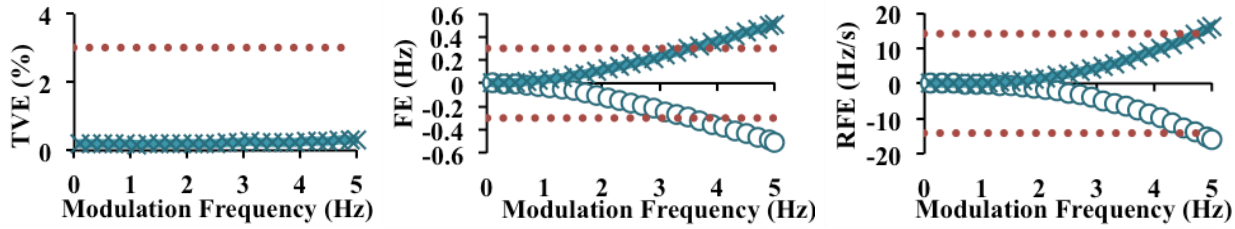

(f) phase modulation test

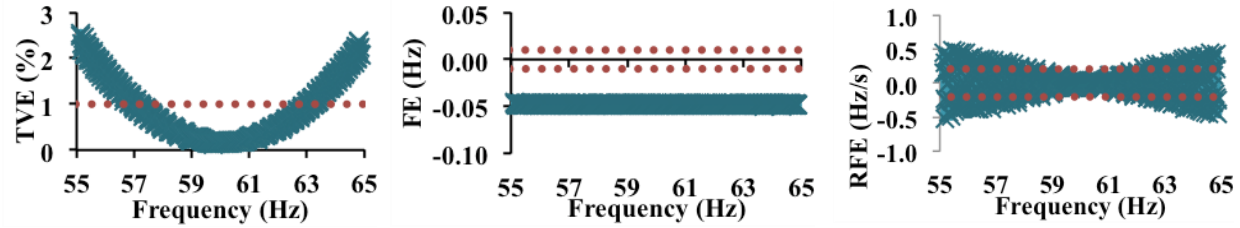

(g) frequency ramp test

Figure 16. Continued.

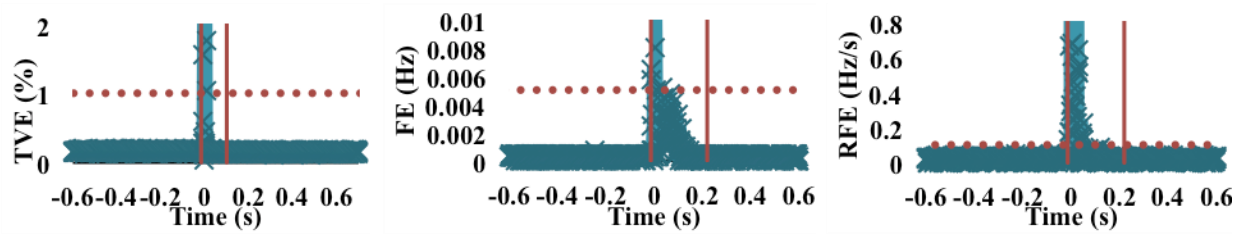

(h) magnitude step test

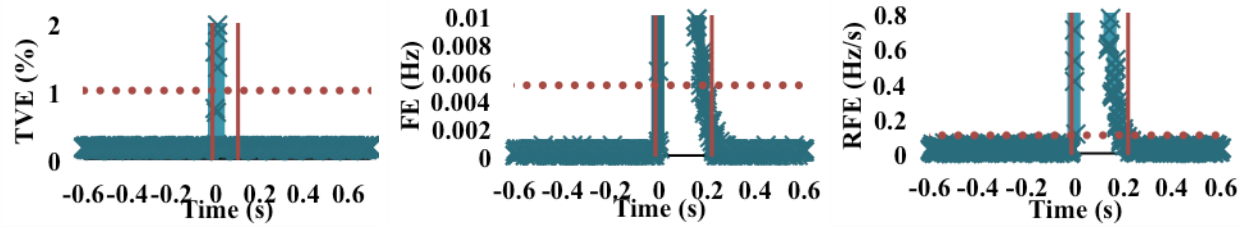

(i) phase angle step test

The suggested probabilistic metrics are calculated for various static and dynamic tests for the PMU under study. The results are tabulated in Table 3. The success probability indicators for various static and dynamic tests are evaluated in columns 3-5. As it can be seen in Table 3, while the error values for some standard tests are perfectly within the desired thresholds in all the test scenarios (e.g., harmonic distortion), the success probability of some other tests is very low (as low as 0.18% for out-of-band test) reflecting the fact that the probability of incorrect or not accurate reported measurements is extremely high with unacceptable level of uncertainty. Taking into account all various error values, the probabilities reported in columns 6-7 demonstrate the PMU integrity values with respect to all the static and dynamic tests, respectively.

Table 3. Probabilistic Metrics for PMU Vulnerability and Integrity Assessment
Adapted with permission from [111]

Test Category	**Test Name**	$P_{TVE,i}^{[.]}$	$P_{FE,i}^{[.]}$	$P_{RFE,i}^{[.]}$	$P_i^{ST_k}$	$P_i^{DT_k}$	$\eta_{TVE,i}^{[.]}$	$\eta_{FE,i}^{[.]}$	$\eta_{RFE,i}^{[.]}$
Steady Tests	Magnitude Sweeping	0.91	1	1	0.91	N/A	0.67	N/A	N/A
	Frequency Sweeping	0.60	1	0.52	0.32	N/A	0.34	0.99	0.99
	Harmonic Distortion	1	1	1	1	N/A	0.83	0.99	N/A
	Out-of-Band Interference	0.18	0.39	1	0.07	N/A	0.06	0.90	N/A
Dynamic Tests	Amplitude Modulation	0.98	1	1	N/A	0.98	0.94	0.99	0.99
	Angle Modulation	1	0.89	0.97	N/A	0.86	0.94	0.99	0.99
	Frequency Ramp	0.48	0	0.69	N/A	0	0.11	0	0.99
	Magnitude Step Change	0.81	1	1	N/A	0.81	0.81	N/A	N/A
	Angle Step Change	0.70	1	1	N/A	0.71	0.82	N/A	N/A

The PMUs may pass all the static and dynamic tests, but the test results do not reflect the uncertainty level of the test acceptance. The probabilistic values calculated in the last three columns of Table 3 show, in the range of 0-1, the distance of the measurement errors to the desired thresholds for various tests. The N/A entries in Table 3 reflect the fact that there is no desirable thresholds reported for a given error metric corresponding to several static and dynamic test in the standards. The closer the distance values $\eta_{e_k,i}^{[.]}$ are to 1, the more reliable the test results are with respect to the desired thresholds. As the probabilistic distance metrics decrease, the test results are vulnerable to failure in the next

test interval and the periodic maintenance plans need to be expedited; otherwise, the PMU measurements and consequently the end-use synchrophasor applications in power system may not be reliable in practice.

It has been shown that assessment of the test results provides an additional insight about: (a) whether the expected functionality and integrity of the PMUs is maintained over time; (b) which synchrophasor standard requirements are most vulnerable for a given device over time; (c) when the maintenance schedule needs to be expedited on certain PMUs based on observed performance degradation probabilities; and (d) the risks of loss of trustworthiness of various end-use synchrophasor-based applications.

4. END-TO-END ASSESSMENT OF SYNCHROPHASOR SYSTEM IN LABORATORY ENVIRONMENT*

4.1. Impact of the Synchrophasor Measurements on the Power System Protection Applications in Transmission System

Various applications for power system protection have different sensitivities to the data errors in the input measurements. Moreover, different PMU algorithms for synchrophasor estimations may have different responses to the input signals experienced during different disturbances. The impacts of such input signal uncertainties and related application errors are largely unknown to the end-users and need to be fully investigated.

Even though the IEEE standards define the basic *type tests* that PMUs have to undergo with certain precision, the test procedure does not reveal the impact of such results on the system-wide applications. In addition, the error impacts of the signal components being present at the time of a specific protection event are not known. The performance is further affected by different requirements in terms of calculation speed, accuracy of estimated frequency, angle and magnitude measurements, etc., which are different for different synchrophasor applications. Making meaningful trade-offs between such performance indicators to reduce the error impact is, hence, an imperative. Since such decisions are made at the time of the PMU design, the user is primarily interested in evaluating the performance under various application scenarios.

---

* Part of this section is reprinted with permission from "Impact of PMU Errors on the Synchrophasor-based Fault Location in Power Systems" by T. Becejac, P. Dehghanian, and M. Kezunovic, Sep. 2016 48th North American Power Symposium, ©2016 IEEE, with permission from IEEE.

One of the essential power system protection applications is certainly detection of the faults and locating where they are on transmission lines. The faults may be caused by a variety of reasons, e.g. failure of different equipment, severe weather conditions, human-induced accidents, animal interferences. Timely detection and location of the faults in the network is of critical importance for maintaining the security and decreasing the risk of the loss of load and consequent financial losses. If efficiently employed, fast and time-synchronized PMU measurements can facilitate a more accurate fault detection and location in power systems. Significant number of studies has focused on the fault location algorithms in the past, some of which are solely based on the synchrophasor measurements. A detailed review of various fault location techniques is reported in [8], and [73].

In order to build a trustworthy mindset for the protection end-users, the first step is to recognize the critical parameters of interest for a given application and then evaluate how the estimation algorithm matches the application requirements using the results acquired from the calibration tests and application tests [113], [114]. Such analyses could build the confidence about the quality of the synchrophasor application outputs. The ability of the synchrophasor-based techniques to pin-point the exact fault locations mainly relies on the accuracy of the measurements fed into the algorithms. PMU performance under such prevailing conditions needs to be judiciously investigated to ensure that the PMU measurements are accurately estimated.

4.2. Testing Environment: Synchrophasor Testbed

At this stage of the testing, full-scale synchrophasor production system is implemented using various commercial solutions from major vendors in this area such as Alstom Grid, OsiSoft, Esri, National Instrument, OPAL-RT and others. The production system is instrumented with software and hardware to allow for testing, calibration and evaluation of various advanced developments in the synchrophasor technology. The testbed platform used for *application* and *system end-to-end testing* in this research, characterizing the PMU response under fault conditions and evaluating the impact of the PMU errors on the fault location application outcome is implemented as shown in Fig 17. The developed infrastructure is generic enough to be employed not only for quantifying the impact of PMU errors on fault location algorithms, but also performing studies on trustworthy assessment of any end-use power system application that uses PMU measurements.

As shown in Fig. 17, the synchrophasor testbed system consists of timing references, signal generator, power amplifiers, PMUs, and data management and analytic tools. Timing reference provides GPS clock reference to the real time simulator and PMUs so that measurements from different devices are synchronized and time-stamped. Model of the network under evaluation is built in the Matlab Simulik software package environment. Various fault scenario use-cases are simulated and waveforms are generated using the low voltage simulators embedded in the Opal-RT. In order to have realistic measurements from the PMU, the applied signals must conform to the nominal level defined by the PMU device (i.e., normally 70 V_{rms} and 5 A_{rms} for voltage and current,

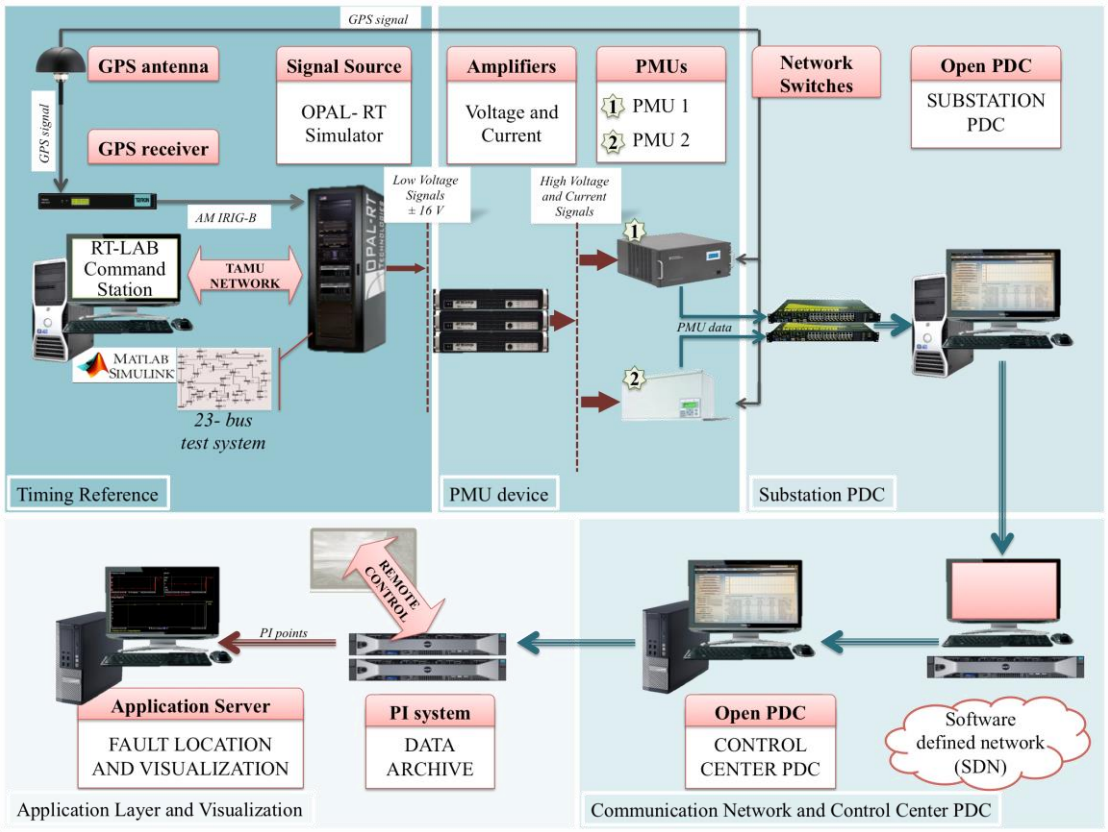

Figure 17. Synchrophasor testbed solution.

respectively). Signals from the simulator are amplified to the nominal level using power amplifiers.

In the case of the *application tests* two PMUs, (PMU under test and reference unit) are fed with the same input waveforms and their outputs are evaluated. In the case of *system end-to-end testing* procedures, since the selected fault location algorithm requires measurements from both ends of the line, two PMU devices were fed simultaneously with the fault signals assuming they are located at both ends of the line. Measurements from the reference PMU are assumed to be correct values, allowing impact assessment of the

DUT to the application outcome. Each PMU is connected to the GPS antenna for the synchronization purposes and measured data streams from the devices are collected and fed to fault location algorithm for further evaluation purposes.

4.3. Application Testing: Definition and Laboratory Set-Up

Application tests are conducted to evaluate the PMU performance under faults and other disturbances in power systems. At this stage of testing, the performance of the stand-alone PMU device is evaluated when PMU is exposed to a set of input waveforms from the field. In this example, various fault scenarios are generated and the PMU under test is exposed to faulty signals with no pre- set waveform characteristics. Phasor estimates and frequency measurements of the DUT are compared with those estimated from the reference PMU (with very accurate algorithm). Accuracy of the reference algorithm was confirmed in the calibration laboratory and the estimation error is at least one order of magnitude better than standard requirements (TVE<0.0x %) which makes this algorithm valid reference even under the unknown inputs. The proposed hypothesis is that such tests will reveal additional, rather unknown, performance characteristics that are crucial for the overall application assessment, nevertheless still in alignment with the results acquired from the *type tests*.

Functional diagram of the testbed implementation is illustrated in Fig. 18. Network models are developed using the graphical system design software in MATLAB which run on a real time (RT) platform. RT simulator is equipped with an I/O FPGA board used to generate the voltage waveforms that are amplified to the nominal level of the PMUs. PMU streams the measurements back to the simulator over fast Ethernet communications for

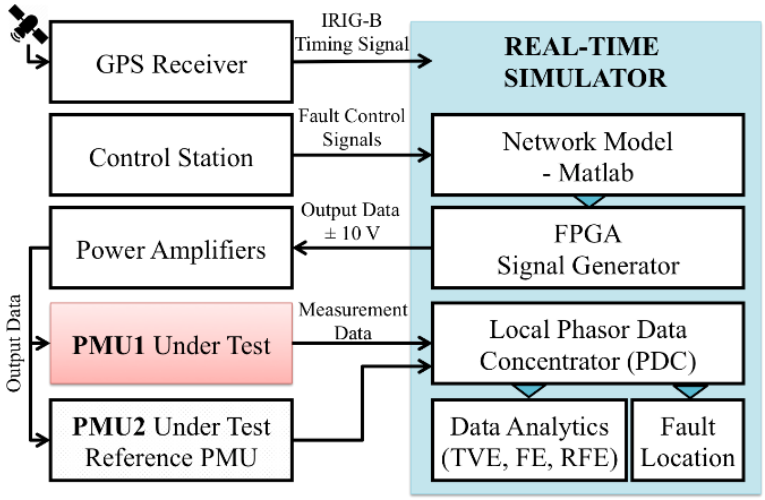

Figure 18. Functional diagram of the synchrophasor testbed developed for *application testing*.

further analysis. An external GPS receiver generates the un-modulated IRIG-B signal that is connected to simulator's spectracom card (TSync-PCIe), providing accurate time-stamps to the RT model allowing local PDC to collect and align the incoming measurements.

4.3.1. Reference Algorithm for PMU Performance Evaluation

An undeniable challenge for PMUs is need to preserve high estimation accuracy, while exposed to non-ideal input signals in presence of noise, numerous power system disturbances, and imbalances. In response to such transients, loss of generation or transmission facilities, or temporal imbalance between generation and load, the system frequency may deviate from its nominal value. When a disturbance such as faults occur, different types of signal distortions (e.g., noise, harmonics, inter-harmonics, voltage sag or dip, etc.) are created and superimposed on the power grid voltage or current signals

[74]. To be able to deal with such non-ideal signals, PMU has to first condition the input signal in order to separate the fundamental frequency component and then estimate its phasor using analog and digital signal processing features accurately.

In contrast with the *type test* procedures, where the measurements are compared against known true values of the input signals, *application tests* require a reference (i.e., more accurate) algorithm to assess the PMU measurements under faults and transients. The reference algorithm is developed via the National Instrument cRIO 9082 platform [75]. Accurate timing information required for the synchrophasor measurement is provided with GPS time stamping and synchronization module 9467 with the ns order of accuracy.

Synchrophasor applications require sampling with respect to an absolute time reference, so the data is acquired at fixed time intervals with the sampling rate of 50 kS/s. The A/D converted data with high sampling rate is sent through multi-stage filters, where the signal frequency is estimated followed by calculation of voltage/current phasors. Data processing is accomplished in two stages: (1) re-sampling and (2) phasor estimation. First, sampled data goes through digital low-pass filters, being decimated with factor 25, and then being sent at the rate of 2 kS/s. Next, data goes through equi-ripple Finite Impulse Response (FIR) Band-Pass Filters (BPF), with the 0.5 dB ripple in the pass band (58-62 Hz) at the 60 Hz nominal frequency, and attenuation of 55 dB in the stop band (55-65 Hz). The designed and developed filter is a 1320 order filter, coefficients of which are predefined and stored in the FPGA memory. Magnitude response of the BPF is depicted in Fig. 19.

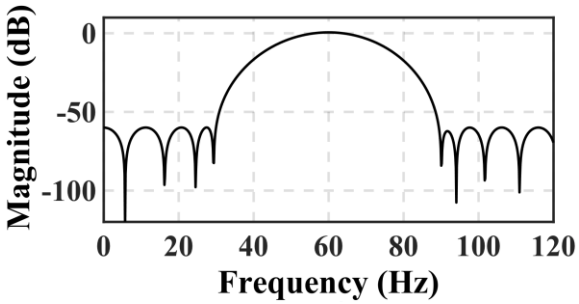

Figure 19. Magnitude response of the BPF in the reference algorithm.

Frequency is estimated using the sine interpolation utilizing the inverse tangent functions. Data is then re-sampled with the new estimated frequency and sent forward to the second stage where the phasors are estimated. Data passes through a two-stage low pass filter, and final corrections are compensated for the delays introduced by the signal processing. Further details on the implemented algorithm can be found in [76].

4.3.2. Accuracy of the Reference PMU

Accuracy of the reference algorithm was confirmed in the calibration laboratory and its estimation error is at least one order of magnitude better than required by the standard for M-class PMUs (TVE<0.0x%). The same observations hold for the FE and RFE metrics. Comprehensive testing was carried out at each reporting rate {10,12,15,20,30,60} fps. Testing results on the reference PMU for the reporting rate of 60 fps are given in Table 4. With the achieved accuracy, it is apparent that the selected PMU algorithm is a good candidate to serve as a reference for the suggested application testing.

Table 4. Performance assessment of the reference PMU.

***Type Test* Item**	**Reference PMU Under Test (@FPS=60)**						**IEEE Std. C37.118.1a**		
	Mean Error			**Maximum Error**			**M Class Limits (@ FPS=60)**		
	TVE (%)	FE (Hz)	RFE (%)	TVE (%)	FE (Hz)	RFE (Hz/s)	TVE (%)	FE (Hz)	RFE (Hz/s)
Signal Magnitude Sweep (10%-200%)	0.008	4.75e-5	0.004	0.028	2.29e-4	0.019	1		
Signal Frequency Sweep (55-65 Hz)	0.006	3.45e-5	0.002	0.016	5.70e-5	0.003	1	0.005	0.1
Harmonic Distortion (up to 50^{th})	0.005	3.00e-5	0.003	0.015	1.34e-4	0.018	1	0.025	-
Out-of-Band Interference (f_0=57 Hz)	0.103	7.1e-4	0.037	0.177	1.56e-3	0.104	1.3	0.01	-
Out-of-Band Interference (f_0=60 Hz)	0.082	4.9e-4	0.042	0.156	1.08e-3	0.100	1.3	0.01	-
Out-of-Band Interference (f_0=63 Hz)	0.058	8.5e-4	0.121	0.156	1.71e-3	0.121	1.3	0.01	-
Frequency Ramp (positive; rate=1 Hz/s)	0.006	1.54e-4	0.008	0.016	7.8e-4	0.035	1	0.01	0.2
Frequency Ramp (negative; rate=1 Hz/s)	0.017	1.57e-4	0.008	0.029	3.7e-4	0.036	1	0.01	0.2
Amplitude Modulation (0.1Hz <f_{mod}< 5Hz)	0.097	5.4e-4	0.017	0.342	1.46e-3	0.047	3	0.3	14
Phase Modulation (0.1 Hz<f_{mod}< 5Hz)	0.058	1.73e-2	0.651	0.249	5.82e-2	2.988	3	0.3	14

***Type Test* Item**	Response Time (sec.)			Response Time to meet limit X* (sec.)		
	TVE	**FE**	**RFE**	**TVE**	**FE**	**RFE**
Magnitude Step (10% of nominal value)	0.026	0.072	0.104	0.117	0.233	0.233
Phase Step (10% of nominal value)	0.048	0.092	0.123	0.117	0.233	0.233

X*: TVE=1%; FE=0.005Hz; RFE=0.1Hz/s (0.4 Hz/s for P-class PMU)

PMU Reporting Latency (sec.)	0.1039	0.1167

4.4. Application Testing Case Study: Power System Faults And Numerical Results

PMU measurements, if judicially employed, can help in more accurate fault detection and fault location. Information on the magnitude and angle of the current signals and voltage phasors are also crucial to accurately locate the faults in electric power systems [77], [78]. In fault location applications, accurate measurement of the frequency is commonly not the priority, but knowledge about the change in frequency can help improve some of the fault-location algorithms. Observations on the performance of various phasor estimation algorithms under such application conditions can offer a more realistic view on whether the PMU measurements can be employed for such applications and which fault location algorithm is expected to be fundamentally more accurate.

Through the proposed approach of PMU testing in a controlled environment and detailed analysis of different estimation techniques used in PMU algorithms, one can gain insights on which estimation technique is most accurate for a certain end-use application. This hypothesis has been validated through series of realistic test scenarios on a 23-bus system running on an Opal Real Time (RT) simulator using the hardware-in-the-loop (HIL) interface.

The network used for simulating faults on transmission lines and studying the PMU responses under such conditions is a modified 23-bus model of a 500 kV transmission network with 7 generating units and 17 load points, the one-line diagram of which is illustrated in Fig. 20. The model is developed in MATLAB Simulink environment and simulated on the Opal-RT platform. The entire system is divided into

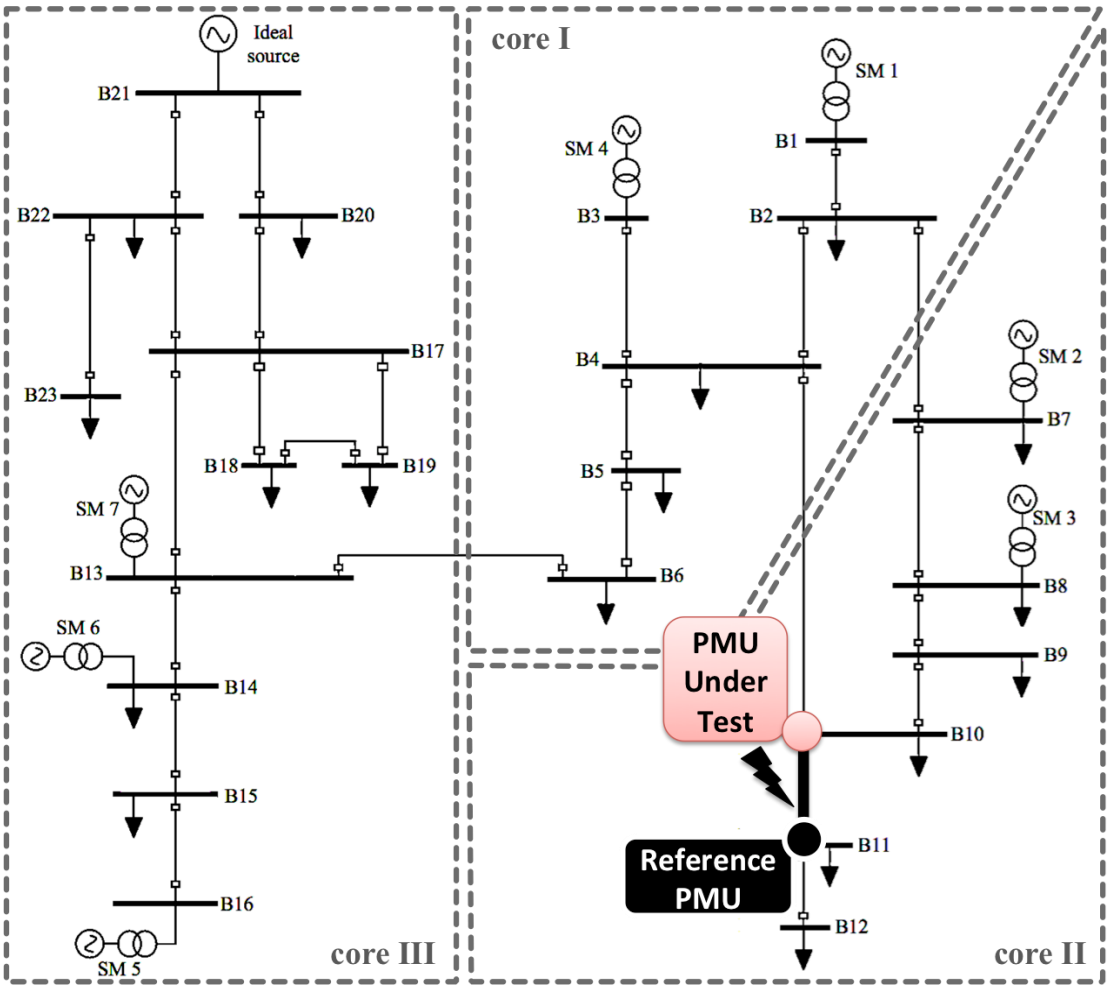

Figure 20. Case Study: 23-bus model of a 500 kV transmission network.

three blocks, each running on separate cores, in order to achieve a fast execution with time steps of 50 us. The system behavior under different scenarios of symmetrical (three-phase) and asymmetrical (single line to ground, double line to ground, and line to line) faults is thoroughly studied. Different scenarios are fed with applied faults of diverse resistance values ranging from 0, 20 and 100 Ohms and different locations on 30%, 50% and 80%

of the line length. Each fault scenario is simulated for 30 seconds. Local frequency is defined in (4.1), where $d\omega$ represents the rotor speed deviation.

$$f = (d\omega + 1) f_{nom} \tag{4.1}$$

The simulation results on the estimated frequency at the generation bus B8, when various fault types are applied on the line connecting busses B10 and B11, are depicted in Fig. 21(a). One can observe, from the simulation results in Fig. 21(a), that the frequency initially increases due to the generation-demand imbalance (load drop), and then returns

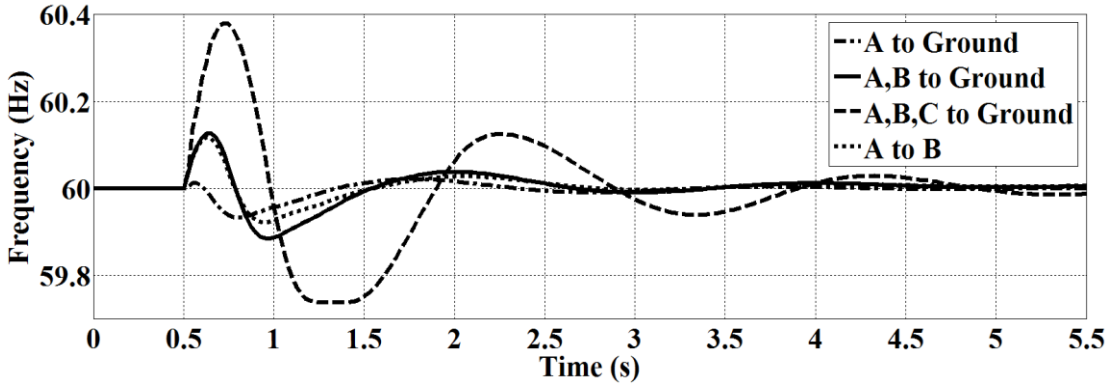

(a)

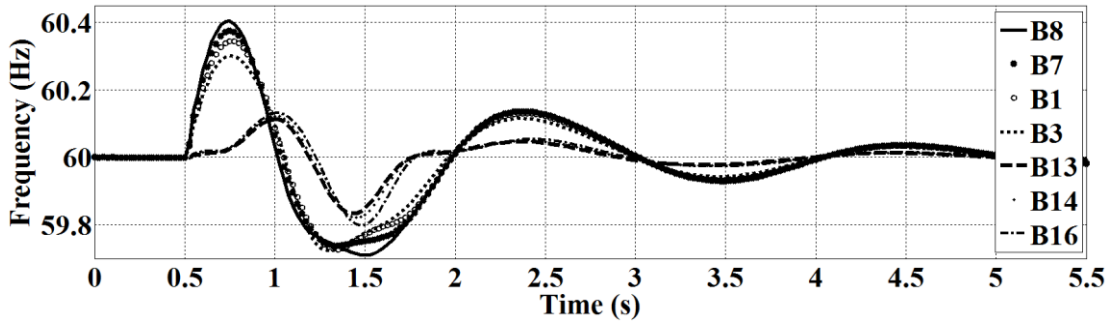

(b)

Figure 21. (a) Frequency measurements at bus B8 during various fault types, (b) Frequency measurements for three-phase fault on the generator buses.

to a new steady state value when the power is rerouted in an updated network topology. The worst-case scenario is during a three-phase fault when the entire demand at load points B11 and B12 is disconnected. This worst-case scenario reveals the maximum expected errors and, hence, is studied for assessment of the PMU estimation errors (*application tests*) as well as evaluating the impact on the fault location applications (*system end-to-end tests*). Occurrence of a fault on a transmission line triggers a sudden change in the system frequency. One can see, from Fig. 21(b) that the frequency at the buses closer to the fault is more affected compared to that measured further away from the fault inception. This leads to a conclusion that the accuracy of PMU measurements located in vicinity of the fault will be more susceptible, and hence, will impose a higher risk to the trustworthiness of the end-use application outcomes.

To verify the conclusions derived from the above simulations, influence of the fault type, fault resistance and fault distance are studied. The metrics used for such performance evaluation are the same as those used in *type tests* and true values for comparison are taken to be measurements of the reference PMU.

First, the influence of different fault types (A-G, AB-G, ABC-G and AB) as well as fault resistance on the FE and TVE metrics is investigated. According to results illustrated in Fig. 22, while variations of fault resistance (R) generally does not have a significant influence on the frequency estimation in most studied scenarios, FE increases as R increases. Its impact on the TVE is noticeable. With an increase in the fault resistance, the TVE decreases. In case of a three-phase fault, the TVE reaches its maximum among all studied scenarios, which complies with the previous observation where the highest

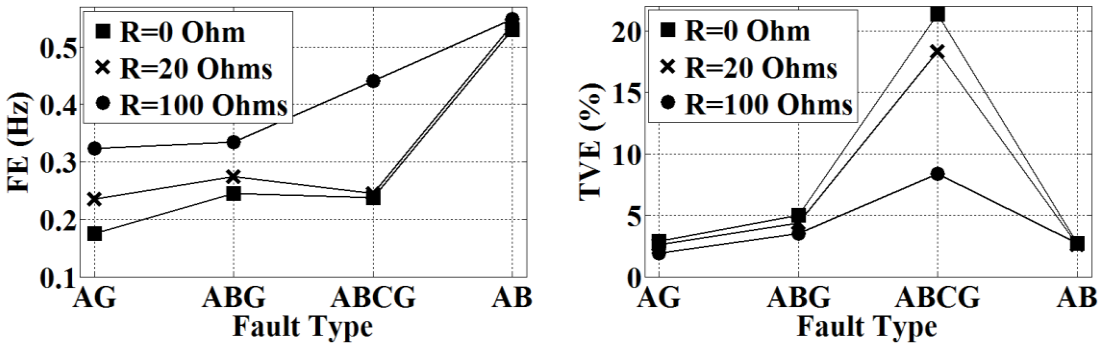

Figure 22. Impact of fault resistance on the FE and TVE metrics (d=80% of line length from B10; Blackman window with length of 6 cycles).

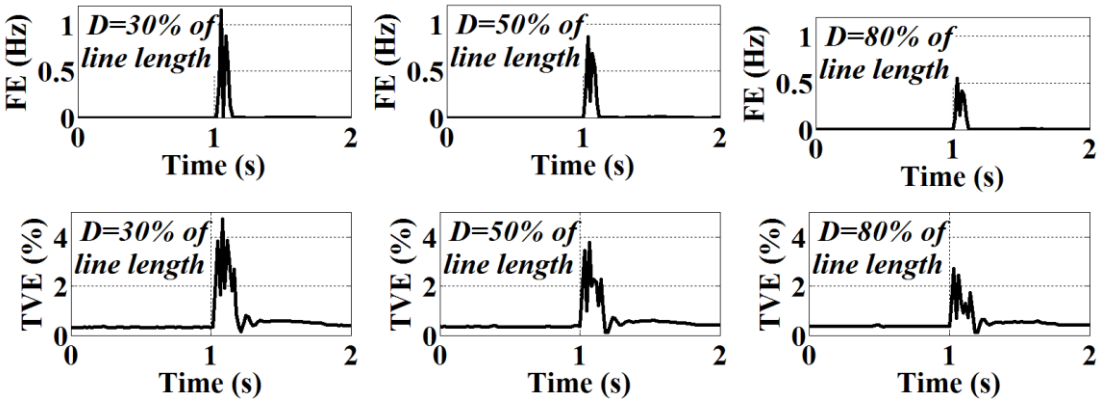

Figure 23. Impact of distance to the fault on the FE and TVE metrics (R=100 Ohms; Blackman window with length of 6 cycles; AB fault).

frequency deviation from nominal value was resulted when an ABC-G fault was simulated. Conversely, the FE has its peak value for AB faults among all studied scenarios.

Next, the impact of the distance to the fault inception is studied where the faults are assumed to occur at 30%, 50% and 80% of the line. Fig. 23 demonstrates the results acquired during an AB fault, with the fault resistance of 100 Ohms. The distance to the

fault from the bus where the PMU under test is located has a significant impact on the TVE metrics. The closer the fault is to the PMU location, the higher the TVE error is. The same observation is valid for FE metrics due to stronger variations in voltage/current signals closer to faults.

Afterward, the performance of four different filtering functions in PMUs as well as the WL under the studied fault scenarios is being researched. Most fault location algorithms use the voltage/current measurements as the input parameters; therefore, this study focuses on cases with potentially higher impacts on the TVE. For further testing, the fault is set to be closer to the PMU under test (D=30% of the line length), with the resistance of R=0 Ohm. Fig. 24 shows the impact of different windowing functions as the input filters. It can be seen that the best frequency estimate is achieved with the Hamming

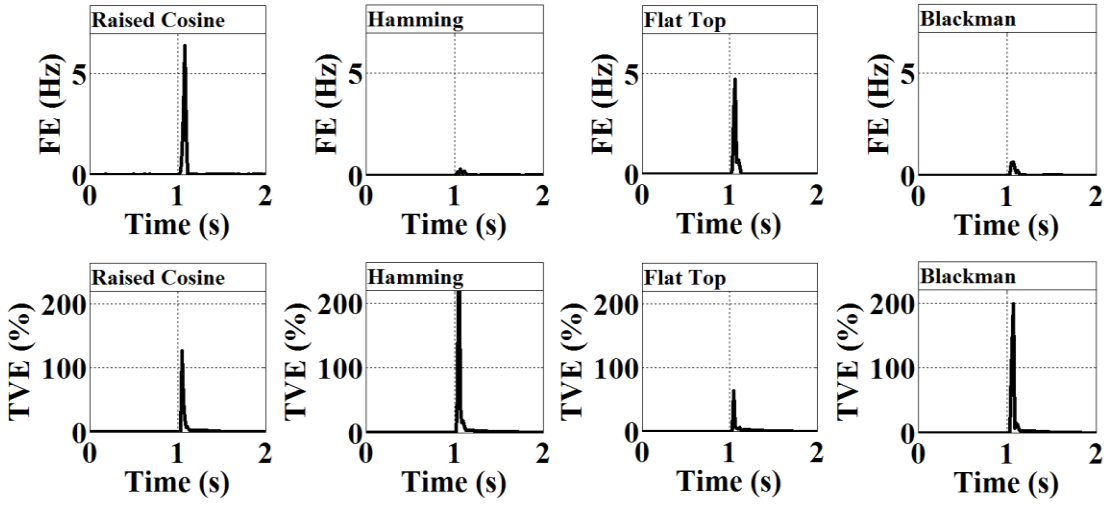

Figure 24. Impact of windowing functions on FE and TVE metrics; (d=30% of line length from B10; R=0 Ohm; ABC-G fault; window length of 6 cycles).

and Blackman filters, while presenting much higher TVE compared to other two filters. The Flat-Top filter has the best performance in terms of the TVE response, which closely matches the former observations in the *type tests*.

The impact of the WL on the accuracy of frequency and phasor estimation is illustrated in Fig. 25. As WL increases, the higher TVE is noticed, while the FE decreases, which make sense, since more data samples are available for higher accuracy of the frequency estimation. In such cases, however, the measurements will be delayed which can be an issue for the applications that mandate a faster data update.

From the acquired testing results, it can be generally concluded that: (1) different PMU algorithms can perform differently for a given application and (2) even if a given algorithm does not pass some *type tests* according to the standard requirements, it still can perform as expected for a specific application in real world scenarios.

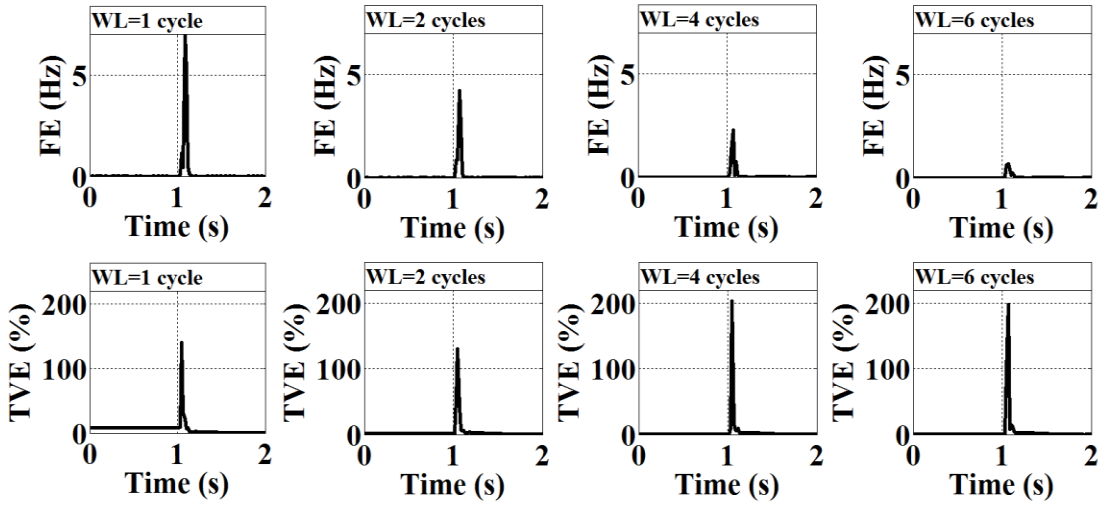

Figure 25. Impact of WL on the FE and TVE metrics (d=30% of the line length from B10; R=0 Ohm; ABC-G fault; Blackman window).

4.5. System End-to-end Testing: Definition and Fault Location Algorithm

Once the lab and commissioning tests are performed to assure that the synchrophasor system elements are intact, a tool that enables *system end-to-end testing* during operation is required since equipment *type testing* may not verify accuracy of the entire synchrophasor system while it is in-service. Therefore, an *system end-to-end test* procedure is defined to verify accuracy of the entire synchrophasor system at both element & system levels. *System end-to-end tests* are conducted by feeding the end-use synchrophasor applications with the measurements from real PMUs and quantifying the impact of measurement errors on the application of interest (e.g., fault location in the studied example). The Synchrophasor Testbed (Fig. 17) has been used for conducting the *system end-to-end tests*.

Impedance based fault location algorithms can be classified into four sub-categories: single, double, multi–end, and wide area methods based on the available sources of data. A double-end fault location algorithm is investigated in this section for *system end-to-end testing*. The studied algorithm [79] is implemented in MATLAB environment using synchrophasor measurements form real PMUs. PMU response errors under the fault conditions are characterized and their impact on the performance of synchrophasor-based fault location algorithms that uses synchronized phasors at both line terminals is quantified.

This use case demonstrates how to evaluate the impact of PMU response errors under fault conditions on the fault location application outcome through *system end to end testing*. The developed infrastructure is generic enough to be employed not only for

quantifying the impact of PMU errors on fault location algorithms, but also performing studies on trustworthy assessment of any end-use power system application that uses PMU measurements.

The fault location technique under study uses symmetrical components, namely the negative, and positive sequence, of voltage and current waveforms as an input to the fault location algorithm. These values can be measured and reported by PMUs, or can be alternatively calculated from the reported voltage and current phasors. The equivalent negative and positive sequence network representations of the transmission line when fault occurs are demonstrated in Fig. 26.

From the equivalent circuits, the following equations can be derived:

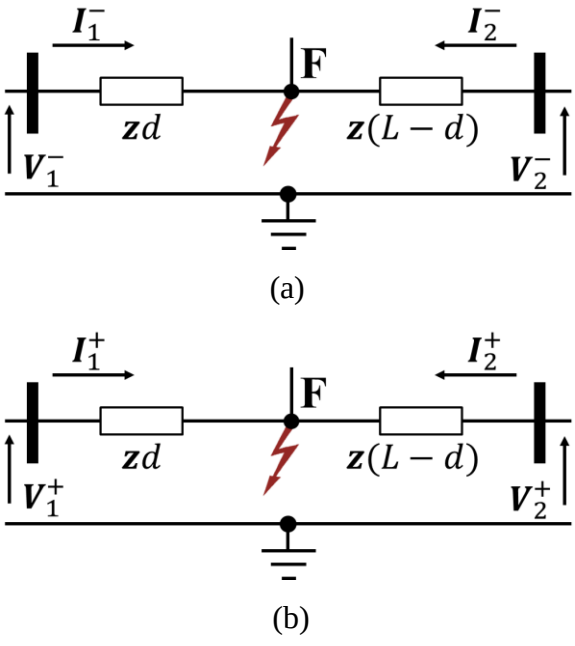

Figure 26. (a). Equivalent negative sequence network of the faulted TL. (b). Equivalent positive sequence network of the faulted TL. Reprinted with permission from [113]

$$V_1^- - zdI_1^- = V_2^- - z\left(L-d\right)I_2^- \tag{4.2}$$

$$V_1^+ - zdI_1^+ = V_2^+ - z\left(L-d\right)I_2^+ \tag{4.3}$$

Where the following nomenclature applies:

z	Negative and positive sequence line impedance.
L	Total length of the transmission line.
d	Distance from the Bus 1 to the fault location.
$V_{1,2}{}^-, V_{1,2}{}^+$	Negative and positive sequence phase voltages at both ends of the line.
$I_{1,2}{}^-, I_{1,2}{}^+$	Negative and positive sequence phase currents at both line terminals.

Distance to the fault can be represented as a percentage of the line length L, as introduced in (4.4):

$$d\% = \frac{d}{L}100 \tag{4.4}$$

Combining equations (4.2) and (4.3), the following expression for the distance to the fault can be obtained:

$$d\% = 100\frac{\left(V_1^+ - V_2^+\right)I_2^- - \left(V_1^- - V_2^-\right)I_2^+}{\left(V_1^+ - V_2^+\right)\left(I_1^- + I_2^-\right) - \left(V_1^- - V_2^-\right)\left(I_1^+ + I_2^+\right)} \tag{4.5}$$

4.6. System End-to-End Testing Case Study: 2-bus Network And Numerical Results

The network model under test is a 400kV network, with 100-mile long transmission line. The selected fault location algorithm was evaluated under 30 different fault use case scenarios: the transmission line was exposed to various types of faults [i.e.,

single phase to ground (ag), phase to phase (ab), two phase to ground (abg), as well as three phase fault (abc)] and various possible locations along the line [e.g., 5%, 20% and 50% of the line length from the bus 1 terminal]. Synchrophasor-based fault location algorithm sensitivity to the changes in the fault resistance was investigated as well. Three values of resistance were used in the simulations: 0, 20, and 100 ohms.

The schematic diagram of the simulated network with three different locations for the fault occurrence is depicted in Fig. 27(a)-(c). Figures 27(d)-(i) demonstrate simulated phase voltages at both ends of the line for the single line to ground (ag) fault with R_f=20

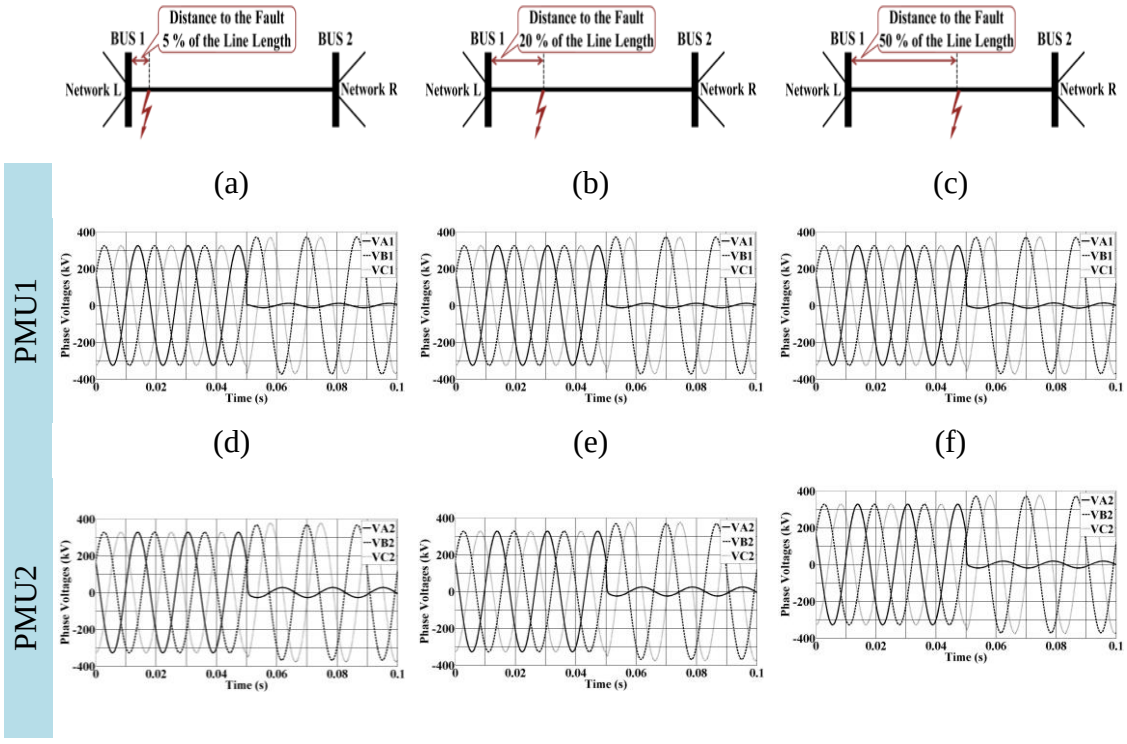

Figure 27. Simulated phase voltages in the transmission line fault use case scenarios. Reprinted with permission from [113]

ohms fault resistance; Fig. 27 (d)-(f) illustrate the phase voltages at Bus 1 while the phase voltages at the Bus 2 are demonstrated in Fig. 27 (g)-(i). The waveform sampling frequency was set to 3.8 kHz. Parameters of the active networks L and R, as well as the transmission line characteristics are listed in Table 5 and Table 6, respectively.

Voltage and current waveforms simulated in the Opal-RT system model are scaled down to the level of ±5V and generated using the simulator's FPGA board. The low voltage signals are then amplified using the power amplifiers; since the simulator is only capable of generating the voltage signals, a voltage controlled current source was used for generating the corresponding three phase current signals. Two PMU devices were then exposed to the generated fault signals. Measurements from both devices are collected, merged, and stored in the database for further analysis. Sample PMU measurements

Table 5. Parameters of the active networks.

Parameters	***Network L***	***Network R***
$\boldsymbol{V_{rms}^{LL}}$ **[V]**	416000	400000
Frequency [Hz]	60	60
$\boldsymbol{R^{zero}}$**[Ω]**	2.0371785	1.2732366
$\boldsymbol{R^{+,-}}$**[Ω]**	1.0185892	0.6366183
$\boldsymbol{L^{zero}}$ **[H]**	0.10185892	0.0636618
$\boldsymbol{L^{+,-}}$**[H]**	0.0509295	0.0318609

Table 6. Transmission line parameters.

Parameters	***Resistance [Ω/km]***	***Inductance [mH/km]***
+ and - sequence	0.065	0.95493
Zero sequence	0.195	2.86479

acquired from both line terminals, during the single-line to ground fault (ag) for the three different location of the fault along the line (5%, 20% and 50% of the line length) are demonstrated in Fig. 28. Figures (a)-(c) and (d)-(f) illustrate the voltage phase magnitudes

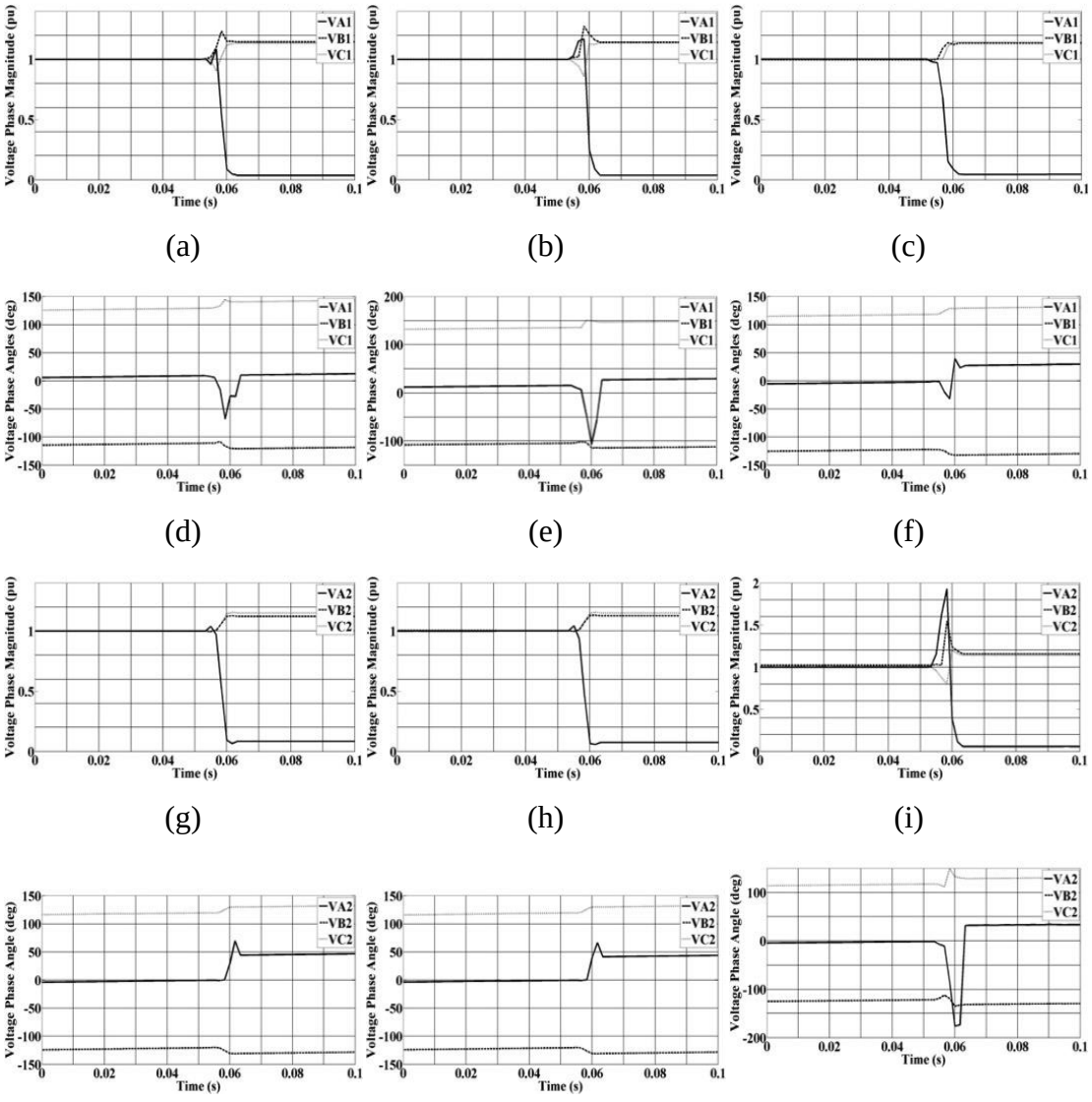

Figure 28. PMU measurements: magnitudes and the phase angles at both ends of the faulted transmission line. Reprinted with permission from [113]

and corresponding phase angle measurements at Bus 1, respectively. Figures (g)-(l) demonstrate the PMU measurements at Bus 2, which actually highlights how this PMU responds under simulated fault conditions. As one can see from the sample results, after the fault occurs (t = 0.05s), there is a short period of time until the PMUs successfully detect the disturbance, which is mainly related to the delay of the signal generator response and another half a cycle period (i.e., 10ms) for the measurements to become reliable.

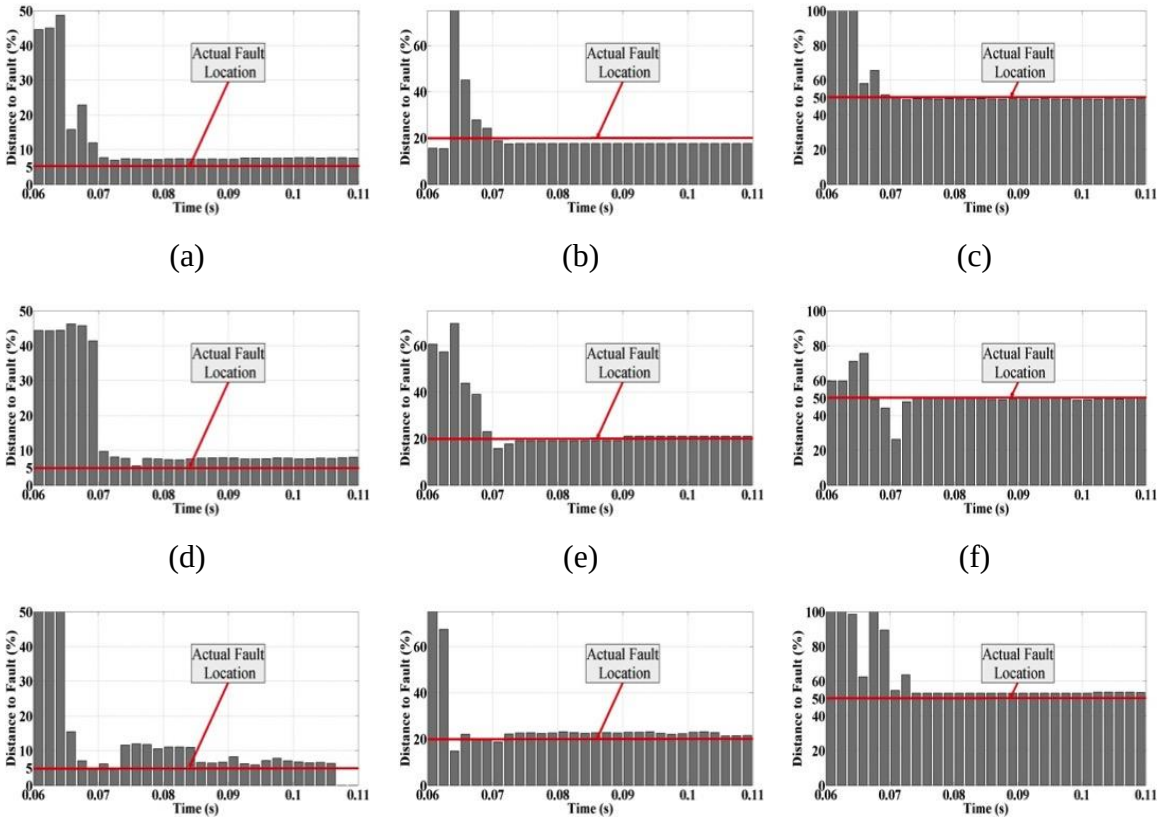

Figure 29. Synchrophasor-based fault location algorithm performance: calculated fault locations for different fault use case scenarios. Reprinted with permission from[113]

PMU measurements are then submitted to the fault location algorithm and the results are depicted in Fig. 29.

Single line to ground fault was simulated with the three values of fault resistance: the bolted fault use case scenario (0 ohm) is illustrated in figures 29(a)-(c); the 20 ohm fault resistance use case scenario is depicted in figures 29(d)-(f); and the high-resistance 100 ohm fault scenario is illustrated in figures 29(g)-(k).

From the results, it can be seen that during the higher resistance fault scenarios, the time taken to locate the fault is comparatively longer. Also it can be noticed that the minimum error is corresponding to the scenario when the fault has happened in the middle of the line, while it is at its highest when the fault occurs at the begging of the line. A summary of the results for all simulated fault scenarios is tabulated in Table 7. All calculated errors corresponding to the studied fault location algorithm are within the 3% of the line length. It is worth mentioning that errors introduced by the communication network and phasor data concentrator have not been incorporated in this test case study while it is very important for such use case to be considered and be researched in future.

Table 7. Summary of the fault analysis. Adapted with permission from [113]

Fault Type	Fault Location (miles)	Fault Resistance (Ω)	Calculated Fault Location (miles)	Fault Location % Error
ag	5 (5%)	0	7.56	2.56%
	20 (20%)		18.24	1.76%
	50 (50%)		49.72	0.28%
	5 (5%)	20	8.6	3.6%
	20 (20%)		20.89	0.89%
	50 (50%)		49.84	0.16%
	5 (5%)	100	7.97	2.97%
	20 (20%)		22.16	2.16%
	50 (50%)		51.07	1.07%
abg	5 (5%)	0	6.93	1.93%
	20 (20%)		21.22	1.22%
	50 (50%)		50.78	0.78%
	5 (5%)	20	-	-
	20 (20%)		21.79	1.79%
	50 (50%)		48.32	1.68%
	5 (5%)	100	6.23	1.23%
	20 (20%)		21.48	1.48%
	50 (50%)		50.88	0.88%
ab	5 (5%)	0	6.13	1.13%
	20 (20%)		-	-
	50 (50%)		47.98	2.02%
abcg	5 (5%)	0	7.03	2.03%
	20 (20%)		22.41	1.41%
	50 (50%)		50.46	1.46%
	5 (5%)	20	3.97	1.03%
	20 (20%)		22.35	2.35%
	50 (50%)		50.84	0.84%
	5 (5%)	100	6.82	1.82%
	20 (20%)		19.07	0.93%
	50 (50%)		49.25	0.75%

4.7. System End-to-End Testing Case Study: 23-bus System – Impact of the PMU Settings and Numerical Results

Same algorithm for the fault location as in previous case study was researched. The real PMU was exposed to a set of faulty signals while the set-up setting parameters (windowing functions and WL) were altered, so as to estimate the influence of such parameters on the accuracy of the synchrophasor measurements as well as the end-use application outcome. On studying the impact of windowing functions, the maximum error in all test scenarios appears to be during the symmetrical three-phase faults (ABC-G). The maximum error in fault location for a fault scenario with R=0 Ohm, d= 30% of the line length from bus B10, and fixed WL of 6 cycles, are tabulated in Table 8. It can be seen that the Raised-Cosine windowing function reveals the highest error in calculating the distance to the fault, mainly due to the low amplitude accuracy of the filter function. On the other hand, performance of the Flat-Top filter is most appealing for the fault location

Table 8. Performance of different windowing functions on the fault location algorithm accuracy.

Filter Function	Raised Cosine	Hamming	Blackman	Flat-Top
Maximum Error (%)	3.76	3.12	1.54	0.97

Table 9. Impact of different windowing lengths on the fault location algorithm accuracy.

Window Length (× 16.66 ms)	1	2	4	6
Maximum Error (%)	4.14	2.05	1.78	1.54

algorithm that uses voltage/current phasor estimates. However, one has to be careful in selecting the PMU settings in the field, as the Flat-Top function has a great performance for the phasor estimation while its frequency resolution is low, making the frequency estimates less accurate compared to other filters. In response to such low frequency resolution of the Flat-Top filter, one can use the Blackman filter that has a close enough phasor estimation with a more accurate frequency estimation compared to Flat-Top filters.

Next, impact of the WL used for the synchrophasor estimation algorithm is studied. Four different values for the WL comprising 1, 2, 4, or 6 cycles are considered. Table 9 shows the impact of WL for the Blackman filter function and the maximum errors in the fault location estimates in case of a fault with R=0 Ohm, d= 30% of the line length from bus B10 are tabulated. It can be seen that the fault location algorithm has the highest accuracy (i.e., minimum error) in case where the WL is longer. However, the WL cannot be large as some synchrophasor applications mandate very fast measurement requirements in real time.

5. END-TO-END ASSESSMENT OF SYNCHROPHASOR SYSTEM IN SIMULATION ENVIRONMENT

5.1. Impact of the PMU Data Quality Issues on Modal Analysis

In power systems, small signal stability problems continue to be a concern for power engineers [80], [81]. Power system disturbances are usually followed by low-frequency oscillations that can decay, sustain, or grow. Additionally, due to a variety of reasons many power systems are vulnerable to stability issues including inter-area oscillations. Inter-area oscillations occur when a group of electrically distant generators oscillates against each other [82]. From an operating point of view, oscillations are acceptable as long as they are quickly damped. In well-damped systems, these oscillations will be absorbed within a few seconds. However, sometimes they may lead to instability and system collapse [83]. Lightly damped electromechanical oscillations are also of concern in the power industry due to their undesirable effect on economics and operational practices. Additionally, even low-magnitude oscillations, if present over an extended period, can cause substantial damage to power system equipment such as generator shafts [84]. Thus, it is essential to detect these oscillations in the early stages of an event to be able to quickly take appropriate preventive controls.

Modal analysis is a mathematical tool used to study and characterize the small signal stability of a power system in the frequency domain [84]. Modal analysis directly extracts modal information from the system response to a perturbation including the mode's magnitude, phase, frequency, and damping factor. Although oscillations cannot be completely eliminated, advanced controls can be added to the system to improve their

damping and modify their frequency, assuming that the modes of the system are correctly identified.

Two main approaches for estimating modal content exist in the power system, 1) the traditional method based on the linearization of power system equations, and 2) the identification approach based on computational techniques that extract the modal information from time domain data. With the deployment of the modern devices that are capable of capturing the dynamic responses of the system, such as PMUs and Digital Fault Recorders (DFRs), an oscillatory response of the system can be measured in real-time. The main idea behind the identification methods is to decompose the system dynamic response into a sum of exponentially damped modes. A significant advantage of the identification methods is that their feasibility does not depend on having a system model [86]. Moreover, as the power grid changes, such as due to load perturbations or transmission switching actions, the modes of the power system also change.

If accurately estimated, system modes may help improve system modeling and the implementation of the control schemes, with a result of increased system reliability. However, PMU data is often delivered with various data quality issues. Data issues in the synchrophasor system can arise for a wide variety of reasons including topology errors, meter failures, and improper configurations. Furthermore, the communication infrastructure brings additional vulnerabilities to the power system, such as allowing intruders to launch various types of cyber-attacks and jeopardize the reliability of the electric grid.

There exist several identification techniques from the signal processing theory for estimating the modes from time-varying waveforms including Prony, Hankel Total Least Square, Matrix Pencil. Prony's method was the first method used for power system small signal stability analyses [87]. Nonetheless, several studies have shown some advantages from using the Matrix Pencil Method for the modal extraction from noisy signals over the traditional Prony method [85], [88]. We are building on these studies to explore the advantages of MPM under not only the presence of noise, but also other issues that can arise in the PMU data measurement set, such as outliers and un-updated data. This dissertation focus on measuring the impact of errors in input data (in this case frequency measurements acquired from the PMUs) on the mode estimation accuracy.

The proposed approach is depicted in the Figure 30. Different quality data issues are applied to the input data (frequency measurements), among which are noise, un-updated data and outliers, with the goal to quantify its impact on the application outcome. One step further, this dissertation investigates the application of the Robust Principal Component Analysis (RPCA) for the data improvement and recovery. It has been shown that RPCA works very well in respect to grossly corrupted observations [52]. After PMU

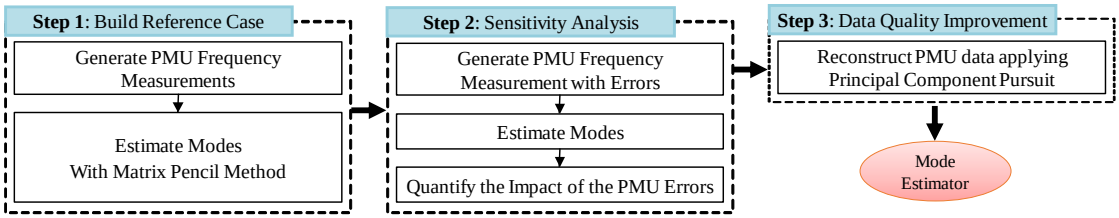

Figure 30. Proposed approach for estimating the impact of the PMU data quality issues on the modal analysis.

data is recovered/repaired, modal analysis are re-run to show the applicability of the proposed approach.

5.2.Modal Analysis

5.2.1. Background

Modal analysis can be formulated as a fitting problem of the pre-specified waveform to an actual time-varying waveform, such that the difference between the proposed and the actual waveform is minimized when estimating the magnitude, phase, frequency, and damping parameters of the fitting function. Estimated coefficients of the modeled waveform determine the modal characteristic of the linear system given as:

$$y(t) \approx \sum_{i=1}^{M} A_i e^{(\sigma_i t)} \cos(\omega_i t + \theta_i) + n(t); \; 0 \le t \le T \tag{5.1}$$

where the following nomenclature applies:

$y(t)$	= observed signal
$n(t)$	= system noise
M	= number of desired modes
$R_i = A_i e^{i\theta_i}$	= complex amplitude
σ_i	= damping factor
ω_i	= angular frequency

The key idea is to model the uniformly sampled data as a linear combination of the exponentially dumped functions. There are several well-known methods used for modal identification: Prony's method, Hankel Total Least Square (HTLS), and Matrix Pencil Method. From a historical perspective, the polynomial type of method (i.e., Prony's method) is much older and is still widely used for the stability studies. Baron de Prony

first developed this method in 1795 [89]. HTLS [90] is a special case of the ESPRIT algorithm [91]. Hua and Sarkar introduced Matrix Pencil Method (MPM) for extracting poles from antennas' transient responses [92]-[94]. MPM was derived from the pencil-of-functions approach [95], and today it is widely applied in the system identification and spectrum estimation areas. As an extension of the MPM, the Iterative Matrix Pencil Method was recently introduced for the modal analyses of the large-scale systems [96]. The Iterative MPM combines the MPM and the cost functions to decrease the computational burden by reducing the number of signals that are processed during the modal extraction. Other methods include variable projection method [97], eigensystem realization method [98], and the dynamic mode decomposition [99].

Unlike the polynomial methods, MPM shows some advantages when dealing with signals with unknown characteristics [100]. Moreover, it has excellent performance even when the input signal has noise, which is usually the case with PMU data [101]. Typically, up to 20-25 dB of signal-to-noise ratio (SNR) can be handled adequately by this technique [94]. The Matrix Pencil approach has a lower variance of estimates of the parameters of interest than a polynomial-type method and is computationally more efficient. While the MPM extracts signal poles directly from the eigenvalues, the Prony method requires a two-step process [82].

The MPM technique belongs to the group of identification methods and hence it can be applied to time-series data (PMU frequency). One of the main limitations of the identification method is the type of modes that can be computed (i.e., only modes that are present in the input data), and the inability to extract some well-damped modes if the input

signals are noisy. Regardless, their practical value has been demonstrated in many studies, such as stability analysis, model validation, and control design [86].

5.2.2. Matrix Pencil Method

With the MPM, signal poles can be found directly from the eigenvalues of a single developed matrix. This method directly estimates all mode parameters by fitting the signal model given in (5.2) to an observed measurement (5.1) that consists of *N* evenly spaced samples.

$$\hat{y}(k) = \sum_{i=1}^{M} R_i z_i^k + n(k);\ k = 0, ..., N-1 \tag{5.2}$$

where $z_i = e^{(\sigma_i + j\omega_i)\Delta t}$ are the poles of the system.

Parameters A_i and θ_i are calculated from the complex residues, whereas σ_i and ω_i are estimated from the eigenvalues of the system poles. Since the poles z_i are found as the solution of a generalized eigenvalue problem, limitation on the number of modes *M* that can be extracted is removed. To calculate the eigenvalues and eigenvectors of the signal, from the sampling sequence given in (5.2), the first step is to form a *(N-L)× (L+1)* Hankel matrix:

$$[Y] = \begin{bmatrix} y(0) & y(1) & \cdots & y(L) \\ y(1) & y(2) & \cdots & y(L+1) \\ \vdots & \vdots & \ddots & \vdots \\ y(N-L-1) & y(N-L) & \cdots & y(N-1) \end{bmatrix}_{(N-L)\times(L+1)} \tag{5.3}$$

where *L* is called pencil parameters, and it represents the free-moving window length. It has been shown that the right choice of the pencil parameter helps when dealing with noisy signals [94]. Performance of the method is maximized if *L* is selected to be *L=N/2*, making

MPM perform close to the optimal Cramer-Rao bound [92]. Cramer-Rao bound represents the best results that one can achieve in a noisy environment.

Furthermore, two additional matrices $[Y_1]$ and $[Y_2]$ are constructed from $[Y]$ by deleting its last and first columns, respectively.

$$[Y_1] = \begin{bmatrix} y(0) & y(1) & \cdots & y(L-1) \\ y(1) & y(2) & \cdots & y(L) \\ \vdots & \vdots & \ddots & \vdots \\ y(N-L-1) & y(N-L) & \cdots & y(N-2) \end{bmatrix}_{(N-L)\times L} \tag{5.4}$$

$$[Y_2] = \begin{bmatrix} y(1) & y(2) & \cdots & y(L) \\ y(2) & y(3) & \cdots & y(L+1) \\ \vdots & \vdots & \ddots & \vdots \\ y(N-L) & y(N-L+1) & \cdots & y(N-1) \end{bmatrix}_{(N-L)\times L} \tag{5.5}$$

Now, from the equations (5.2), (5.4) and (5.5) we can write:

$$[Y_1] = [Z_L][R][Z_R] \tag{5.6}$$

$$[Y_2] = [Z_L][R][Z_0][Z_R] \tag{5.7}$$

where

$$[R] = diag[R_1, R_2, ..., R_M] \tag{5.8}$$

$$[Z_0] = diag[z_1, z_2, ..., z_M] \tag{5.9}$$

$$[Z_L] = \begin{bmatrix} 1 & 1 & \cdots & 1 \\ z_1 & z_2 & \cdots & z_M \\ \vdots & \vdots & \ddots & \vdots \\ z_1^{(N-L-1)} & z_2^{(N-L-1)} & \cdots & z_M^{(N-L-1)} \end{bmatrix}_{(N-L)\times M} \tag{5.10}$$

$$[Z_R]=\begin{bmatrix}1 & z_1 & \cdots & z_1^{(L-1)}\\ 1 & z_2 & \cdots & z_2^{(L-1)}\\ \vdots & \vdots & \ddots & \vdots\\ 1 & z_M & \cdots & z_M^{(L-1)}\end{bmatrix}_{M\times L} \tag{5.11}$$

diag[] represents the diagonal matrix.

Next, we defined the matrix pencil as given in (5.12):

$$[Y_2]-\lambda[Y_1]=[Z_L][R]\{[Z_0]-\lambda[I]\}[Z_R] \tag{5.12}$$

where [*I*] is an identity matrix.

If pencil parameter *L* satisfies $M\leq L\leq N-M$, then the rank of $[Y_2]-\lambda[Y_1]$ is equal to *M* [92]. On the other hand, if $\lambda=z_i$, the *i*th row of $[Y_2]-\lambda[Y_1]$ is equal to zero, and the rank decreases to *M-1*. Therefore, the z_i is the generalized eigenvalue of the matrix pencil pair $\{[Y_2], [Y_1]\}$. To find poles, one should find the eigenvalues of the:

$$[Y_1]^{+}[Y_2]=\left\{[Y_1]^H[Y_1]\right\}^{-1}[Y_1]^H[Y_2] \tag{5.13}$$

The superscript "+" denotes the Moore-Pensore inverse or pseudoinverse matrix, superscript "H" stand for Hermitian (conjugate) transpose, and "-1" denotes inverse.

After solving (5.13) and obtaining z_i and *M*, the residues R_i can be calculated from the least square problem as given in (5.14);

$$\begin{bmatrix}y(0)\\ y(1)\\ \vdots\\ y(N-1)\end{bmatrix}=\begin{bmatrix}1 & 1 & \cdots & 1\\ z_1 & z_2 & \cdots & z_M\\ \vdots & \vdots & \ddots & \vdots\\ z_1^{(N-1)} & z_2^{(N-1)} & \cdots & z_M^{(N-1)}\end{bmatrix}_{N\times M}\begin{bmatrix}R_1\\ R_2\\ \vdots\\ R_M\end{bmatrix} \tag{5.14}$$

Finally, we can get the amplitudes, phases, frequencies, and damping factors as follows:

$$A_i = |R_i| \tag{5.15}$$

$$\theta_i = \arctan\left[\mathrm{Im}(R_i)/\mathrm{Re}(R_i)\right] \tag{5.16}$$

$$\omega_i = \arctan\left[\mathrm{Im}(z_i)/\mathrm{Re}(z_i)\right]/\Delta t \tag{5.17}$$

$$\sigma_i = \ln|z_i|/\Delta t \tag{5.18}$$

The damping ratio can be calculated using the following equation:

$$\zeta_i = \frac{1}{\sqrt{1+\left(\frac{2\pi}{\sigma_i}\right)^2}} \frac{\omega_i}{2\pi} \times 100\% \tag{5.19}$$

In the case of data that contains noise before estimating the desired number of poles, the sampled sequence should be conditioned to reduce the impact of the input noise. This can be achieved by applying the Singular Value Decomposition (SVD) of the matrix in (5.3). The SVD is a method for factorization of matrices of the form:

$$[Y] = [U][\Sigma][V]^H \tag{5.20}$$

where [Σ] is the rectangular diagonal matrix. The diagonal matrix elements σ_i, are the singular values of the matrix [Y]. The columns of [U] and [V] are unitary matrices containing the left-singular vectors and right-singular vectors of [Y], respectively. The SVD reduces the dimension of the data set while preserving the primary relationships within the set and ignoring the variations below some predefined threshold.

The Matrix Pencil decomposes [Y] with the SVD with the result being the poles and residuals. In this case, the SVD is also used to determine the number of modes (model order) M, in the observed signal. In the noiseless case, M is equal to the number of non-

zero singular values. However, in the presence of noise, singular values that were previously zero are perturbed and become non-zero. Now, the best way to approximate *M* is to look into the ratio of singular values of [*Y*], σ_i, to the largest singular value, σ_{max}, and compare to predefined Singular Value Threshold (SVT), defined as $SVT=10^{-p}$, where *p* represents the number of significant decimal digits. In this case, all singular values with the ratio below the threshold are considered noise and discarded. This step is reflected as a built-in pre-filtering process [94].

$$\frac{\sigma_i}{\sigma_{\max}} \approx SVT \tag{5.21}$$

Next, we can use the first *M* significant singular values to reconstruct the original matrix [*Y*], and the pair {[Y_1], [Y_2]}:

$$\begin{aligned} [V_s] &= [v_1, v_2, ..., v_M] \\ [Y_1] &= [U_s][\Sigma_s][V_{1s}]^H \\ [Y_2] &= [U_s][\Sigma_s][V_{2s}]^H \end{aligned} \tag{5.22}$$

where [Σ_s] is the first *M* columns of [Σ], and [V_{1s}] and [V_{2s}] are obtained from [V_s] by deleting its last and first rows respectively. Using the set of equations from (5.13)-(5.18), all desired shapes and parameters can be calculated.

5.3. Quantify the Impact of the Defected Data Sets – Case Studies

Evaluation and quantification of the PMU data errors impact on the application outcome is a vital step for target application credibility. One way to test sensitivity of the application is to artificially augment errors in the input data [116]ss.

The impact of the synchrophasors errors on the performance of the MPM is demonstrated through two examples:

- Artificially created single data sequence with known modal parameters.
- The transient stability simulation of a 2000-bus synthetic grid [102].

5.3.1. Single Synthetic Signal

a) Simulated signal decomposition, without noise

First, the signal given in (5.23) is used to generate an example data sequence with known modes:

$$y(t) = e^{-0.075t}\cos(2\pi * 0.15t) + e^{-0.15t}\cos(2\pi * 0.35t) + n(t) \tag{5.23}$$

where *n(t)* represents any flawed data (i.e., noise, outliers, and un-updated data), *y(t)* contains 300 points, and the signal is sampled at a rate of 30 Hz (a total of 10 seconds of sampled data is used for the analysis). This signal clearly has two modes at 0.15 Hz and 0.35 Hz with damping ratios of 7.96% and 6.82%, respectively. Fig. 31 shows the original clean data curve.

In order to apply the MPM to this data set, the pencil parameter *L* and the Singular Value Threshold need to be defined first. Values for the pencil parameter between *N/3* and *2N/3* are preferred, where *N* is the number of data points [94]. The fixed value of *L* in this study is calculated as follows:

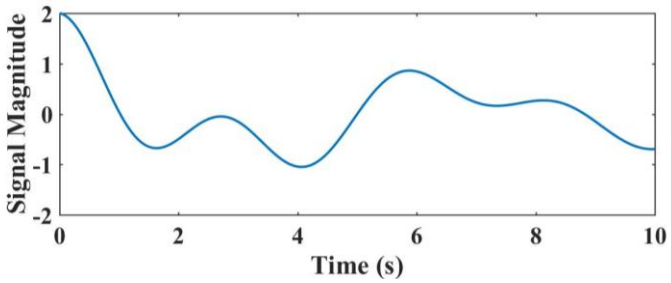

Figure 31. Original simulated signal.

$$L = ceil\left(1/2*\left(ceil\left(N/3\right)+ floor\left(N/2\right)\right)\right) \tag{5.24}$$

The MPM is very sensitive to the value of the SVT. For this example, all values in the range 0<SVT<0.692 allow correct extraction of the modes and its damping ratios. However, if the SVT is 0.693 then the MPM detects only one mode with a frequency of 0.147 Hz, which is relatively close to the original value of 0.15 Hz. However, the damping ratio is underestimated, with the values of 4.67% compared to 7.96%. Thus, the SVT plays a critical role in a case that signal is not "clean". In the following analysis, the optimal value of the parameter SVT is determined in the presence of noise and other flawed data.

b) Decomposition of the simulated signal with noise

In order to determine the optimal value of the SVT, white Gaussian random noise is added to the original synthetic signal with four values of the signal-to-noise ratio (SNR) ranging from 10-40dB. The number of estimated modes and the mean error between the original waveform without noise and one reconstructed from the modes calculated with the MP algorithm are considered. One hundred simulation runs for each test case were done and Fig. 32 shows the results from these analyses. The "stars" represent the value of the SVT for which the MPM correctly calculated the number of modes present in the original signal. The findings are summarized in Table 10.

The SVT max value mostly depends on the signal content while the SVT min value controls the process of removing the noise. With increasing the SVT, more noise is removed from the signal, and the reconstructed waveforms better fit the original, giving a highly accurate estimation of the mode parameters. However, a large value for the SVT could remove actual existing modes, so one has to be careful with the choice of the

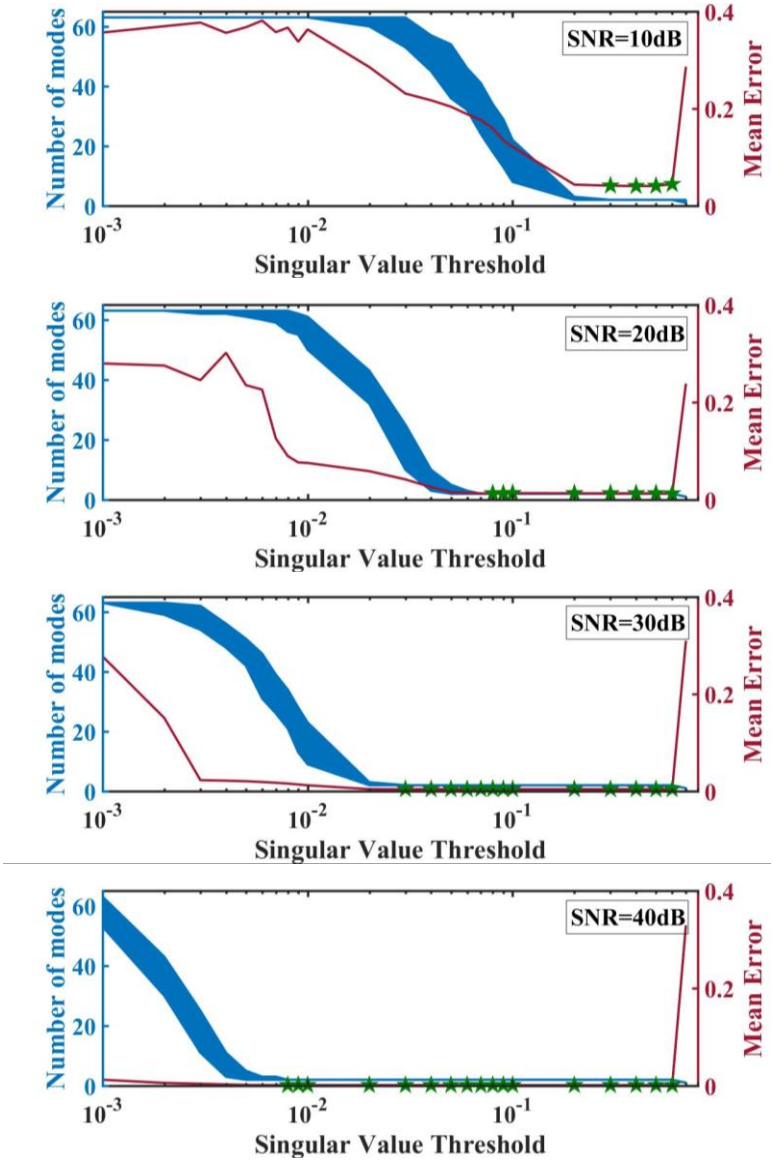

Figure 32. Number of modes and mean error of the reconstructed signal with four different values of additive noise.

threshold. Typical noise level present in PMU data is around 40 dB [101], which means that parameter SVT can take value as low as 0.008. To accommodate for the uncertainties and possible higher noise, we fixed the threshold value to 0.05. Later it will be shown that

Table 10. Limits of the singular value threshold in the presence of noise.

SNR (dB)	**Singular Value Threshold**	
	min	***max***
10	0.3	0.7
20	0.07	0.7
30	0.03	0.7
40	0.008	0.7

even value of 0.05 is some cases is too low, depending on the type of errors considered in the observed signal.

c) Decomposition of the simulated signal with arbitrary data injection

Table 11. Estimated mode parameters in the presence of arbitrary data injection.

Singular Value Threshold=0.05			
Frequency (Hz)	**Damping Ratio (%)**	**Lambda**	**Amplitude**
0.149	**8.32**	**-0.0779**	**0.992**
2.845	0.67	-0.1203	0.016
2.614	0.91	-0.1488	0.019
2.388	1.10	-0.1655	0.002
0.350	**7.59**	**-0.1671**	**1.022**
0.593	4.55	-0.1697	0.021
2.162	1.30	-0.1761	0.018
1.936	1.50	-0.1832	0.014
1.711	1.75	-0.1879	0.012
1.485	2.05	-0.1912	0.019
0.811	3.75	-0.1913	0.011
1.259	2.44	-0.1933	0.001
1.035	2.98	-0.194	0.020
Singular Value Threshold≥0.06			
0.149	8.24	-0.0772	0.988
0.350	7.53	-0.1659	1.0156

Here the tested data sequence is modified to contain data spikes lasting for a total of 0.13s in samples 172 to 175. These spikes could occur in real PMU data due to either time skew in the GPS or a cyber-attack [62]. Once again, the values of the SVT were swept with the results of the analyses presented in Fig 33. The calculated mode parameters are given in Table 11.

When the SVT is equal to 0.05 the number of estimated modes is 13, much higher than the original. However, it is not hard to differentiate "real" modes from the spurious

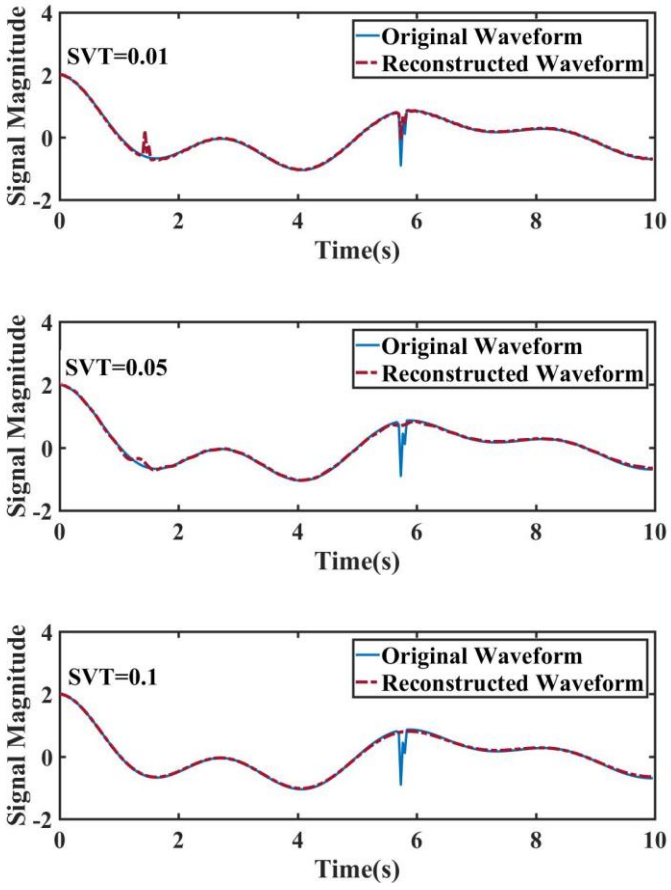

Figure 33. Simulated and reconstructed waveforms in the presence of data spikes.

based on the amplitude values that are at least one order higher for the present modes. Furthermore, both "real" mode frequencies are calculated with a maximum error of 0.01 Hz. The damping ratio is overestimated for both modes with the maximum error equal to 0.77%. Increasing the value of SVT to 0.06 gives the exact number of modes and a slightly better estimate of the damping ratio. However, if the SVT decreases to 0.01, the number of modes is 63, and the error is much higher. In addition, it was observed that by increasing the length of the corrupted data segments the higher value of the SVT is required.

d) Decomposition of the simulated signal with un-updated data

Next, a 0.5s long sequence of un-updated data from 6.5s to 7s is added to the clean data sequence with the results shown in Fig 34. For all values of the SVT higher than 0.05,

Table 12. Limits of the singular value threshold in the presence of un-updated data.

Singular Value Threshold≥0.05			
Frequency (Hz)	Damping Ratio (%)	Lambda	Amplitude
0.150	6.58	-0.0621	0.978
0.347	7.41	-0.1616	1.033

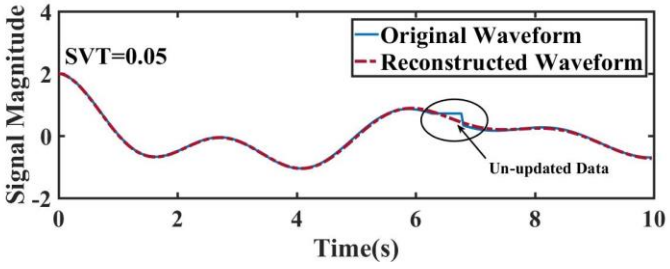

Figure 34. Simulated and reconstructed waveforms with the un-updated data.

the MPM was able to correctly estimate the number of modes with the results given in Table 12.

5.3.2. Large Synthetic Network

A 2000-bus network that is publicly available at [104] is used to generate the synthetic synchrophasor measurements. Figure 35 shows 500kV part of the transmission network along with the 13 synchrophasors located in the substations with the large generators. The waveforms used for this study are from the virtual PMU frequency measurements in response to the loss of generator in the substation "MIAMI". The sampling frequency is initially set to 0.5 cycles, and data is later re-sampled with the factor four, to get the reporting rate of 30 frames per second. The simulation duration is 20s, producing 600 points per PMU channel. Figure 36 shows the original measurements, where each curve represents the frequency measurement acquired from one of the PMUs in the system. The authors in [103] developed the approach to tune the model dynamics, so that the synthetic data created using this fictitious network has the characteristics of actual networks.

To apply the MPM on the synthetic PMU data set, the following parameters for the algorithm are used: pencil parameter of L=250 is calculated using the (5.24) and the SVT is initialized to 0.05.

One additional step that need to be considered before the MPM could be applied onto the PMU data is data-detrending. The term "trend" designates a downwards or upwards shift in the data set over time. Removing a trend from the data set allows the analyses to focus on the underlying fluctuations. Hence, the data set is pre-conditioned.

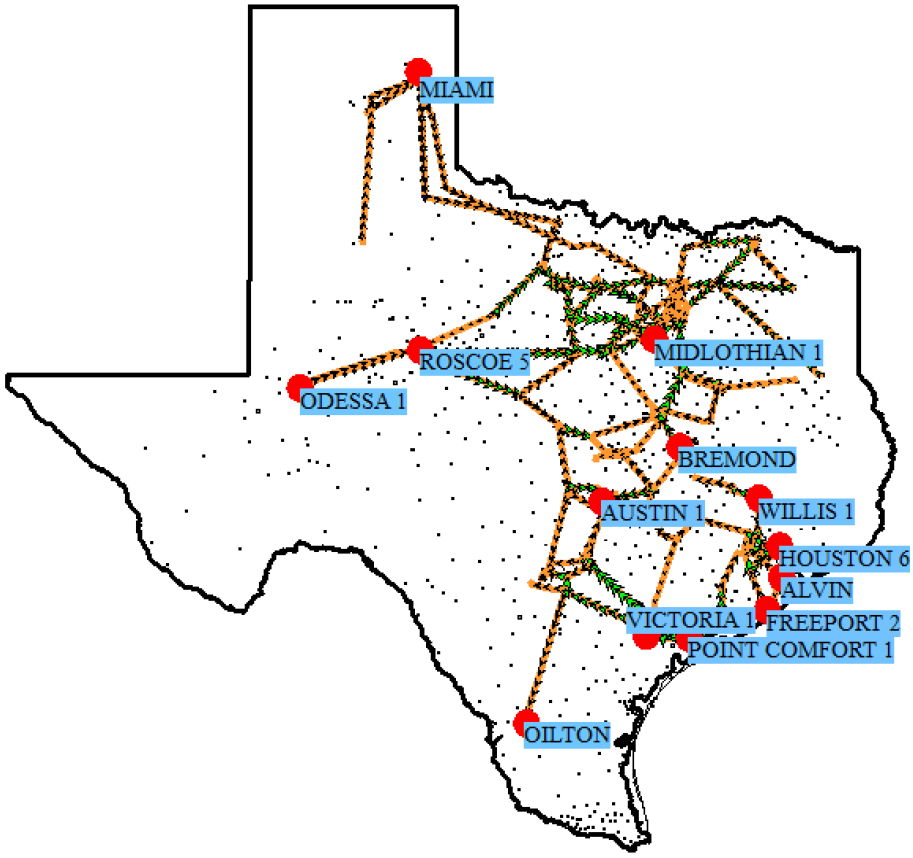

Figure 35. 2000 bus system with 13 virtual PMUs.

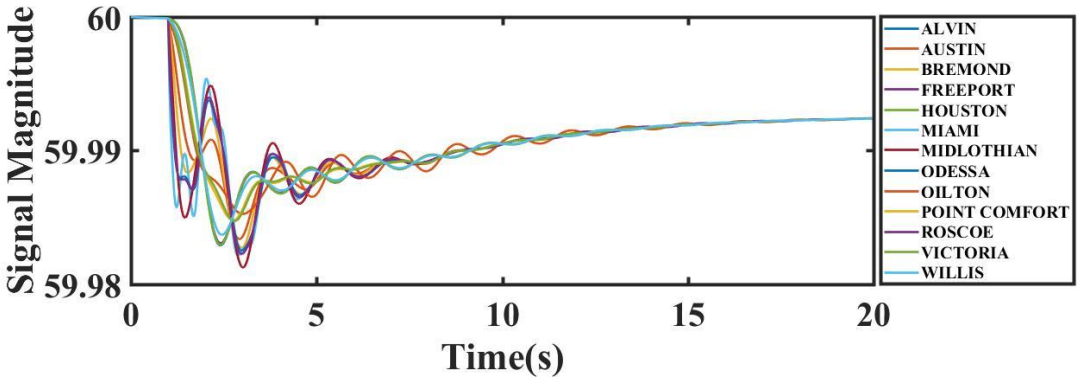

Figure 36. Original clean frequency measurements from 13 PMUs.

scaled by its respective standard deviation. Example of the de-trending processes is depicted in Fig. 37.

In general, the MPM is designed to process single signals. However, with small adjustments it can be used on the multi-channel data set. First, the Henkel matrix as given in (5.3) for each signal is constructed and at the end, all matrices are vertically concatenated to form one single matrix.

$$[Y] = \begin{bmatrix} [Y]_1 \\ [Y]_2 \\ \vdots \\ [Y]_k \end{bmatrix}_{(k(N-L))\times(L+1)} \tag{5.25}$$

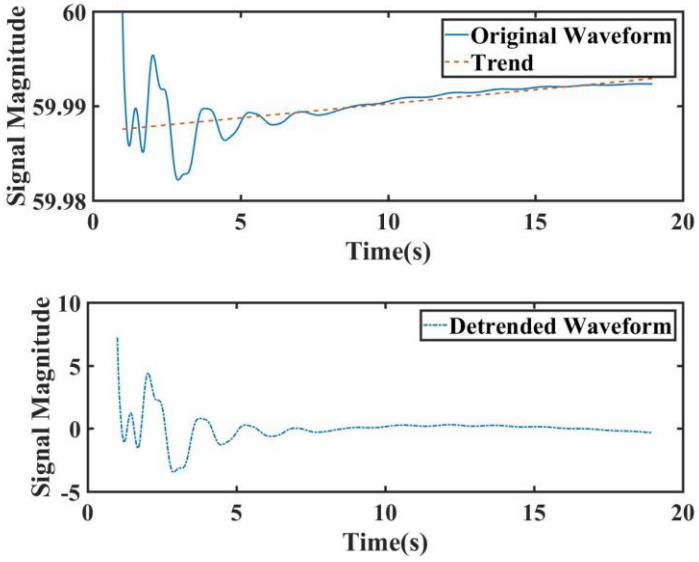

Figure 37. PMU frequency measurement (a) before detrending (b) with trend removed

Once the modes are estimated, (5.14)-(5.19) are used to evaluate the mode shapes and frequencies in each channel separately.

To verify the finding from the first set of case studies regarding the optimal value of SVT, additional sensitivity analysis was conducted, now on the synchrophasor frequency measurements, and the best results were achieved with the value of SVT=0.05. Figure 38 shows the solution of the MPM when the SVT is 0.05 and the estimated parameters are given in Table 13, including dominant modes frequencies, damping ratios, and lambdas. The tested case has seven dominant modes, and these results were utilized

Table 13. Modal parameters estimated from the 13 PMU frequency measurements.

Singular Value Threshold≥0.05		
Frequency (Hz)	**Damping Ratio (%)**	**Lambda**
0.061	24.55	-0.094
0.223	35.30	-0.496
0.329	34.36	-0.716
0.633	9.04	-0.360
0.660	7.96	-0.330
0.942	6.86	-0.407
1.828	8.78	-1.022

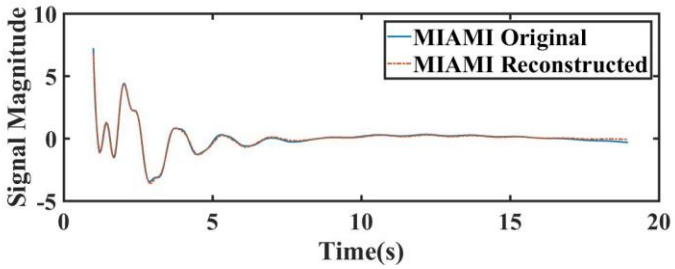

Figure 38. Clean frequency measurement and reconstructed signal.

as the reference point for the following analyses. In the next three case studies low-quality measurements were introduced to demonstrate the effectiveness of the MPM. In each case, one type of flawed PMU data has been randomly inserted into the data set.

a) Synchrophasor data with noise

First, Gaussian random noise with SNRs ranging from 40 to 20 dB were added to the original clean PMU data set. Figure 39 shows one data curve with the applied noise with SNR=20 dB and the reconstructed waveform using the results from the MPM algorithm. Detail results are presented in Table 14.

As expected, the MPM could effectively extract all the modes with high accuracy despite the additive noise. It can be seen that this algorithm shows great resistance to the noise and successfully identifies all the dominant modes. The maximum frequency error is 0.003 Hz and the damping ratio error is 1.2%.

b) Synchrophasor data with outliers

Next, the test data set of the 13 synthetic PMU frequency measurements was modified with small constant values of random "data spikes" added to all of them. The length of

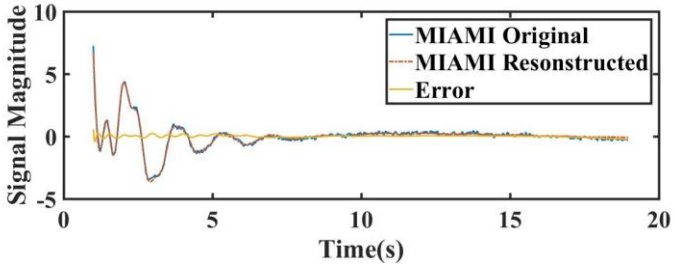

Figure 39. Noisy frequency measurement and the reconstructed signal.

Table 14. Modal parameters estimates from 13 PMU frequency measurements with noise and respective errors.

SNR (dB)	Frequency (Hz)	Frequency Error (Hz)	Damping Ratio (%)	Damping Ratio Error
40	0.061	0	24.48	-0.075
	0.223	-0.0002	35.21	-0.090
	0.329	-0.0003	34.50	0.147
	0.633	0.0002	9.04	-0.002
	0.659	-0.0004	7.96	0.001
	0.943	0.0005	6.84	-0.016
	1.828	-0.0001	8.77	-0.012
30	0.061	0	24.40	-0.148
	0.222	-0.0011	36.50	1.200
	0.331	0.0016	33.81	-0.549
	0.633	0.0000	8.82	-0.216
	0.659	-0.0005	8.19	0.234
	0.945	0.0028	6.80	-0.056
	1.827	-0.0010	8.80	0.014
20	0.061	0.0001	24.90	0.346
	0.222	-0.0014	36.38	1.076
	0.334	0.0044	33.60	-0.762
	0.632	-0.0009	8.52	-0.519
	0.661	0.0015	8.61	0.656
	0.946	0.0033	6.72	-0.139
	1.832	0.0038	8.71	-0.078

each corrupted data segment is 0.13s. Figure 40 shows the reconstructed waveform with the presence of spike; the results are summarized in the Table 15. It can been seen that the MPM is relatively immune to this type of flawed PMU data.

c) Synchrophasor data with un-updated data segments

In this test case a 0.5s duration of the tested sequence was modified to contain an un-updated segment for all 13 waveforms simultaneously. This type of error can arise due to the issues in PDC or the communication traffic. Figure 41 shows one of the original

Table 16. Modal parameters estimates from 13 PMU frequency measurements with spikes and respective errors.

Frequency (Hz)	Frequency Error (Hz)	Damping Ratio (%)	Damping Ratio Error
0.061	0.0003	21.12	-3.436
0.202	-0.0207	48.76	13.456
0.345	0.0154	23.97	-10.386
0.629	-0.0043	9.47	0.435
0.665	0.0053	7.19	-0.766
0.945	0.0025	5.87	-0.988
1.829	0.0010	7.98	-0.806

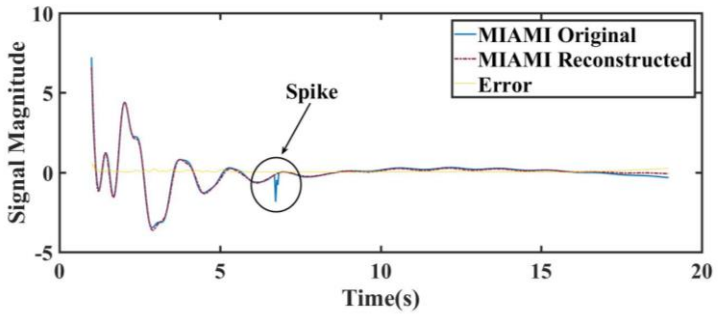

Figure 40. Frequency measurement with the spikes and the reconstructed signal.

measurement curves along with the reconstructed one. Mode parameters are given in Table 16. Even though all the real modes are detected, in this test case, there is one additional “fake” mode extracted with the low damping ratio. This leads to the conclusion that some pre-screening of PMU data should take place, to avoid false detection and alarms.

Table 17. Modal parameters estimates from 13 PMU frequency measurements with un-updated and respective errors.

Frequency (Hz)	Frequency Error (Hz)	Damping Ratio (%)	Damping Ratio Error
0.063	0.0015	25.16	0.613
0.197	-0.0262	53.43	**18.129**
0.369	**0.0394**	25.78	-8.574
0.639	0.0060	12.96	3.923
0.673	0.0134	5.73	-2.231
0.935	-0.0071	5.30	-1.560
1.162	**1.1618**	**2.13**	**2.134**
1.804	-0.0248	8.03	-0.755

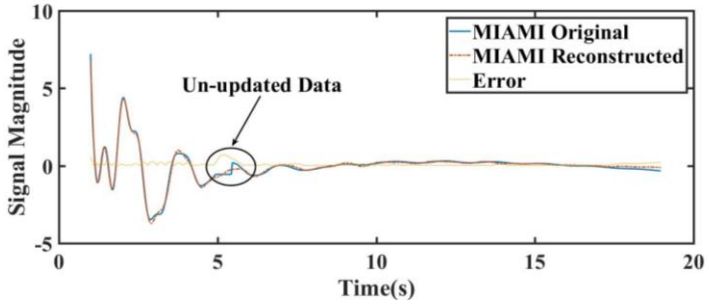

Figure 41. Frequency measurement with un-updated data and the reconstructed signal.

5.4.Principal Component Pursuit

Issues in the synchrophasor data are direct consequence of the measurement equipment limitations (e.g., accuracy, limited precision, and failure), communication gear noise, and cyber-attacks. Many of the bad data detection methods are still based on SE, though it has been shown that when smart cyber-attack is launched, traditional SE methods

will fail (bypass) to detect it, putting the system in danger. To deploy the SE-based BD detection and correction technique, previous knowledge on the system model is necessary, which in turn may result in non-reliable bad data detection when system topology is inaccurate. Therefore, the detection accuracy of the SE-based approaches may be affected when gross errors are presented in system topology or parameters. Furthermore, these methods cannot operate successfully when state estimation diverges because of gross measurement errors, system physical disturbances, or stressful operating conditions.

Techniques that require prior knowledge of the network parameters and/or system topology might be affected by the errors in the topology/parameters, giving the significant advantage to the purely data-driven methods, among which are: Principal Component Analyses (PCA), low-rank matrix approach, density based Local Outlier Factor detection techniques (LOF), clustering. Due to the inherent temporal correlation of power grid states and the strong spatial correction, matrix whose columns are PMU measurements exhibits the low-rank structure. Low-rank matrix techniques are block-based processing methods, and potential applications include the recovery of missing PMU data, detection of the outliers, cyber-attacks. One interesting approach for the recovery of a low-rank matrix is the Principal Component Pursuit (PCP), which is based on a convex problem that can be solved by applying an augmented Lagrangian multiplier (ALM)-based algorithm [64]. In contrast to PCA, PCP guaranties recovery of the low-rank matrix despite the gross sparse errors. The PCP is also called Robust Principal Component Analysis.

5.4.1. Mathematical Formulation

The matrix *M* whose columns are the time-series PMU measurements can be represented as a sum of two matrices, low rank matrix L_0 and the sparse matrix S_0 that contains any error present in the data set.

$$M = L_0 + S_0 \tag{5.26}$$

S_0 is a sparse matrix with a few non-zero entries. Compared to the PCA, here both matrices, L_0 and S_0 can have arbitrary magnitudes. Moreover, the column and row space of the L_0 are unknown. To recover the L_0 from the *M*, following convex optimization problem needs to be solved:

$$\min_{L,S} \|L\|_* + \lambda \|S\|_1 \quad subject\,to\, M = L + S \tag{5.27}$$

where $\|\cdot\|_*$ denotes the nuclear norm and $\|\cdot\|_1$ is the l_1 norm. Nuclear norm is equal to the sum of the singular values ($\|X\|_* = \sum_i \sigma_i(X)$), and l_1 norm is sum of the absolute values of the matrix elements ($\|X\|_1 = \sum_{ij} |X_{ij}|$). λ represents a regularization parameter. PCP simply minimizes a weighted combination of the two norms (nuclear and l_1).

Singular Value Decomposition of $L_0 \in \mathbb{R}^{n_1 \times n_2}$ is given as:

$$L_0 = U \Sigma V^* = \sum_{i=1}^{r} \sigma_i u_i v_i^* \tag{5.28}$$

where *r* is the rank, σ_i are the singular values, and *U* and *V* are the matrices of the left- and right- singular vectors of the *L*, respectively.

The PCP solves the optimization problem under rather week assumption that the matrix S_0 is not a low-rank matrix and that the L_0 is not sparse. Given assumption solves

the identifiability issue of S_0, and it is satisfied if S_0 is uniformly random in being sparse for all subsets of size m, where m (support of S_0) denotes the number of nonzero entries of the matrix S_0 ($m = \|S_0\|_0$).)

Theorem 1 [105]: Suppose $L_0 \in \mathbb{R}^{n \times n}$ satisfies the incoherency conditions (5.29) with parameter μ on right- and left- singular vectors matrices of L_0 given in (5.28).

$$\max_i \|U^* e_i\|^2 \le \frac{\mu r}{n_1}, \max_i \|V^* e_i\|^2 \le \frac{\mu r}{n_2}, \|UV^*\|_\infty \le \sqrt{\frac{\mu r}{n_1 n_2}} \tag{5.29}$$

where e_i's are the canonical basis vectors, and $\|\cdot\|$ denotes the 2-norm and $\|\cdot\|_\infty$ is the $l\infty$ norm, such that $\|X\| = \sqrt{\sum_{ij} \left(X_{ij}\right)^2}$ and $\|X\|_\infty = \max_{i,j} |X_{i,j}|$.

Moreover, supposed that the S_0 is uniformly distributed. Then there is a constant c such that with probability at least $1\text{-}cn^{-10}$ (over the choice of support of S_0), Principal Component Pursuit (5.27) with $\lambda = 1/\sqrt{n}$ recovers L_0 and S_0 exactly, provided that:

$$rank\left(L_0\right) \le \rho_r n \mu^{-1} \left(\log n\right)^{-2} \quad and \quad m \le \rho_s n^2 \tag{5.30}$$

where ρ_r and ρ_s are some positive numerical constants.

In more general case, when L_0 is not a square matrix Principal Component Pursuit with $\lambda = 1/\sqrt{n_{(1)}}$ exactly recovers L, with the probability at least $1\text{-}cn_{(1)}^{-10}$, provided that:

$$rank\left(L_0\right) \le \rho_r n \mu^{-1} \left(\log n_{(2)}\right)^{-2} \quad and \quad m \le \rho_s n_{(1)} n_{(2)} \tag{5.31}$$

where $n_{(1)} = \max(n_1, n_2)$ and $n_{(2)} = \min(n_1, n_2)$.

As per definition λ parameter is data independent and even a large rank matrices can be recovered from the sparse errors. The PCP method works because the corrupted

data stream can be recovered based on the previous behavior of all signals and current behavior of the uncorrupted data streams by capturing the low-rank subspace for the current data window.

5.4.2. Algorithm

Several efficient algorithms have been proposed to solve the PCP convex optimization problem among which are interior point method [106], iterative tresholding approach [107], and accelerated proximal gradient method [108]. However, interior point method is limited to a small set of data ($n<100$) due to the high computational burden in finding the step direction, consequently its approach on the synchrophasor data blocks is not suitable. Although the scalability problem was resolved using the iterative methods, it has been shown that the convergence of this methods is not sufficient. Empirical results show that the convergence rate of the accelerated proximal gradient method is up to 50 times faster, while practical performance of the above-mentioned method exhibits certain accuracy issues during the recovery process, and it requires many tunings. In this dissertation, the Augmented Lagrange Multiplier (ALM) -based Algorithm is utilized to solve the PCP problem. Main advantages of this group of algorithms are the higher accuracy and the fast convergence. Further, the minimal settings are required, making the ALM attractive solution.

Constrained optimization problem (5.27) is solved by converting it to the series of unconstrained minimization problems. The ALMA operates in the augmented Lagrangian defined with:

$$l(L,S,Y) = \|L\|_* + \lambda\|S\|_1 + \langle Y, M - L - S\rangle + \frac{\mu}{2}\|M - L - S\|_F^2 \tag{5.32}$$

Where Y denotes the Lagrange multiplier matrix and μ is the regularization parameter. $\|\cdot\|_F$ represents the Forbenius Norm of the matrix, defined as the square root of the sum of the absolute squares of its elements, $\|X\|_F = \sqrt{\sum_i \sum_j |X_{i,j}|^2} = \sqrt{\sum_i^{\min\{n_1,n_2\}} \sigma_i^2(X)}$. Operator $\langle\cdot\rangle$ designates the sum of product of corresponding elements defined as $\langle X, Y\rangle = \sum_i \sum_j X_{ij} Y_{ij}$. Objective of the ALMA is to minimize the $l(L,S,Y)$. The generic LM algorithm solves the PCP by repeating two steps:

1: Solve: $(L_i, S_i) = \arg\min_{L,S} l(L,S,Y_i)$

2: Update Lagrange multiplier matrix: $Y_{i+1} = Y_i + \mu(M - L_i - S_i)$

Sequence of the convex programs that need to be solved in the first step does not have an optimal solution [105], and more efficient method called *alternating directions* that is based on the ALMA is utilized instead [109]. Here, step one is divided into two sub-steps, where $l(L,S,Y)$ is first minimized in respect to L with fixed S (5.33). Next, the same problem is solved, this time with respect to S while keeping L fixed (5.34).

$$\arg\min_L l(L,S,Y) = \mathcal{D}_{1/\mu}\left(M - S + \mu^{-1}Y\right) \tag{5.33}$$

$$\arg\min_S l(L,S,Y) = \mathcal{S}_{\lambda/\mu}\left(M - L + \mu^{-1}Y\right) \tag{5.34}$$

$\mathcal{D}_\tau(X)$ is the singular value thresholding operator given by (5.35). and $\mathcal{S}_\tau : \mathbb{R} \to \mathbb{R}$ is the shrinkage operator defined as in (5.36).

$$\mathcal{D}_{\tau}\left(X\right)=U\mathcal{S}_{\tau}\left(\Sigma\right)V^{*} \tag{5.35}$$

$$\mathcal{S}_{\tau}\left[x\right]=\operatorname{sgn}\left(x\right)\max\left(\left|x\right|-\tau,0\right) \tag{5.36}$$

Steps of the utilized algorithm are as follows:

1: Initialize: $S_0 = L_0 = Y_0 = 0,\ \mu > 0$

2: While not (stop criteria), do

a. compute: $L_{i+1} = \mathcal{D}_{1/\mu}\left(M - S_i + \mu^{-1}Y_i\right)$

b. compute: $S_{i+1} = \mathcal{S}_{\lambda/\mu}\left(M - L_{i+1} + \mu^{-1}Y_i\right)$

c. update: $Y_{i+1} = Y_i + \mu(M - L_{i+1} - S_{i+1})$

3: end while

The major computational burden is related to the computation of the low-rank matrix, *L*, by performing the SVT in each iteration. According to the (5.35)-(5.36) only the singular vectors that correspond to the singular values larger than the threshold μ need to be calculated. Choice of the threshold μ and the stopping criteria is the crucial for the efficient implementation of the algorithm.

In this work we conducted sensitivity analyses to previously mentioned settings and the results are given in the following section.

5.4.3. Numerical Examples

In this section, the performance of the Principal Component Pursuit for the recovery of the defected PMU data is explored. We demonstrated the effectiveness of the PCP through series of the examples of synthetic PMU data sets containing various data quality issues.

Once again, we considered a positive-sequence 2000-bus synthetic network with PMUs placed at the high voltage (500kV) buses shown in Fig. 35. Total of 120 PMU frequency measurements of 20s duration are captured for the analyses. A PMU reporting rate is set to 30 frames per second, with a total number of points equal to 600 per channel. Before applying the PCP first-order de-trending was performed removing the linear trend from all signals. We considered three types of data issues named: noise, outliers, and un-updated data, under both, ambient and transient conditions.

a) Ambient Conditions

To create the ambient synthetic data we injected the white Gaussian noise in the load terminals. Figure 42 shows the 20s long high-quality PMU frequency measurements used as the reference case in the following analyses. The objective of those analyses is to explore the ability of the PCP algorithm to recover the corrupted measurements while preserving the underlying data behavior.

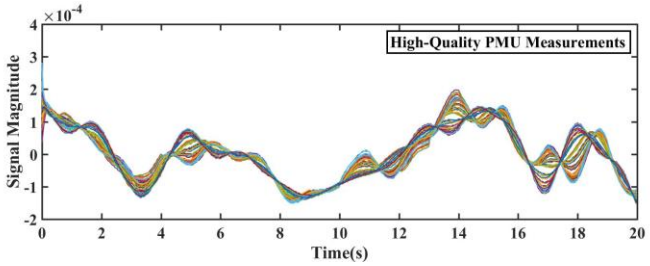

Figure 42. Clean de-trended PMU frequency measurement: ambient condition.

Synthetic PMU data with noise

First, we considered presence of the noise. We added additional white Gaussian noise to the twenty percent of the waveforms simultaneously (total of 24 measurements). Figure 43 shows PMU frequency measurements before and after the PCP was applied to the data set along with the error between reconstructed and original noise-free measurements. Duration of the inserted high-sensing noise segments is 0.5s. The results

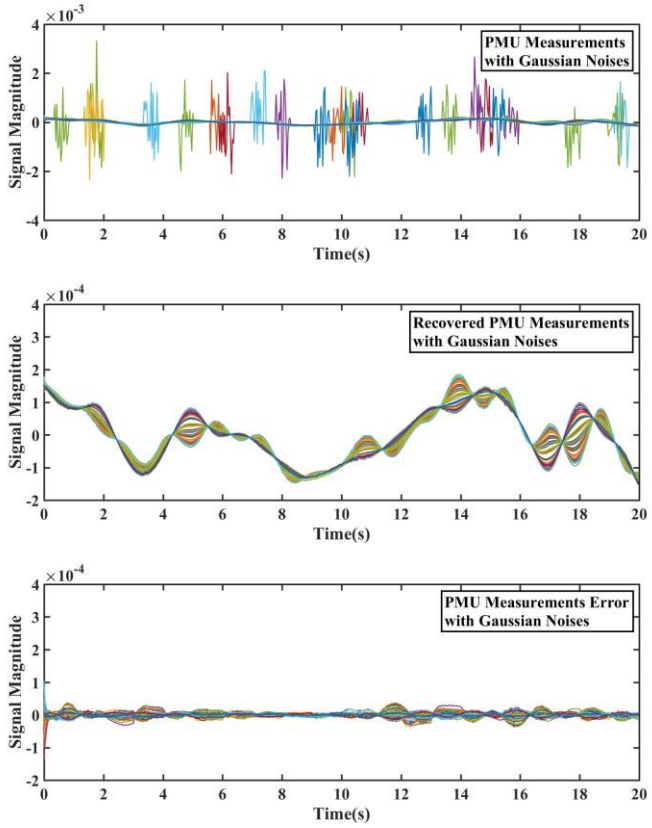

Figure 43. Synthetic PMU frequency measurements with noise under ambient conditions.

show that the PCP was able to successfully smooth measurement curves and remove the inserted noises. All 24 noisy segments are removed from the PMU measurements.

Synthetic PMU data with outliers

Next, we explored the performance of the PCP in a case when the PMU data contains the "spikes". The test data set contains 120 frequency measurements, of which 20% contain outliers. The magnitude and position of the outlier in the measurement sequence are arbitrary injected. The results of the analyses are depicted in Fig. 44. The top

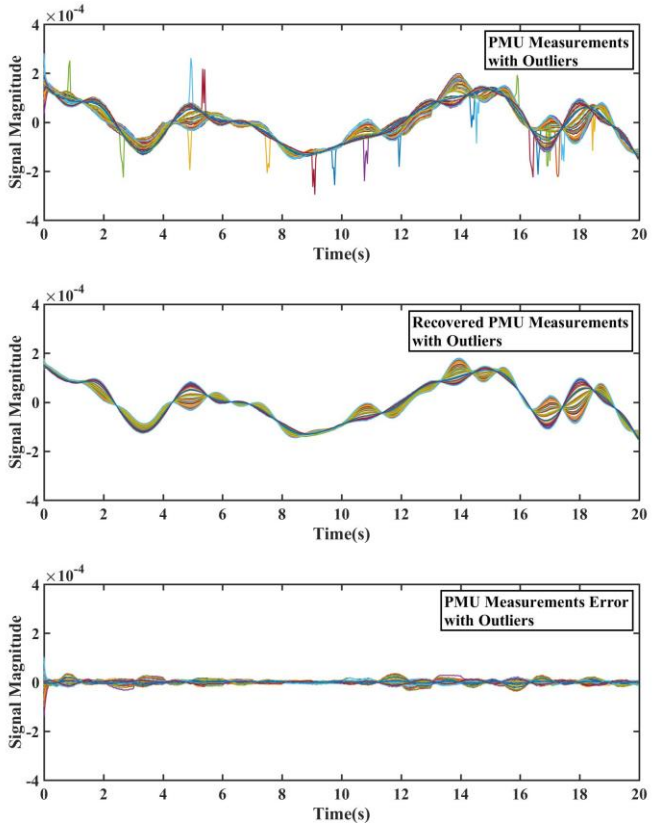

Figure 44. Synthetic PMU frequency measurements with outliers under ambient conditions.

graph shows the PMU frequency measurements with the spikes. Next, we plotted the recoved measurements followed by the error. It can be seen that the error is close to zero which means that the PCP successfully removed all the corrupted segments.

Synthetic PMU data with un-updated data segments

Lastly, we illustrated the ability of the PCP to recover the measurement points in a case when the waveforms contain un-updated segments. Figure 45 shows three curves

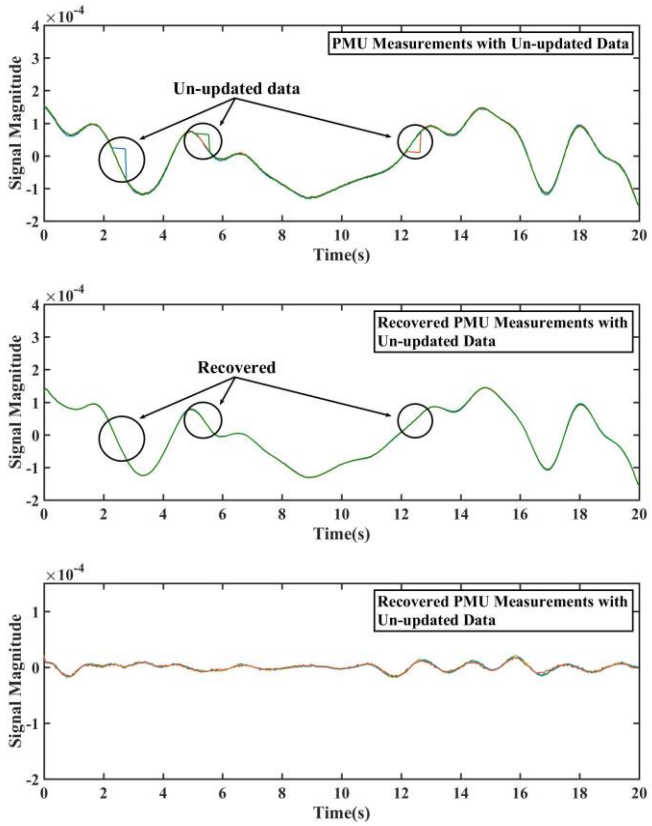

Figure 45. Synthetic PMU frequency measurements with un-updated data segments under ambient conditions.

that contain 0.5s long un-updated data. In all the corrupted signals proposed method detected the error and recovered the PMU curves.

In all the above case studies under ambient conditions, results show that the proposed methodology is suitable for detection and correction of the PMU data measurements.

b) Transient Conditions

In this section, we investigated the performance capabilities of the PCP method when the signals under considerations are generated from the large synthetic system during disturbance. The objective of these studies is to show the advantages of using the PCP method as a pre-screening tool for the Matrix Pencil Method for the modal extraction. In the section 5.3.2 of this dissertation, we proposed the MPM algorithm for the modal analyses when the synthetic PMU data curves are corrupted. From the results of some of the cases, MPM extracted incorrect modes, imposing a need to employ the data pre-screening tool.

We repeat studies from the section 5.3.2, but now the data set is pre-condition and cleaned with the PCP method before we applied the MPM.

Figures 46-48 show three case studies introduced in the section 5.3.2, where the original PMU frequency curves were corrupted with the noise, outliers, or contain un-updated data segments. Top figures depict three data curves when the corruption is applied to the original clean frequency measurements; the reconstructed signals from the MPM estimates are presented in the middle and the errors are given at the bottom graph. The

Table 18. Modal parameters estimates error from synthetic PMU frequency measurements with noise with and without PCP.

Frequency Error (Hz)		**Damping Ratio Error**	
Without PCP	**With PCP**	**Without PCP**	**With PCP**
0.0001	-0.0037	0.346	0.407
-0.0014	0.0115	1.076	**0.384**
0.0044	0.0054	-0.762	**-0.103**
-0.0009	**-0.0006**	-0.519	**-0.127**
0.0015	0.0059	0.656	**0.381**
0.0033	0.0114	-0.139	-0.303
0.0038	0.0033	-0.078	-1.201

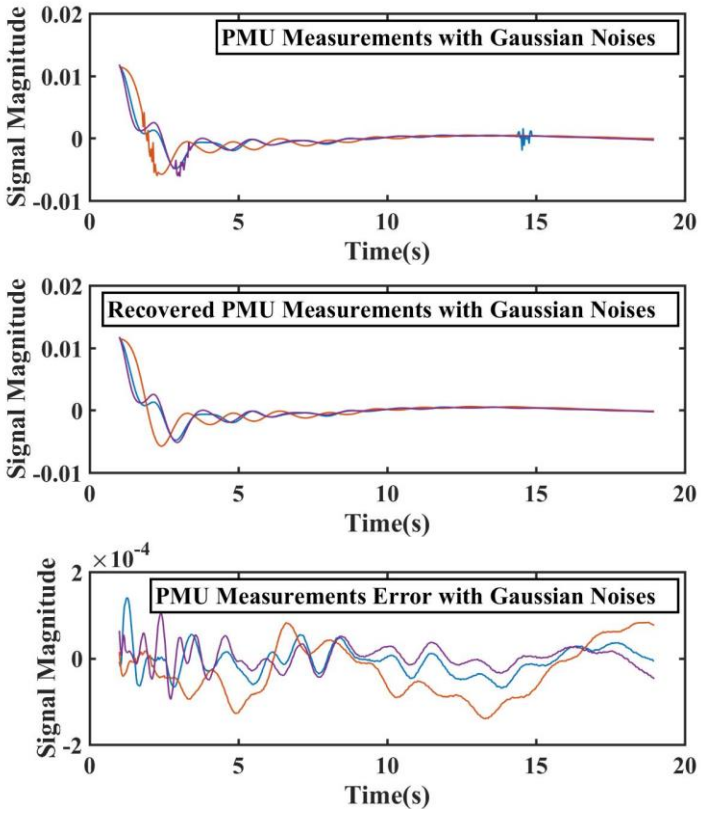

Figure 46. Synthetic PMU frequency measurements with noise under transient conditions.

Table 19. Modal parameters estimates errors from synthetic PMU frequency measurements with spikes with and without PCP.

Frequency Error (Hz)		**Damping Ratio Error**	
Without PCP	**With PCP**	**Without PCP**	**With PCP**
0.0003	-0.0036	-3.436	**0.383**
-0.0207	**0.0111**	13.456	**0.708**
0.0154	**0.0055**	-10.386	**-0.344**
-0.0043	**-0.0007**	0.435	**-0.067**
0.0053	0.0062	-0.766	**0.311**
0.0025	0.0119	-0.988	**-0.340**
0.0010	0.0041	-0.806	-1.219

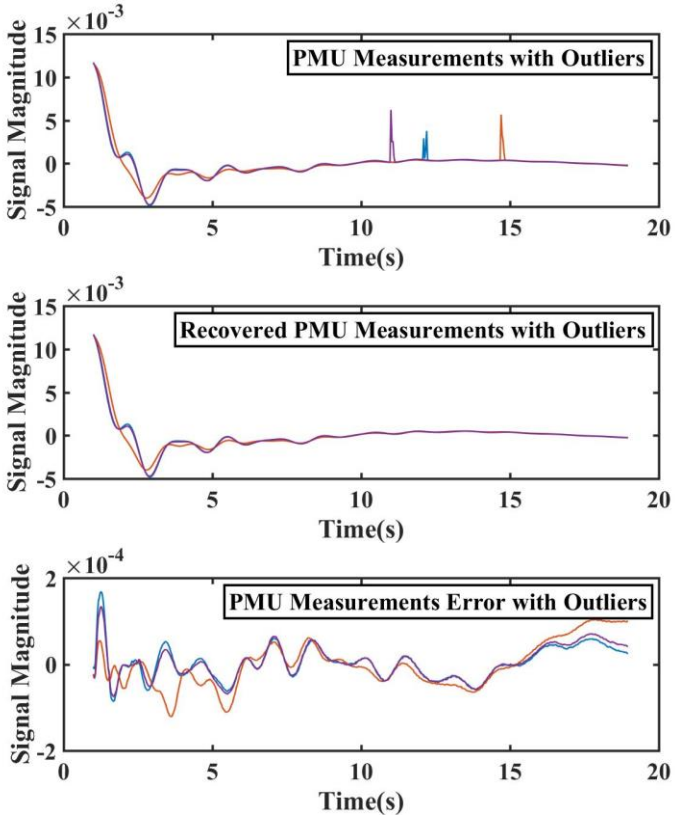

Figure 47. Synthetic PMU frequency measurements with outliers under transient conditions.

Table 20. Modal parameters estimates errors from synthetic PMU frequency measurements with un-updated with and without PCP.

Frequency Error (Hz)		Damping Ratio Error	
Without PCP	**With PCP**	**Without PCP**	**With PCP**
0.0015	-0.0037	0.613	**0.252**
-0.0262	**0.0113**	18.129	**0.308**
0.0394	**0.0055**	-8.574	**-0.036**
0.0060	**-0.0008**	3.923	**-0.139**
0.0134	**0.0063**	-2.231	**0.393**
-0.0071	0.0112	-1.560	**-0.317**
1.1618	**N/A**	**2.134**	**N/A**
-0.0248	**0.0053**	-0.755	-1.270

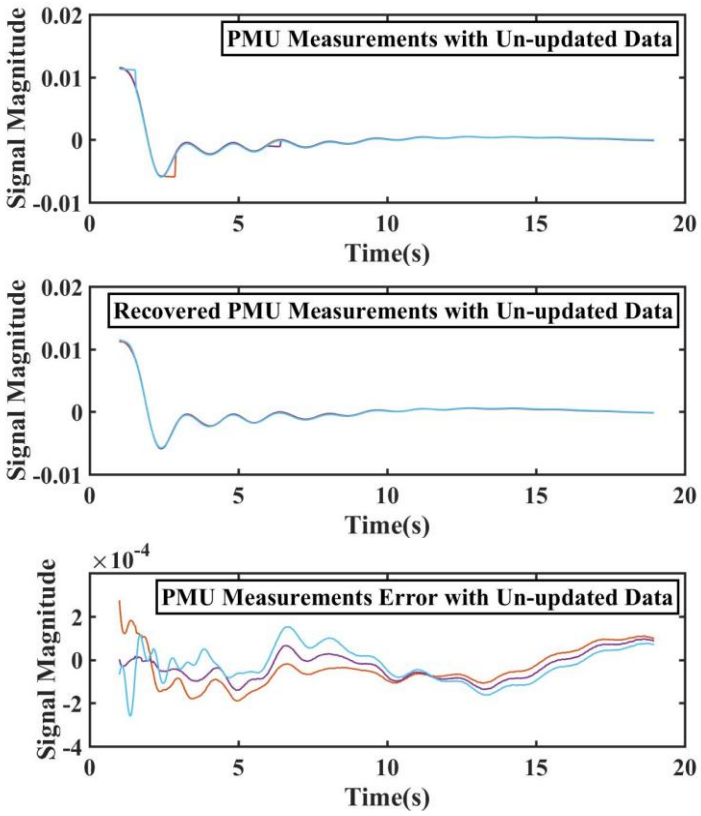

Figure 48. Synthetic PMU frequency measurements with un-updated data under transient conditions.

error is defined as a difference between the original curve without corruption and a reconstructed curve from the MPM analyses.

To highlight the advantages of using the PCP as a pre-screening tool for the MPM algorithm, we compared the errors in the frequency and damping ratios in the case when only the MPM algorithm was used for the modal analyses and when we applied the PCP algorithm. Results from the three case studies, when PMU data contains noise, outliers and un-updated segments are reported in the Tables 17-19. It can be seen that in most of the cases, the error is lower, and if not, it is in the same order as in case when there was no pre-screening tool applied. In the case when the PMU data contains the un-updated segments, MPM alone extracted the “fake” mode, with very low damping ratio which in return could trigger the false alarms and reduce the reliability of the monitored grid. However, when we applied the PCP this problem was resolved.

6. CONCLUSION

6.1. Summary of Contributions

The synchrophasor infrastructure is a mission-critical system and, it is expected to operate reliably each time it is called upon. However, the PMU data is often delivered with various data quality issues, hindering PMUs to be fully incorporated and deployed in control and operation practices. Regardless of the application, certain testing and performance validation of PMUs and the end-to-end synchrophasor system are essential to confirm measurement accuracy and continuously ensure high reliability and trustworthiness.

This research examines a number of procedures and testing tool implementation techniques to reach a better understanding of the PMU measurement limitations imposed on the synchrophasor applications, and improve the quality of synchrophasor data.

The main contributions and achievements of this research are summarized as follows:

- *Testing framework for the PMUs and synchrophasor systems.*

  This dissertation introduces the comprehensive framework for testing and evaluation of the PMU devices and synchrophasor end-to-end system. The proposed testing framework conducts the synchrophasor performance assessment in three steps:

1: *Type testing*: conducted in the synchrophasor calibration laboratory according to accepted industrial standards;

2: *Application testing*: conducted to evaluate the performance of the PMUs under faults, transients, and other disturbances in power systems;

3: *End-to-end testing*: conducted to assess the risk and quantify the impact of measurement errors on the applications of interest. Two critical power system applications were considered in this dissertation, i.e. fault location and the modal analyses.

The developed testing methodology helps the end users to assess the benefits and to evaluate the risks associated with the use of PMU measurements in any or certain synchrophasor-based application.

- *Synchrophasor calibration laboratory.*

  In this effort, a unique PMU calibration lab is constructed to execute standardized PMU acceptance tests according to IEEE and IEC standards, such as the IEEE C37.118.1a among others. PMU test platform is developed to verify the performance of PMU device exposed to *type tests*. The validity of the testing and calibration procedure is confirmed with the systematic characterization of the testing hardware and software modules that was carried out in all stages of testing. Overall accuracy of the calibration system is assessed based on the following metrics: (a) the accuracy and stability of the timing reference, and (b) the ability to curtail the angle and magnitude uncertainties in the generated waveforms.

- *New metrics for the PMU performance evaluation.*

  In section 3, in conjunction with the standard performance requirements, this dissertation defines novel “metrics” for PMU performance evaluations under any static and dynamic conditions that may unfold in the grid. The new statistical metrics offer a more realistic understanding of the overall PMU performance and help the users to choose the appropriate device/settings for the target application. Rather than solely a pass/failed status, we proposed metric that highlights the success rate of all the test scenarios within a given *type test* and, as a result, is a reliable measure to recognize sustainable problems in a PMU device and differentiate them from ephemeral conditions that might have led to a test failure. The proposed probabilistic technique can quantitatively reveal the PMU response to various test performance thresholds specified by corresponding IEEE standards as well as the probability of specific failures to meet the standard requirements. The trends revealed by such probabilistic metrics could help in better planning the maintenance periods and future in-filed testing procedures.

- *Synchrophasor testbed.*

  In section 4, we introduced full-scale synchrophasor production system that is instrumented with software and hardware to allow for testing, calibration and evaluation of various advanced developments in the synchrophasor technology. The testbed platform used for *application* and system *end-to-end testing* in this research, characterizing the PMU response under fault conditions and evaluating the impact of the PMU errors on the fault location application outcome is

implemented. Additionally, the developed infrastructure is generic enough to be employed not only for quantifying the impact of PMU errors on fault location algorithms, but also performing studies on trustworthy assessment of any end-use power system application that uses PMU measurements.

- *Application testing procedure.*

  Power system applications have different sensitivities to the data errors in the input measurements. The impacts of such input signal uncertainties and related application errors are largely unknown to the end-users and impose the need for the additional testing and evaluation beyond the standard.

  In this work, in section 4 we proposed the testing methodology named *application testing*. Application testing analysis and PMU performance evaluation under faults and other prevailing conditions offers a realistic assessment of the PMU measurement errors in real-world field scenarios and reveal additional performance characteristics that are crucial for the overall application evaluation. We generated a large set of the fault scenarios, and conducted the sensitivity analyses of various PMU settings. The performance of the stand-alone PMU device is evaluated when PMU is exposed to a set of input waveforms from the field. The testing results revealed additional, rather unknown, performance characteristics that are crucial for the overall application assessment, nevertheless still in alignment with the results acquired from the *type tests*. Following conclusions are derived at this stage of testing:

  1: Different PMU settings enhance or degrade performance of the device;

2: Even if a given algorithm does not pass some *type tests* according to the standard requirements, it still can perform satisfactory for a specific application in real world scenarios.

- *System end-to-end assessment in laboratory environment.*

  End-to-end tests are designed to quantify the impact of synchrophasor estimation errors and their propagation from the PMU toward the end-use applications and to evaluate the associated risk. *System end-to-end tests* are conducted by feeding the end-use synchrophasor applications with the measurements from real PMUs and quantifying the impact of measurement errors on the application of interest (e.g., fault location in the studied example). PMU response errors under the fault conditions are characterized and their impact on the performance of synchrophasor-based fault location algorithms that uses synchronized phasors at both line terminals is quantified. This use case demonstrates how to evaluate the impact of PMU response errors under fault conditions on the fault location application outcome through *system end to end testing*. The proposed methodology is generic enough to be employed not only for quantifying the impact of PMU errors on fault location algorithms, but also performing studies on trustworthy assessment of any end-use power system application that uses PMU measurements.

- *System end-to-end assessment in simulation environment.*

  With the deployment of the modern devices that are capable of capturing the dynamic responses of the system, such as PMUs an oscillatory response of the

system can be measured in real-time. If accurately estimated, system modes may help improve system modeling and the implementation of the control schemes, with a result of increased system reliability. However, PMU data is often delivered with various data quality issues. Data issues in the synchrophasor system can arise for a wide variety of reasons including topology errors, meter failures, and improper configurations. In section 5 of this dissertation, we focused on quantifying the impact of errors in input data on the modal extraction application. Different quality data issues are be applied to the input data (i.e. PMU frequency measurements), among which are noise, un-updated data and outliers. We used the Matrix Pencil Method for the modal extraction. The applicability of the MPM for the modal extraction from the time-domain data sequence was examined, and results were presented through two case examples. In this study, we found the optimal value of the singular value threshold for the proposed method, for which the MPM was able to accurately calculate the modes parameters in the presence of the flawed data, i.e., noise, outliers, and un-updated data. We also showed how the method could be applied on sets of multiple PMU streams, and we showed its ability to correctly detect and accurately characterize dominant modes after a major disturbance in the large-scale system in majority of the testing cases.

- *Recovery of the corrupted data.*

  Through series of the case studies for the modal extraction, we found that under some circumstances additional "fake" modes were extracted. Such results let to conclusion that certain pre-screening technique is mandatory for the reliable

application performance. Also, the Section 5 of this dissertation, investigates the application of the Robust Principal Component Analysis (RPCA) for the PMU data improvement and recovery. We demonstrated the effectiveness of the proposed method through series of the examples of synthetic PMU data sets containing various data quality issues. We considered three types of data issues: noise, outliers, and un-updated data, under both, ambient and transient conditions. From the results, it is clear that the applied technique was able to improve the quality of the PMU data set as well as the performance of the modal analyses.

6.2. Future work

The research proposed in this dissertation can be continued in several different directions in the future. The following aspects could be further addressed:

- Novel statistical metrics that were applied to the *type test* results could be further improved. During the testing in the calibration laboratory, PMUs are exposed to the test waveforms that are less likely to happen in the real system. One of the possible improvements is to add the **weighted** assessment to the performance evaluation, rather than treat each test case equally important.
- We showed that it is possible to derive the useful conclusions, and predict the behavior of the PMU under the transients by examining only the testing results from the calibration laboratory. Developing the methodology that will relate the results from the PMU *type testing* to the application of interest and predict the PMU behavior is another possible direction for the future research.

- We presented the application of the Principal Component Pursuit for the detection and correction of the bad data in the PMU blocks. Considered issues are as follows: high sensing noise, spikes and un-updated data. In the future, the spectrum of errors can be extended to include the missing data points as well. Furthermore, investigating the impact of the cyber attacks was not considered either.

REFERENCES

[1] S. Mukherjee, R. Nateghi, and M. Hastak, "A multi-hazard approach to assess severe weather-induced major power outage risks," in *US. Reliability Engineering & System Safety*, 175, 283-305., 2018

[2] (2009, Feb.). American Recovery and Reinvestment Act of 2009. [Online]. Available: https://www.energy.gov/oe/information-center/recovery-act

[3] A. G Phadke and J. S. Thorp, *Synchronized Phasor Measurements and Their Applications*, ISBN 978-0-387-76537-2, Springer, 2008.

[4] North American Electric Reliability Corporation (NERC), "Real-time application of synchrophasor for improving reliability," NY, Oct. 2010.

[5] B. Singh, N. K. Sharma, A. N. Tiwari, K. S. Verma and S. N. Singh, "Applications of phasor measurement units (PMUs) in electric power system networks incorporated with FACTS controllers," *International Journal of Engineering, Science and Technology*, Vol. 3, No. 3, pp. 64-82, 2011.

[6] A. Gómez-Expósito and A. Abur, "Foreword for the special section on synchrophasor applications in power systems," *IEEE Trans. Power Sys.*, vol. 28, no. 2, pp. 1907-1909, May 2013.

[7] M. Kezunovic, S. Meliopoulos, S. Venkatasubramanian, and V. Vittal, *Application of Time-Synchronized Measurements in Power System Transmission Networks*, ISBN 978-3-319-06218-1 Springer, 2014.

[8] F. Aminifar, *et al*., "Synchrophasor measurement technology in power systems: panorama and state-of-the-art," *IEEE Access*, vol. 2, pp. 1607-1628, Jan. 2015.

[9] K. E. Martin, J. F. Hauer, T. J. Faris, "PMU Testing and Installation Considerations at the Bonneville Power Administration," *in Proc. IEEE PES General Meeting*, pp. 1-6, 24-28 June 2007.

[10] IEEE Standard for Synchrophasor Measurements for Power Systems, *IEEE Std. C37.118.1-2011 (Revision of IEEE Std. C37.118-2005)*, pp.1-61, Dec. 28, 2011.

[11] IEEE Standard for Synchrophasor Data Transfer for Power Systems, *IEEE Std. C37.118.2-2011 (Revision of IEEE Std. C37.118-2005)*, pp.1-53, Dec. 28, 2011.

[12] IEEE Standard for Synchrophasor Measurements for Power Systems -- Amendment 1: Modification of Selected Performance Requirements, *IEEE Std. C37.118.1a-2014 (Amendment to IEEE Std. C37.118.1-2011)*, pp.1-25, April 30, 2014.

[13] IEEE Synchrophasor Measurement Test Suite Specification--Version 2, pp.1-43, Sept. 28, 2015.

[14] Erich Gunther, at all., Webinar "What's new with the Interoperability Process Reference Manual", [Online] available at: http://sgip.org/SGIP/files/ccLibraryFiles/Filename/000000001580/SGIP_Nov20_Webinar_Final.pdf

[15] V. Centeno (Dec. 2007). PMU system testing and calibration guide. North American Synchro Phasor Initiative (NASPI), [Online]. Available: https://www.naspi.org/File.aspx?fileID=555

[16] IEEE Guide for Synchronization, Calibration, Testing, and Installation of Phasor Measurement Units (PMUs) for Power System Protection and Control, *IEEE Std. C37.242-2013*, pp.1-107, March 6, 2013.

[17] IEEE Guide for Phasor Data Concentrator Requirements for Power System Protection, Control, and Monitoring, *IEEE Std. C37.244-2013*, pp.1-65, May 10, 2013.

[18] G. Stenbakken, T. Nelson, "NIST Support of Phasor Measurements to Increase Reliability of the North American Electric Power Grid," *IEEE PES General Meeting*, pp1-3, 18-22 June 2006.

[19] Y.-H. Tang, G. N. Stenbakken, and A. Goldstein, "Calibration of phasor measurement unit at NIST," *IEEE Trans. Instrum. Meas.*, vol. 62, no. 6, pp. 1417-1422, Jun. 2013.

[20] R. M. Moraes, *et al.*, "PMU interoperability, steady-state and dynamic performance tests," *IEEE Trans. Smart Grid*, vol. 3, no. 4, pp. 1660-1669, Dec. 2012.

[21] H. Liu, T. Bi, and Q. Yang, "The evaluation of phasor measurement units and their dynamic behavior analysis," *IEEE Trans. Instrum. Meas.*, vol. 62, no. 6, pp. 1479-1485, Jun. 2013.

[22] G. Barchi, D. Macii, and D. Petri, "Synchrophasor estimators accuracy: A comparative analysis," *IEEE Trans. Instrum. Meas.*, vol. 62, no. 5, pp. 963-973, May 2013.

[23] U. Pogliano, J. Braun, B. Voljc, and R. Lapuh, "Software platform for PMU algorithm testing," *IEEE Trans. Instrum. Meas.*, vol. 62, no. 6, pp. 1400-1406, Jun. 2013.

[24] A. J. Roscoe, "Exploring the relative performance of frequency-tracking and fixed-filter phasor measurement unit algorithms under C37.118 test procedures, the effects of inter-harmonics, and initial attempts at merging P-class response with M-class filtering," *IEEE Trans. Instrum. Meas.*, vol. 62, no. 8, pp. 2140-2153, Aug. 2013.

[25] D. Belega and D. Petri, "Accuracy analysis of the multi-cycle synchrophasor estimator provided by the interpolated DFT algorithm," *IEEE Trans. Instrum. Meas.*, vol. 62, no. 5, pp. 942-953, May 2013.

[26] I. Kamwa, S. R. Samantaray, and G. Joos, "Compliance analysis of PMU algorithms and devices for wide-area stabilizing control of large power systems," *IEEE Trans. Power Syst.*, vol. 28, no. 2, pp. 1766-1778, May 2013.

[27] D. R. Gurusinghe, A. D. Rajapakse, and K. Narendra, "Testing and enhancement of the dynamic performance of a phasor measurement unit," *IEEE Trans. Power Del.*, vol.29, no.4, pp.1551–1560, Aug. 2014.

[28] S.S. Biswas, A.K. Srivastava, J. S. Park, and J. Castaneda, "Tool for testing of phasor measurement units: PMU performance analyzer," *IET Gen., Trans. & Dist.*, vol. 9, no. 2, pp. 154-163, Jan. 2015.

[29] "Phasor measurement units gain credibility through improved test and calibration standards" [Online] available at: https://us.flukecal.com/products/electrical-calibration/electrical-calibrators/6135apmucal-phasor-measurement-unit-calibrati

[30] Z. Huang, J. F. Hauer and K. E. Martin, "Evaluation of PMU dynamic performance in both lab environments and under field operating conditions," *Proc. IEEE PES General Meeting*, pp.1-6, Florida, 2007.

[31] A. G. Phadke and B. Kasztenny, "Synchronized phasor and frequency measurement under transient conditions," *IEEE Trans. Power Del.*, vol. 24, no. 1, pp. 89-95, Jan. 2009.

[32] G. Barchi, D. Macii, D. Belega, and D. Petri, "Performance of synchrophasor estimators in transient conditions: A comparative analysis," *IEEE Trans. Instrum. Meas.*, vol. 62, no. 9, pp. 2410-2418, Sep. 2013.

[33] J. C. Zhao, *et al*., "Impact of Measurement Error on Synchrophasor Applications," ORNL/TM-2015/314 report, Oak Ridge National Laboratory, Oak Ridge, 2015.

[34] A. Guzman, S. Samineni, and M. Bryson. "Protective relay synchrophasor measurements during fault conditions," *SEL Journal of Reliable Power,* vol. 2, no. 2, May 2011.

[35] P. Meinhardt, "Time Synchro1nized End to End Testing Using IRIG-B," IET 9th *International Conference on Developments in Power System Protection,* Glasgow, March 2008.

[36] A. Apostolov, B. Vandiver, "Can End-to-End testing satisfy NERC/ FERC?," *65th Annual Conference for Protective Relay Engineers,* College Station, TX, 2012.

[37] S. Turner, "End-to-end testing transmission line protection schemes and double-ended fault locators," *66th Annual Conference for Protective Relay Engineers,* College Station, TX, 2013.

[38] A. Apostolov, B. Vandiver, "End to End Testing - What Should You Know?," *67th Annual Conference for Protective Relay Engineers,* College Station, TX, 2014.

[39] California ISO, “Five year synchrophasor plan,” California ISO, Tech. Rep., Nov 2011.

[40] NASPI, PMU. “Synchrophasor Data Quality Attributes and a Methodology for Examining Data Quality Impacts upon Synchrophasor Applications.” (2016).

[41] K. Narendra and H. Kirkham, “A report on using PMU data under fault conditions,” NASPI PSRTT WG Report.

[42] L. Zhang and A. Abur, “Impact of tuning on bad data detection of PMU measurements,” *IEEE PES Innovative Smart Grid Technologies*, Tianjin, 2012, pp. 1-5

[43] L. Vanfretti, J. H. Chow, S. Sarawgi and B. Fardanesh, “A Phasor-Data-Based State Estimator Incorporating Phase Bias Correction,” in *IEEE Transactions on Power Systems*, vol. 26, no. 1, pp. 111-119, Feb. 2011.

[44] S. G. Ghiocel *et al*., “Phasor-Measurement-Based State Estimation for Synchrophasor Data Quality Improvement and Power Transfer Interface Monitoring,” in *IEEE Transactions on Power Systems*, vol. 29, no. 2, pp. 881-888, March 2014.

[45] W. Xu, M. Wang, J. F. Cai and A. Tang, “Sparse Error Correction From Nonlinear Measurements With Applications in Bad Data Detection for Power Networks,” in *IEEE Transactions on Signal Processing*, vol. 61, no. 24, pp. 6175-6187, Dec.15, 2013.

[46] K. D. Jones, A. Pal and J. S. Thorp, “Methodology for Performing Synchrophasor Data Conditioning and Validation,” in *IEEE Transactions on Power Systems*, vol. 30, no. 3, pp. 1121-1130, May 2015.

[47] J. Zhang, G. Welch, G. Bishop and Z. Huang, "A Two-Stage Kalman Filter Approach for Robust and Real-Time Power System State Estimation," in *IEEE Transactions on Sustainable Energy*, vol. 5, no. 2, pp. 629-636, April 2014.

[48] H. Li, L. Lai and S. M. Djouadi, "Combating False Reports for Secure Networked Control in Smart Grid via Trustiness Evaluation," *2011 IEEE International Conference on Communications (ICC)*, Kyoto, 2011, pp. 1-5.

[49] Y. Fan, Z. Zhang, M. Trinkle, A. D. Dimitrovski, J. B. Song and H. Li, "A Cross-Layer Defense Mechanism Against GPS Spoofing Attacks on PMUs in Smart Grids," in *IEEE Transactions on Smart Grid*, vol. 6, no. 6, pp. 2659-2668, Nov. 2015.

[50] Q. Zhang, V. Vittal, G. Heydt, Y. Chakhchoukh, N. Logic and S. Sturgill, "The time skew problem in PMU measurements," *2012 IEEE Power and Energy Society General Meeting*, San Diego, CA, 2012, pp. 1-6.

[51] Z. Mao, T. Xu and T. J. Overbye, "Real-time detection of malicious PMU data," *2017 19th International Conference on Intelligent System Application to Power Systems (ISAP)*, San Antonio, TX, 2017, pp. 1-6.

[52] K. Mahapatra, N. R. Chaudhuri and R. Kavasseri, "Bad data detection in PMU measurements using principal component analysis," *2016 North American Power Symposium (NAPS)*, Denver, CO, 2016, pp. 1-6.

[53] L. Liu, M. Esmalifalak and Z. Han, "Detection of false data injection in power grid exploiting low rank and sparsity," *2013 IEEE International Conference on Communications (ICC)*, Budapest, 2013, pp. 4461-4465.

[54] L. Liu, M. Esmalifalak, Q. Ding, V. A. Emesih and Z. Han, "Detecting False Data Injection Attacks on Power Grid by Sparse Optimization," in *IEEE Transactions on Smart Grid*, vol. 5, no. 2, pp. 612-621, March 2014.

[55] M. Wang *et al*., "A Low-Rank Matrix Approach for the Analysis of Large Amounts of Power System Synchrophasor Data," *2015 48th Hawaii International Conference on System Sciences*, Kauai, HI, 2015, pp. 2637-2644.

[56] M. Wang *et al*., "Identification of "unobservable" cyber data attacks on power grids," *2014 IEEE International Conference on Smart Grid Communications (SmartGridComm)*, Venice, 2014, pp. 830-835.

[57] P. Gao et al., "Identification of Successive "Unobservable" Cyber Data Attacks in Power Systems Through Matrix Decomposition," in *IEEE Transactions on Signal Processing*, vol. 64, no. 21, pp. 5557-5570, Nov.1, 1 2016.

[58] P. Gao, M. Wang, S. G. Ghiocel and J. H. Chow, "Modeless reconstruction of missing synchrophasor measurements," *2014 IEEE PES General Meeting Conference & Exposition*, National Harbor, MD, 2014, pp. 1-5.

[59] P. Gao, M. Wang, S. G. Ghiocel, J. H. Chow, B. Fardanesh and G. Stefopoulos, "Missing Data Recovery by Exploiting Low-Dimensionality in Power System Synchrophasor Measurements," in *IEEE Transactions on Power Systems*, vol. 31, no. 2, pp. 1006-1013, March 2016.

[60] P. Gao, R. Wang, M. Wang and J. H. Chow, "Low-rank matrix recovery from quantized and erroneous measurements: Accuracy-preserved data privatization in

power grids," *2016 50th Asilomar Conference on Signals, Systems and Computers*, Pacific Grove, CA, 2016, pp. 374-378.

[61] M. Wu and L. Xie, "Online identification of bad synchrophasor measurements via spatio-temporal correlations," *2016 Power Systems Computation Conference (PSCC)*, Genoa, 2016, pp. 1-7.

[62] M. Wu and L. Xie, "Online Detection of Low-Quality Synchrophasor Measurements: A Data-Driven Approach," in *IEEE Transactions on Power Systems*, vol. 32, no. 4, pp. 2817-2827, July 2017.

[63] S. Dutta and T. J. Overbye, "Information processing and visualization of power system wide area time varying data," *2013 IEEE Computational Intelligence Applications in Smart Grid (CIASG)*, Singapore, 2013, pp. 6-12.

[64] K. Mahapatra and N. R. Chaudhuri, "Malicious Corruption-Resilient Wide-Area Oscillation Monitoring using Principal Component Pursuit," in *IEEE Transactions on Smart Grid*, in press.

[65] K. Mahapatra, N. R. Chaudhuri, R. Kavasseri and S. Brahma, "Online Analytical Characterization of Outliers in Synchrophasor Measurements: A Singular Value Perturbation Viewpoint," in *IEEE Transactions on Power Systems*, vol. PP, no. 99, pp. 1-1.

[66] H. Sedghi and E. Jonckheere, "Statistical structure learning of smart grid for detection of false data injection," *2013 IEEE Power & Energy Society General Meeting*, Vancouver, BC, 2013, pp. 1-5.

[67] Q. Zhang, Xiaochuan Luo, D. Bertagnolli, S. Maslennikov and B. Nubile, "PMU data validation at ISO New England," *2013 IEEE Power & Energy Society General Meeting*, Vancouver, BC, 2013, pp. 1-5.

[68] Dongliang Duan, Liuqing Yang and L. L. Scharf, "Phasor state estimation from PMU measurements with bad data," *2011 4th IEEE International Workshop on Computational Advances in Multi-Sensor Adaptive Processing (CAMSAP)*, San Juan, 2011, pp. 121-124.

[69] Q. F. Zhang and V. M. Venkatasubramanian, "Synchrophasor time skew: Formulation, detection and correction," *2014 North American Power Symposium (NAPS)*, Pullman, WA, 2014, pp. 1-6.

[70] C. P. Steinmetz, "Complex quantities and their use in electrical engineering," In *Proceedings of the International Electrical Congress*, pp. 33-74, 1893

[71] J.O.Smith III, *Spectral Audio Signal Processing*, ISBN 978-0-9745607-3-1, W3K Publishing, 2011

[72] Available:https://www.tek.com/sites/default/files/media/media/resources/3MW_17750_8_0.pdf

[73] M. Harrysson, "Fault location algorithms in transmission grids," M.S. thesis, Dept. Elect. Eng., Halmstad Univ., Halmstad, Sweden, 2014.

[74] S. M. Mohan, J. J. Izykowski, E. Rosolowski, *Fault location on power networks*. Springer Science & Business Media, 2009.

[75] NI CompactRIO Controller Specifications [Online]. Available: http://www.ni.com/pdf/manuals/376904b_02.pdf

[76] National Instruments (May 2016). Open PMU LabVIEW Project. [Online]. Available: http://www.ni.com/white-paper/52975/en/

[77] V. Terzija, M. Kezunovic, "Synchronized Measurement Technology for Analysis of Transmission Lines Faults," in *44th Hawaii International Conference on System Sciences* (HICSS), pp.1-8, 4-7 Jan. 2011.

[78] E. Nashawati, R. Garcia and T. Rosenberger, "Using synchrophasor for fault location identification," in *Proc. 65th Annual Conference for Protective Relay Engineers*, pp. 14-21, College Station, TX, 2012.

[79] Z. M. Radojević, et al., "New approach for fault location on transmission lines not requiring line parameters", *Int. Conf. on Power System Transients*, Kyoto, Japan, 2009, pp. 1-6.

[80] P. W. Sauer, M. A. Pai, J. H. Chow, "Small-Signal Stability," in *Power System Dynamics and Stability: With Synchrophasor Measurement and Power System Toolbox*, , IEEE, 2017, pp.

[81] C. Canizares *et al*., "Benchmark Models for the Analysis and Control of Small-Signal Oscillatory Dynamics in Power Systems," in *IEEE Transactions on Power Systems*, vol. 32, no. 1, pp. 715-722, Jan. 2017.

[82] M. Klein, G. J. Rogers, P. Kundur, "A Fundamental Study of Inter-Area Oscillations in Power Systems," *IEEE Trans. Power Systems*, vol. 6, pp. 914-921, Aug. 1991.

[83] V. Venkatasubramanian and Y. Li, “Analysis of 1996 western american electric blackouts”, in *Proc. Bulk Power System Phenomena-Stability and Control*, Venice, Italy, 2004.

[84] P. Kundur, “Power System Stability and Control” in New York:McGraw-Hill, Inc., 1994.

[85] F. Dussaud “An application of modal analysis in electric power systems to study inter-area oscillations” in Degree Project In Electric Power System Second Level, STOCKHOLM, Sweden, 2015.

[86] J. Hauer, E. Martinez, A. R. Messina, and J. Sanchez-Gasca. “Identification of Electromechanical Modes in Power Systems.” *Special Publication, TP462, IEEE Power & Energy Society, Tech. Rep.* 2012.

[87] J. F. Hauer, C. J. Demeure, L. L. Scharf, “Initial Results in Prony Analysis of Power System Response Signals”, *IEEE Trans. Power Systems*, vol. 5, pp. 80-89, Feb. 1990.

[88] L. L. Grant and M. L. Crow, “Comparison of Matrix Pencil and Prony methods for power system modal analysis of noisy signals,” *2011 North American Power Symposium*, Boston, MA, 2011, pp. 1-7.

[89] G. R. B. Prony, “Essai experimental et analytique sur les lois de la dilatalrlite de fluids elastiques et sur cells de la vapeur de l'alcool a differents tempoeratures,” *Journal de l'Ecole Polytechnique (París)*, vol. 1, pp. 24-76, 1795.

[90] S. Van Huffel, H. Chen, C. Decanniere, and P. Van Hecke, “Algorithm for time-domain NMR data fitting based on total least squares,” *J. Mag. Res*., vol. A110, pp. 228–237, 1994.

[91] R. Roy and T. Kailath, “ESPRIT – estimation of signal parameters via rotational invariance technique,” *IEEE Trans. Acoust. Speech Signal Process.*, vol. 37, no. 7, pp. 984–995, Jul. 1989.

[92] Y. Hua and T. K. Sarkar, “Matrix pencil method and its performance,” *ICASSP-88., International Conference on Acoustics, Speech, and Signal Processing*, New York, NY, USA, 1988, pp. 2476-2479 vol.4.

[93] Y. Hua and T. K. Sarkar, “Generalized pencil-of-function method for extracting poles of an EM system from its transient response,” in *IEEE Transactions on Antennas and Propagation*, vol. 37, no. 2, pp. 229-234, Feb. 1989.

[94] Y. Hua and T. K. Sarkar, “Matrix pencil method for estimating parameters of exponentially damped/undamped sinusoids in noise,” in *IEEE Transactions on Acoustics, Speech, and Signal Processing*, vol. 38, no. 5, pp. 814-824, May 1990"

[95] V. K. Jain, T. K. Sarkar, “High-performance signal-modeling by Pencil-of-Functions method: band-pass case”, *IEEE Trans. on ASSP*, Aug. 1986.

[96] W. Trinh, K. S. Shetye, I. Idehen, and T. J. Overbye, “Iterative Matrix Pencil Method for Power System Modal Analysis,” 2019 *Hawaii International Conference on System Sciences (HICSS)*, Wailea, HI, January 2019., in press.

[97] A. R. Borden, B. C. Lesieutre, "Variable projection method for power system modal identification," *IEEE Trans. Power Syst.*, vol. 29, no. 6, pp. 2613-2620, Nov. 2014.

[98] R. A. DeCallafon, B. Moaveni, J. P. Conte, X. He, E. Udd, "General realization algorithm for modal identification of linear dynamic systems", *ASCE J. Eng. Mech.*, vol. 134, no. 9, pp. 712-722, 2009.

[99] S. Mohaptra, T. J. Overbye, "Fast modal identification monitoring and visualization for large-scale power systems using dynamic mode decomposition," *Proc. 2016 Power Systems Computation Conference (PSCC)*, pp. 1-7.

[100] A. R. Borden, B. C. Lesieutre and J. Gronquist, "Power system modal analysis tool developed for industry use,"*2013 North American Power Symposium (NAPS)*, Manhattan, KS, 2013, pp. 1-6.

[101] M. Brown, M. Biswal, S. Brahma, S. J. Ranade and H. Cao, "Characterizing and quantifying noise in PMU data," *2016 IEEE Power and Energy Society General Meeting (PESGM)*, Boston, MA, 2016, pp. 1-5.

[102] A. B. Birchfield, T. Xu, K. M. Gegner, K. S. Shetye and T. J. Overbye, "Grid Structural Characteristics as Validation Criteria for Synthetic Networks," in *IEEE Transactions on Power Systems*, vol. 32, no. 4, pp. 3258-3265, July 2017.

[103] T. Xu, A. B. Birchfield and T. J. Overbye, "Modeling, Tuning, and Validating System Dynamics in Synthetic Electric Grids," in *IEEE Transactions on Power Systems*, vol. 33, no. 6, pp. 6501-6509, Nov. 2018.

[104] https://electricgrids.engr.tamu.edu/electric-grid-test-cases/activsg2000/

[105] E. J. Candes, X. Li, Y. Ma, and J. Wright, "Robust principal component analysis?" *Journal of the ACM (JACM),* vol. 58, no. 3, p. 11, 2011.

[106] M. Grant, S. Boyd, Y. Ye, "Cvx: Matlab software for disciplined convex programming", 2008.

[107] J. Wright, A. Ganesh, S. Rao, Y. Peng, and Y. Ma, "Robust principal component analysis: Exact recovery of corrupted low-rank matrices via convex optimization," in *Advances in neural information processing systems*, 2009, pp. 2080–2088.

[108] Z. Lin, A. Ganesh, J. Wright, L. Wu, M. Chen, and Y. Ma, "Fast convex optimization algorithms for exact recovery of a corrupted low-rank matrix," *Computational Advances in Multi-Sensor Adaptive Processing (CAMSAP),* vol. 61, no. 6, 2009.

[109] X. Yuan, and J. Yang. "Sparse and low-rank matrix decomposition via alternating direction methods," *preprint* 12 (2009): 2.

[110] M. Kezunovic, A. Esmaeilian, T. Becejac, P. Dehghanian, and C. Qian, "Life-Cycle Management Tools for Synchrophasor Systems: Why We Need Them and What They Should Entail", *The 2016 IFAC CIGRE/CIRED Workshop on Control of Transmission and Distribution Smart Grids,* October 11-13, 2016, Prague, Czech Republic.

[111] T. Becejac, P. Dehghanian, and M. Kezunovic, "Probabilistic Assessment of PMU Integrity for Planning of Periodic Maintenance and Testing", *IEEE Conference on Probabilistic Methods Applied to Power Systems (PMAPS),* October 2016, Beijing, China.

[112] T. Becejac, P. Dehghanian, and M. Kezunovic, "Analysis of PMU Algorithm Errors During Fault Transients and Out-of-Step Disturbances", *IEEE Power and Energy Society (PES) Transmission & Distribution (T&D) Latin America*, September 21-24, 2016, Morelia, Mexico.

[113] T. Becejac, P. Dehghanian, and M. Kezunovic, "Impact of PMU Errors on the Synchrophasor-based Fault Location in Power Systems", *48th North American Power Symposium, (NAPS),* Sep. 2016, Denver, Colorado, USA.

[114] T. Becejac, and P. Dehghanian, "PMU Multilevel End-to-End Testing to Assess Synchrophasor Measurements during Faults," under review

[115] T. Becejac, and T. Overbye, "Overview of Synchrophasor Data Quality Issues and Bad Data Detection Techniques," under review

[116] T. Becejac, and T. Overbye, "Impact of PMU Data Errors on Modal Extraction Using Matrix Pencil Method," *IEEE International Conference on Smart Grid Synchronized Measurements and Analytics 2019 (SGSMA 2019),* under review